

Exploration of molecular defense mechanisms against viral infections exemplified in COVID-19

Doctoral thesis

to obtain a doctorate (PhD)

from the Faculty of Medicine

of the University of Bonn

Jasper Henning Justin Spitzer

from Ennigerloh, Germany

2024

Written with authorization of
the Faculty of Medicine of the University of Bonn

First reviewer: Prof. Dr. Eicke Latz

Second reviewer: Prof. Dr. Jan Hasenauer

Day of oral examination: 11.01.2024

From the Institute of Clinical Chemistry and Clinical Pharmacology

Director: Prof. Dr. Hartmann

Contents

List of Abbreviations	4
1 Abstract	5
2 Introduction with references	6
2.1 SARS-CoV-2	6
2.2 COVID-19 and the defending immune response.....	6
2.3 Immune response in severe COVID-19.....	7
2.4 Vaccine response	8
2.5 Vaccination against COVID-19	8
2.6 Vaccine failure and cirrhosis-associated immune dysfunction.....	8
2.7 Aims	9
2.8 References.....	9
3 Publications	13
3.1 Publication 1: Comparative Analysis of Antibody Titers against the Spike Protein of SARS-CoV-2 Variants in Infected Patient Cohorts and Diverse Vaccination Regimes.....	13
3.2 Publication 2: Interferon-induced IL-10 drives systemic T-cell dysfunction during chronic liver injury	33
3.3 Publication 3: CD4+ T cell calibration of antigen-presenting cells optimizes antiviral CD8+ T cell immunity.....	52
4 Discussion with references.....	70
4.1 Antibody-response to SARS-CoV-2 vaccines.....	70
4.2 IFN-induced IL10 weakens the T cell response.....	70
4.3 Interactions of T cells and antigen presenting cells	71
4.4 References	72
5 Acknowledgement	74

List of Abbreviations

ACE2	Angiotensin converting enzyme 2
APC	Antigen presenting cell
ARDS	Acute respiratory distress syndrome
BALF	Bronchoalveolar fluid
CAID	Cirrhosis associated immune dysfunction
CCR2	Cc-chemokine receptor 2
CD4	Cluster of differentiation 4
CD40	Cluster of differentiation 40
CD40L	Cluster of differentiation 40 ligand
COVID-19	Coronavirus disease 2019
HBV	Hepatitis B virus
IFN	Interferon
IL-1 β	Interleukin-1 β
IL-6	Interleukin-6
IL-8	Interleukin-8
IL-10	Interleukin-10
mRNA	Messenger ribonucleic acid
N protein	Nucleocapsid protein
SARS-CoV-2	Severe Acute Respiratory Syndrome Coronavirus 2
S protein	Spike protein

1 Abstract

Studying the immune response to Severe Acute Respiratory Syndrome Coronavirus 2 (SARS-CoV-2) has been an international research focus ever since the start of the pandemic in early 2020. In the first part of this thesis, the antibody response to both infection with and vaccination against SARS-CoV-2 was analysed; while multiple vaccines exist, with regard to resulting antibody titres and short-term inflammatory response, no large differences between the immunization approaches exist. Initial antibody responses waned after 6 months but were restored robustly by booster vaccinations. Antibody responses were weaker against variants of SARS-CoV-2, with the beta-variant showing the strongest immune evasion. In the second section, the T cell exhaustion characteristic for liver cirrhosis was found to be driven by Interleukin-10 (IL-10), which was itself caused by bacterial translocation-induced type I interferon derived from myeloid cells in the liver. Interestingly, this T cell exhaustion was critical for vaccine responses, including the vaccine response to SARS-CoV-2, and could be repressed using IL-10 blockade, restoring vaccine responsiveness. The third part of the thesis is focused on the interactions of T cells and antigen presenting cells (APCs): while preconditioning through Interferon is necessary and leads to an immune activation, for an optimal response, an additional trigger via interaction between cluster of differentiation (CD) 40 and CD40 ligand (CD40L) is essential: thus, myeloid cells need T cell help to participate to their fullest extent. A signature of important immune activators, including IL-15 and several other cytokines, as well as driving transcription factors like p65, IRF1 and FOS, could only become activated by the combinatorial signals. In severe forms of Coronavirus disease 2019 (COVID-19), APCs lack either one or both parts of this activation, rendering the immune response less directed and effective.

2 Introduction with references

2.1 SARS-CoV-2

In December 2019, a new respiratory virus emerged in the Wuhan region of China. Initially termed “Wuhan pneumonia”, the virus was identified through sequencing as a member of the *Coronaviridae* family of viruses and designated SARS-CoV-2, with its disease named COVID-19 (Wu *et al.*, 2020). Over the following months, the virus would go on to infect over 700 million patients worldwide (August 2023; *WHO Coronavirus (COVID-19) Dashboard*, 2023). Along with this infamy came the growing interest of the global scientific community, studying and deciphering SARS-CoV-2 to prevent further infections and deaths.

SARS-CoV-2 is part of the Betacoronavirus genus and as such an enveloped, positive-strand RNA virus. Of the encoded proteins, the spike (S)-protein is of special importance: its subunits bind to the angiotensin converting enzyme 2 (ACE2; Hoffmann *et al.*, 2020). Thus, affinity for and the distribution of ACE2 which determines the spectrum of infection, both on a cell-to-cell and a species-to-species level (Sun *et al.*, 2020). In addition to the S protein, the structural nucleocapsid (N) protein can play an important role for the diagnosis and monitoring of SARS-CoV-2 infections (Shan *et al.*, 2021).

As it is the central protein for viral entry into the cell, the S protein is the focus of both therapeutic interventions as well as host immune responses (Zhu *et al.*, 2020). These pressures drive the evolution of SARS-CoV-2, leading to a range of different variants to emerge over time, which on a genetic level mostly differ in their S proteins, whereas on a physiological level they also differ with regards to transmissibility and virulence (Markov *et al.*, 2023).

2.2 COVID-19 and the defending immune response

The disease caused by SARS-CoV-2 has been termed Coronavirus disease 2019 (COVID-19). It is transmitted via droplet infection with an average incubation period of 5 days. In 35% percent of cases, the infection resolves without any symptoms, but in other cases the symptoms can include cough, fever, loss of taste and smell as well as general flu-like symptoms (N. Chen *et al.*, 2020). In most cases, the disease is self-resolving. The WHO distinguishes four levels of severity: 1) mild diseases, which are any cases that meet the definition for COVID-19 but show no signs of pneumonia, 2) moderate disease, manifesting with pneumonia but not severe pneumonia, 3) severe cases include with pneumonia and increased respiratory rate or low oxygen saturation,

and 4) critical disease includes acute respiratory distress syndrome (ARDS), as well as sepsis, septic shock and multisystemic inflammatory syndrome (*Clinical Spectrum*, 2023).

While overall the case fatality rate is manageable, in its more severe forms, COVID-19 is a deadly disease; in the early phases of the pandemic, estimated 5% of all cases in the US and 20% of hospitalised cases experienced severe symptoms, with 75% of hospitalised patients needing supplemental oxygen (Wiersinga *et al.*, 2020).

2.3 Immune response in severe COVID-19

The immune response to COVID-19 has been extensively studied ever since early 2020. While initial reports mostly focussed on excessive hyper-inflammation (Wang *et al.*, 2020), more recent studies contribute to illuminate the complex network of interactions underlying the disease in all its severities.

Patients usually develop a robust antibody response against COVID-19 within the first week after symptom onset (Long *et al.*, 2020). Recovered patients show a population of T follicular helper cells as well as class-switched B cells (Juno *et al.*, 2020). However, not all cases resolve on their own:

The hallmarks of severe COVID-19 are 1) an overabundance of pro-inflammatory cytokines, 2) a deficiency in virus-specific responses including lack of robust interferon (IFN) and T cell responses, and 3) an imbalance in the myeloid cell compartment. All three of these hallmarks interrelate and influence each other: The amount of pro-inflammatory cytokines and chemokines such as interleukin-6 (IL-6), interleukin-8 (IL-8), and in some studies interleukin-1 β (IL-1 β) are increased in patients with more severe forms of disease (G. Chen *et al.*, 2020; Lucas *et al.*, 2020), whereas the IFN, particularly the type 1 IFN response, is less pronounced in severer cases (Galani *et al.*, 2021). This difference in these soluble factors is accompanied by differences in cell populations: in more severe cases of COVID-19, lymphocytopenia is present (Guan *et al.*, 2020), with a special emphasis on cytotoxic T cells (Wilk *et al.*, 2020).

Similarly, cells of the myeloid lineage have been implicated in this immune disbalance: bronchoalveolar fluid (BALF) from patients is enriched for chemokines attracting cc-chemokine receptor 2 (CCR2) positive monocytes to the site of infection, where they make up the majority of cells. This accumulation is stronger in more severe cases (Liao *et al.*, 2020). The disbalance of the myeloid cell compartment is however not localised

to the site of infection; multiple studies have found peripheral hyper-inflammatory monocytes in severe cases of COVID-19 which do produce a large amount of inflammatory cytokines like IL-6, while showing lower levels of key molecules for antigen presentation and engagement of the T cell compartment (Schulte-Schrepping *et al.*, 2020; Zhou *et al.*, 2020).

2.4 Vaccine response

In dealing with pathogenic agents, vaccines have proven to be invaluable against numerous diseases, such as small as small pox (Meyer, Ehmann and Smith, 2020) or diphtheria (Sharma *et al.*, 2019). All currently applied vaccine approaches are measured by their outcomes with regards to antibody and T cell responses: antibody titre as well as antibody affinity for the relevant target of the infection are used; with the vaccine against hepatitis B virus (HBV), the resulting antibody titre is used as a measure of immunity (Schillie *et al.*, 2013). However, some studies suggest that an antibody response alone is not sufficient for immunisation, but instead T cell help is necessary (Malley *et al.*, 2005).

2.5 Vaccination against COVID-19

Aside from containment measures, in the first year of the pandemic there was a strive for a vaccine, as immunisation would allow for the lifting of other measures. In 2020, the first vaccines against SARS-CoV-2 were approved; among them the first ever messenger ribonucleic acid (mRNA) based vaccines for a human disease (Zhang, Shen and Chang, 2022). With these vaccines, large proportions of the European population could be successfully vaccinated against SARS-CoV-2 (*COVID-19 Vaccine Tracker*, 2023). While the approval of these vaccines depended on proven safety and efficacy, at the time, long-term sustainability of the immune responses induced by the vaccines was not yet established.

2.6 Vaccine failure and cirrhosis-associated immune dysfunction

In the strive to immunise large parts of the world, numerous logistic and scientific challenges had to be overcome. However, other challenges also play an important role in the immunisation, which can be vaccine-related or host-related (Wiedermann, Garner-Spitzer and Wagner, 2016). Of the host-related vaccine failures, the vast majority is directly related to immune deficiencies like after organ transplantation (Mavundza *et al.*, 2020) or immune cell depletion (Vijenthira *et al.*, 2021).

In addition, some conditions, such as liver cirrhosis can result in vaccine unresponsiveness: the immunological effects of liver cirrhosis have been termed cirrhosis associated immune dysfunction (CAID) and include immunodeficiency and systemic inflammation (Albillos, Lario and Álvarez-Mon, 2014), which is associated with enhanced bacterial translocation (Berg and Garlington, 1979). Under homeostatic conditions, the liver is exposed to large amounts of bacterial antigens and neutralizes the pathogens (Jenne and Kubes, 2013). However, this function is lost under cirrhosis conditions and instead, patients show increased susceptibility to infection (Premkumar *et al.*, 2019) and a poor vaccination response (Alter, 2012; See, 2022). While myeloid cells have been identified as primary responders to bacterial dislocation, the interactions between immune cells driving vaccine failure are still not elucidated.

2.7 Aims

Conceptualised in the beginning of the COVID-19 pandemic, this project aimed to elucidate the immune response to the SARS-CoV-2 virus. In the first part, responses to the vaccines broadly used in Germany were characterised in selective cohorts with a focus on long-term follow up. In the second part, a possible reason for vaccination failure is explored – liver cirrhosis associated immune dysfunction, manifesting in the effects of myeloid cells on T cells in the liver and systemically. In the third part of this thesis, severe courses of COVID-19 are analysed with a continuing focus of myeloid-T cell interactions, as the failure of myeloid cells to adequately induce a T cell response may not be driven myeloid cells alone.

2.8 References

- Albillos, A., Lario, M. and Álvarez-Mon, M. (2014) 'Cirrhosis-associated immune dysfunction: Distinctive features and clinical relevance', *Journal of Hepatology*, 61(6), pp. 1385–1396. Available at: <https://doi.org/10.1016/j.jhep.2014.08.010>.
- Alter, M.J. (2012) 'Vaccinating Patients with Chronic Liver Disease', *Gastroenterology & Hepatology*, 8(2), pp. 120–122.
- Berg, R.D. and Garlington, A.W. (1979) 'Translocation of Certain Indigenous Bacteria from the Gastrointestinal Tract to the Mesenteric Lymph Nodes and Other Organs in a Gnotobiotic Mouse Model', *Infection and Immunity*, 23(2), pp. 403–411. Available at: <https://doi.org/10.1128/iai.23.2.403-411.1979>.
- Chen, G. *et al.* (2020) 'Clinical and immunological features of severe and moderate coronavirus disease 2019', *The Journal of Clinical Investigation*, 130(5), pp. 2620–2629. Available at: <https://doi.org/10.1172/JCI137244>.
- Chen, N. *et al.* (2020) 'Epidemiological and clinical characteristics of 99 cases of 2019 novel coronavirus pneumonia in Wuhan, China: a descriptive study', *The Lancet*,

395(10223), pp. 507–513. Available at: [https://doi.org/10.1016/S0140-6736\(20\)30211-7](https://doi.org/10.1016/S0140-6736(20)30211-7).

Clinical Spectrum (2023) *COVID-19 Treatment Guidelines*. Available at: <https://www.covid19treatmentguidelines.nih.gov/overview/clinical-spectrum/> (Accessed: 10 August 2023).

COVID-19 Vaccine Tracker (2023). Available at: <https://vaccinetracker.ecdc.europa.eu/public/extensions/COVID-19/vaccine-tracker.html#uptake-tab> (Accessed: 11 August 2023).

Galani, I.-E. *et al.* (2021) ‘Untuned antiviral immunity in COVID-19 revealed by temporal type I/III interferon patterns and flu comparison’, *Nature Immunology*, 22(1), pp. 32–40. Available at: <https://doi.org/10.1038/s41590-020-00840-x>.

Guan, W. *et al.* (2020) ‘Clinical Characteristics of Coronavirus Disease 2019 in China’, *New England Journal of Medicine*, 382(18), pp. 1708–1720. Available at: <https://doi.org/10.1056/NEJMoa2002032>.

Hoffmann, M. *et al.* (2020) ‘SARS-CoV-2 Cell Entry Depends on ACE2 and TMPRSS2 and Is Blocked by a Clinically Proven Protease Inhibitor’, *Cell*, 181(2), pp. 271–280.e8. Available at: <https://doi.org/10.1016/j.cell.2020.02.052>.

Jenne, C.N. and Kubes, P. (2013) ‘Immune surveillance by the liver’, *Nature Immunology*, 14(10), pp. 996–1006. Available at: <https://doi.org/10.1038/ni.2691>.

Juno, J.A. *et al.* (2020) ‘Humoral and circulating follicular helper T cell responses in recovered patients with COVID-19’, *Nature Medicine*, 26(9), pp. 1428–1434. Available at: <https://doi.org/10.1038/s41591-020-0995-0>.

Liao, M. *et al.* (2020) ‘Single-cell landscape of bronchoalveolar immune cells in patients with COVID-19’, *Nature Medicine*, 26(6), pp. 842–844. Available at: <https://doi.org/10.1038/s41591-020-0901-9>.

Long, Q.-X. *et al.* (2020) ‘Antibody responses to SARS-CoV-2 in patients with COVID-19’, *Nature Medicine*, 26(6), pp. 845–848. Available at: <https://doi.org/10.1038/s41591-020-0897-1>.

Lucas, C. *et al.* (2020) ‘Longitudinal analyses reveal immunological misfiring in severe COVID-19’, *Nature*, 584(7821), pp. 463–469. Available at: <https://doi.org/10.1038/s41586-020-2588-y>.

Malley, R. *et al.* (2005) ‘CD4+ T cells mediate antibody-independent acquired immunity to pneumococcal colonization’, *Proceedings of the National Academy of Sciences*, 102(13), pp. 4848–4853. Available at: <https://doi.org/10.1073/pnas.0501254102>.

Markov, P.V. *et al.* (2023) ‘The evolution of SARS-CoV-2’, *Nature Reviews Microbiology*, 21(6), pp. 361–379. Available at: <https://doi.org/10.1038/s41579-023-00878-2>.

Mavundza, E.J. *et al.* (2020) ‘A systematic review of immunogenicity, clinical efficacy and safety of human papillomavirus vaccines in people living with the human

immunodeficiency virus', *Human Vaccines & Immunotherapeutics*, 16(2), pp. 426–435. Available at: <https://doi.org/10.1080/21645515.2019.1656481>.

Meyer, H., Ehmann, R. and Smith, G.L. (2020) 'Smallpox in the Post-Eradication Era', *Viruses*, 12(2), p. 138. Available at: <https://doi.org/10.3390/v12020138>.

Premkumar, M. *et al.* (2019) 'A/H1N1/09 Influenza is Associated With High Mortality in Liver Cirrhosis', *Journal of Clinical and Experimental Hepatology*, 9(2), pp. 162–170. Available at: <https://doi.org/10.1016/j.jceh.2018.04.006>.

Schillie, S. *et al.* (2013) 'CDC guidance for evaluating health-care personnel for hepatitis B virus protection and for administering postexposure management', *MMWR. Recommendations and reports: Morbidity and mortality weekly report. Recommendations and reports*, 62(RR-10), pp. 1–19.

Schulte-Schrepping, J. *et al.* (2020) 'Severe COVID-19 Is Marked by a Dysregulated Myeloid Cell Compartment', *Cell*, 182(6), pp. 1419-1440.e23. Available at: <https://doi.org/10.1016/j.cell.2020.08.001>.

See, K.C. (2022) 'Vaccination for the Prevention of Infection among Immunocompromised Patients: A Concise Review of Recent Systematic Reviews', *Vaccines*, 10(5), p. 800. Available at: <https://doi.org/10.3390/vaccines10050800>.

Shan, D. *et al.* (2021) 'N-protein presents early in blood, dried blood and saliva during asymptomatic and symptomatic SARS-CoV-2 infection', *Nature Communications*, 12(1), p. 1931. Available at: <https://doi.org/10.1038/s41467-021-22072-9>.

Sharma, N.C. *et al.* (2019) 'Diphtheria', *Nature Reviews Disease Primers*, 5(1), pp. 1–18. Available at: <https://doi.org/10.1038/s41572-019-0131-y>.

Sun, K. *et al.* (2020) 'Atlas of ACE2 gene expression reveals novel insights into transmission of SARS-CoV-2', *Heliyon*, 7(1), p. e05850. Available at: <https://doi.org/10.1016/j.heliyon.2020.e05850>.

Vijenthira, A. *et al.* (2021) 'Vaccine response following anti-CD20 therapy: a systematic review and meta-analysis of 905 patients', *Blood Advances*, 5(12), pp. 2624–2643. Available at: <https://doi.org/10.1182/bloodadvances.2021004629>.

Wang, J. *et al.* (2020) 'Cytokine storm and leukocyte changes in mild versus severe SARS-CoV-2 infection: Review of 3939 COVID-19 patients in China and emerging pathogenesis and therapy concepts', *Journal of Leukocyte Biology*, 108(1), pp. 17–41. Available at: <https://doi.org/10.1002/JLB.3COVR0520-272R>.

WHO Coronavirus (COVID-19) Dashboard (2023). Available at: <https://covid19.who.int> (Accessed: 23 August 2023).

Wiedermann, U., Garner-Spitzer, E. and Wagner, A. (2016) 'Primary vaccine failure to routine vaccines: Why and what to do?', *Human Vaccines & Immunotherapeutics*, 12(1), pp. 239–243. Available at: <https://doi.org/10.1080/21645515.2015.1093263>.

Wiersinga, W.J. *et al.* (2020) 'Pathophysiology, Transmission, Diagnosis, and Treatment of Coronavirus Disease 2019 (COVID-19): A Review', *JAMA*, 324(8), pp. 782–793. Available at: <https://doi.org/10.1001/jama.2020.12839>.

Wilk, A.J. *et al.* (2020) 'A single-cell atlas of the peripheral immune response in patients with severe COVID-19', *Nature Medicine*, 26(7), pp. 1070–1076. Available at: <https://doi.org/10.1038/s41591-020-0944-y>.

Wu, F. *et al.* (2020) 'A new coronavirus associated with human respiratory disease in China', *Nature*, 579(7798), pp. 265–269. Available at: <https://doi.org/10.1038/s41586-020-2008-3>.

Zhang, Z., Shen, Q. and Chang, H. (2022) 'Vaccines for COVID-19: A Systematic Review of Immunogenicity, Current Development, and Future Prospects', *Frontiers in Immunology*, 13. Available at: <https://www.frontiersin.org/articles/10.3389/fimmu.2022.843928> (Accessed: 15 August 2023).

Zhou, Y. *et al.* (2020) 'Pathogenic T-cells and inflammatory monocytes incite inflammatory storms in severe COVID-19 patients', *National Science Review*, 7(6), pp. 998–1002. Available at: <https://doi.org/10.1093/nsr/nwaa041>.

Zhu, F.-C. *et al.* (2020) 'Safety, tolerability, and immunogenicity of a recombinant adenovirus type-5 vectored COVID-19 vaccine: a dose-escalation, open-label, non-randomised, first-in-human trial', *The Lancet*, 395(10240), pp. 1845–1854. Available at: [https://doi.org/10.1016/S0140-6736\(20\)31208-3](https://doi.org/10.1016/S0140-6736(20)31208-3).






3 Publications

- 3.1 Publication 1: Comparative Analysis of Antibody Titers against the Spike Protein of SARS-CoV-2 Variants in Infected Patient Cohorts and Diverse Vaccination Regimes



Article

Comparative Analysis of Antibody Titers against the Spike Protein of SARS-CoV-2 Variants in Infected Patient Cohorts and Diverse Vaccination Regimes

Alexandru Odainic ^{1,2,†}, Jasper Spitzer ^{1,†} , Jennifer Barbara Szlapa ³, Simon Schade ¹, Tim Jonas Krämer ¹, Jakob Neuberger ¹, Christian Bode ⁴ , Folkert Steinhagen ⁴, Ricarda Maria Schmithausen ⁵ , Gero Wilbring ⁵, Esther Sib ⁵, Nico Tom Mutters ⁵, Frederik Rabenschlag ⁶, Lisa Kettel ⁶, Maike Woznitza ⁶, Kathrin van Bremen ⁷, Tina Peers ⁸, Gez Medinger ⁹, Anushka Kudaliyanage ¹, Maike Kreutzenbeck ¹, Ulrike Strube ¹, Joseph M. Johnson ¹⁰, Dawn Mattoon ¹⁰, Andrew J. Ball ¹⁰ , Stefan Scory ¹¹, Richard McGuire ¹¹, Christian Putensen ⁴, Zeinab Abdullah ³, Catharina Latz ^{12,‡}  and Susanne Viktoria Schmidt ^{1,*,‡}

¹ Institute of Innate Immunity, University Hospital Bonn, 53127 Bonn, Germany

² Department of Microbiology and Immunology, The Peter Doherty Institute for Infection & Immunity, University of Melbourne, Melbourne, VIC 3010, Australia

³ Institute of Experimental Immunology, University Hospital Bonn, 53127 Bonn, Germany

⁴ Department of Anesthesiology and Intensive Care Medicine, University Hospital Bonn, 53127 Bonn, Germany

⁵ Institute for Hygiene and Public Health, University Hospital Bonn, 53127 Bonn, Germany

⁶ Medical Corps of the German Armed Forces, German Armed Forces Central Hospital, 56072 Koblenz, Germany

⁷ Department of Internal Medicine I, University Hospital Bonn, 53127 Bonn, Germany

⁸ Clare Park Hospital, Farnham GU10 5XX, UK

⁹ Department of Paramedic Science, School of Health and Social Work, University of Hertfordshire, Hatfield AL10 9AB, UK

¹⁰ Quanterix Corporation, Billerica, MA 01821, USA

¹¹ Meso Scale Diagnostics, Rockville, MD 20850, USA

¹² Dardenne Eye Hospital, 53177 Bonn, Germany

* Correspondence: susanne.schmidt@uni-bonn.de

† These shared first-authors contributed equally to this work.

‡ These shared last-authors contributed equally to this work.



Citation: Odainic, A.; Spitzer, J.; Szlapa, J.B.; Schade, S.; Krämer, T.J.; Neuberger, J.; Bode, C.; Steinhagen, F.; Schmithausen, R.M.; Wilbring, G.; et al. Comparative Analysis of Antibody Titers against the Spike Protein of SARS-CoV-2 Variants in Infected Patient Cohorts and Diverse Vaccination Regimes. *Int. J. Mol. Sci.* **2022**, *23*, 12231. <https://doi.org/10.3390/ijms232012231>

Academic Editors: Jeffrey L. Platt, Manlio Ferrarini and Vincenzo Barnaba

Received: 23 September 2022

Accepted: 11 October 2022

Published: 13 October 2022

Publisher's Note: MDPI stays neutral with regard to jurisdictional claims in published maps and institutional affiliations.



Copyright: © 2022 by the authors. Licensee MDPI, Basel, Switzerland. This article is an open access article distributed under the terms and conditions of the Creative Commons Attribution (CC BY) license (<https://creativecommons.org/licenses/by/4.0/>).

Abstract: The presence of neutralizing antibodies against SARS-CoV-2 correlates with protection against infection and severe COVID-19 disease courses. Understanding the dynamics of antibody development against the SARS-CoV-2 virus is important for recommendations on vaccination strategies and on control of the COVID-19 pandemic. This study investigates the dynamics and extent of α -Spike-Ab development by different vaccines manufactured by Johnson & Johnson, AstraZeneca, Pfizer-BioNTech and Moderna. On day 1 after vaccination, we observed a temporal low-grade inflammatory response. α -Spike-Ab titers were reduced after six months of vaccination with mRNA vaccines and increased 14 days after booster vaccinations to a maximum that exceeded titers from mild and critical COVID-19 and Long-COVID patients. Within the group of critical COVID-19 patients, we observed a trend for lower α -Spike-Ab titers in the group of patients who survived COVID-19. This trend accompanied higher numbers of pro-B cells, fewer mature B cells and a higher frequency of T follicular helper cells. Finally, we present data demonstrating that past infection with mild COVID-19 does not lead to long-term increased Ab titers and that even the group of previously infected SARS-CoV-2 patients benefit from a vaccination six months after the infection.

Keywords: antibody response; SARS-CoV-2; vaccination; inflammation; Long-COVID; lymphocytes

1. Introduction

In December 2019, a new coronavirus named SARS-CoV-2 spread from China, leading to a worldwide pandemic [1]. According to the World Health Organization, multiple

SARS-CoV-2 variants of interest and concern, among them B.1.617.2 (Delta) and the latest B.1.1.529 (Omicron) [2] led to up to 594 million registered cases through August 2022 [3]. Up to the beginning of April 2022, it caused over 6 million deaths by an acute respiratory distress syndrome (ARDS) and associated complications, as all organs are affected by SARS-CoV-2 infection. Viral clearance by the host's immune system is essential to restrain viral infections and maintain the host's cellular homeostasis. Cells of the innate immune system recognize viruses via extra- and intracellular PRRs (pattern recognition receptors). These, in turn, activate immune-defensive signaling cascades via inflammasome activation and secretion of inflammatory cytokines such as IL1 α , IL6 and IFN γ (summarized by Diamond and Kanneganti [4]). In severe and critical COVID-19 cases with a poor outcome, hyperinflammation is observed. This hyperinflammation is caused by a dysregulated cytokine release from infected cells and/or subsequent activated immune cells (neutrophils, tissue-resident macrophages, peripheral monocytes and T cells) [5]. Therefore, the staple of treatment for hospitalized patients consists of corticosteroids and non-steroidal anti-inflammatory drugs (NSAR), antibodies (Ab) against the IL6 receptor or inhibitors of inflammatory cytokine-driven signaling cascades [6–8].

Binding of the Spike (S)-protein—a part of the viral capsid—to the host's ACE2 expressing cells allows SARS-CoV-2 to enter human cells [9,10]. The innate immune system responds to the SARS-CoV-2 infection with opsonizing and neutralizing antibodies secreted by B cells, which are taught by antigen-specific T cells. IgG and IgM antibodies usually develop roughly two weeks after symptom onset, with 100% of patients achieving seroconversion after 20 days [11]. The generation of neutralizing antibodies in patients with recovered SARS-CoV-2 infection correlated to the presence of CD134⁺CD25⁺ positive circulating follicular T helper cells and class-switched CD19⁺IgD⁻ B cells specific for the S-protein [12]. At the time of publication, the WHO lists over 300 vaccine projects. The intent is to raise specific Ab titers, thereby preventing the viral transmission and reducing the likelihood of severe and critical COVID-19 disease courses. At the beginning of 2020, only one year after the pandemic emerged, two forms of novel vaccines (mRNA- and vector-based) were approved for use in Europe. Initially, one dose of the vector-based vaccine from Johnson & Johnson (COVID-19 Vaccine Janssen[®]; [13]) and two doses of AstraZeneca (Vaxzevria[®]; [14,15]) were considered sufficient to achieve a primary immunization. Subsequently, a booster with an mRNA-based vaccine was recommended [16]. Both vaccines use a recombinant, replication-incompetent vector of the human adenovirus type Ad26 (Johnson & Johnson, JJ) or chimpanzee adenoviral vector ChAdOx1 (AstraZeneca, AZ, Cambridge, UK), which carries the genetic information for the S-protein of SARS-CoV-2. The general recommended vaccination scheme [17,18] for mRNA-based vaccines from Moderna (Spikevax [19]) or Pfizer–BioNTech (Comirnaty [20]) includes two inoculations with a temporal difference of 4 to 8 weeks and a recommended booster after six months. Both vaccines use mRNA transcripts which encode the full-length Spike protein with a transmembrane anchor and an intact S1–S2 cleavage site [21]. The presence of plasmablasts and germinal B-cell responses, including cross-reactive memory B cells, provides a robust humoral immunity against SARS-CoV-2 after vaccination [22].

The herein-delineated study investigates the dynamics of α -Spike-Ab (α -Spike-Ab) titers in SARS-CoV-2-infected patients with different disease outcomes and diverse vaccination cohorts over a time frame of up to one year. We quantified cytokines, markers for neuroinflammation and phenotypes of B and T cell populations longitudinally via flow cytometry. Infection with SARS-CoV-2 induced S-protein specific antibodies within one week. These Ab titers were significantly reduced after six months. Ab titers after vaccination followed a similar time course, independent of the vaccine. Our data support the current recommendation to boost every 6th or 7th month to maintain a sufficient Ab concentration in the peripheral blood. Our study further demonstrates that recovered COVID-19 patients benefit from booster vaccinations.

2. Results

2.1. *A-Spike-Ab Titers Differ with Disease Severity of COVID-19 and Correlate to Elevated Numbers of Class-Switched B Cells and Tfh Cells*

2.1.1. Mild Cohort

We analyzed Ab development in the initial stage of SARS-CoV-2 infection, its persistence throughout hospitalization and the duration of Ab presence over a period of up to 12 months in three independent cohorts (Figure 1A). Patients of similar age (mean_{yr}: Controls = 57, Mild = 54, Critical = 63; Supplementary Figure S1A) and with comparable systemic diseases such as hypertension (21–41%) and diabetes (7–12%) served as controls. We observed equal sex ratios in all cohorts, except for the critically ill patients. Male patients were overrepresented (88%) in this group—a phenomenon described early on during the first year of the SARS-CoV-2 pandemic [23].

We analyzed the development of α -Spike-Ab (Wuhan variant) in the early stages of the infection in 15 patients with mild COVID-19 disease. This group of patients did not need medical attention and recovered from the infection at home. Blood samples were collected at multiple timepoints during the first eight days and on day 15 after enrolment into the study (Figure 1B). As the onset of infection cannot be defined precisely in most cases, we quantified the patients' highest serum level for SARS-CoV-2 Nucleoprotein (N-protein). The day of the highest concentration of N-protein in serum of SARS-CoV-2-infected patients was set as t_0 and this enabled us to harmonize the analysis for the complete cohort [24]. The samples collected at preceding timepoints were designated t_{-1} and t_{-2} , whereas timepoints following t_0 were set as t_{1-4} . The onset of infection is presumed to be up to 8 days before t_0 . Concentrations of α -Spike-Ab started to increase after one-to-three days (t_1) of infection. They became significantly upregulated from day seven on after t_0 (t_2 , Figure 1B). N-protein levels showed an opposite trend, which we interpret as a sign of viral clearance as demonstrated by us before [24]. Titers of α -Spike-Ab against the alpha-, beta- and gamma-variant of SARS-CoV-2 were quantified (Supplementary Figure S1B,C). Low titers of specific α -Spike-Ab against the respective SARS-CoV-2 variants were observed at t_2 (Supplementary Figure S1B). Moreover, rising α -Spike-Ab titers (Wuhan variant) resulted in increasing differences in variant immunity (t_2 and t_3 , Supplementary Figure S1C). To enable the comparison between the antibody response against the different virus strains, we plotted their respective concentration reduction when compared to the Wuhan strain in percent: for example, Ab concentrations against the Spike protein of the alpha (17%), beta (51%) or gamma (50%) variant were lower than α -Spike-Ab concentrations against the Wuhan variant at t_2 (Supplementary Figure S1C).

To investigate the dynamics of B and CD4⁺ T cells contributing to the humoral immune responses in SARS-CoV-2 infected patients, we performed flow cytometry analysis for different B cell subpopulations and T follicular helper cells (Tfh) in the peripheral blood of the different groups. In comparison to the control group, SARS-CoV-2-infected patients showed higher percentages of pro-B cells (mean and SEM for Ctrl: $33 \pm 3\%$; Mild _{t_0} : $93 \pm 1\%$), especially at t_0 of infection (Supplementary Figure S1D). The percentage of mature B cells was decreased at t_0 (mean and SEM for Ctrl: $53 \pm 4\%$; Mild _{t_0} : $3 \pm 0\%$) whereas the percentage of immature B cells increased from t_0 on (mean and SEM for Mild _{t_0} : $3 \pm 1\%$; Mild _{t_2} : $7 \pm 2\%$). Significantly elevated numbers of IgD⁻CD38^{low}CD27⁺ class-switched B cells (Ctrl: 58 (52–64)%; Mild _{t_2} : 78 (73–80)%; Figure 1C) correlated with increased concentrations of α -Spike-Ab after 7 days (t_2) after the onset of infection (t_2 , $p = 0.01$, $r = 0.59$). In contrast, no significant changes were detected for non-class-switched B cells (IgD⁺CD38^{low}CD27⁺) (median, interquartile range for Ctrl: 10 (6–16)%; Mild _{t_2} : 9 (9–10)%; Supplementary Figure S1E). Furthermore, percentages of CD4⁺CXCR5⁺CD3⁺ Tfh cells, required for the differentiation of the Ab production by plasma cells, were elevated in the SARS-CoV-2 infection in comparison to numbers detected in uninfected controls (median, interquartile range for Ctrl: 7 (6–9)%; Mild _{t_2-t_3} : 32–51%; Figure S1D).

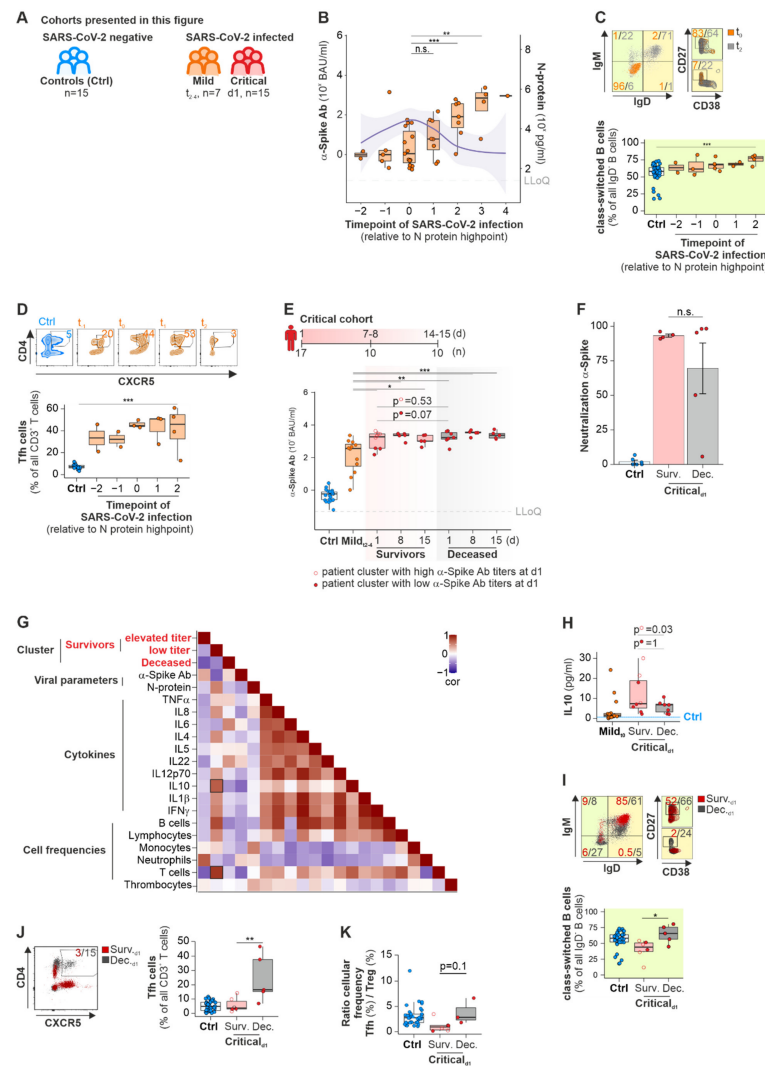


Figure 1. Dynamics of Ab titers against Wuhan SARS-CoV-2 Spike-protein in different COVID-19 disease stages in correlation of B and T cell maturation. **(A)** Scheme of patient cohorts and number of patients. **(B)** Development of α -Spike-Ab titers in SARS-CoV-2 infected patients with a mild disease course harmonized to the timepoint of highest N-protein concentrations (t_0) in sera. The shaded area indicates the 95% confidence interval of N-protein concentrations. **(C)** Representative dot plot (upper panel) and summarized box plot (lower panel) of B cells (C) in patients with mild SARS-CoV-2 disease course. **(D)** Representative contour plots (left panel) and summarized boxplot (right panel) of T follicular helper cells in mildly ill COVID-19 patients. **(E)** Titers of Wuhan α -Spike-Ab concentrations in sera of patients with a critical COVID-19 disease course; non-filled points show the cluster of patients with an increased Ab titer. **(F)** Neutralization capacity of the antibodies against the RBD of Spike protein in healthy non-vaccinated controls and critically ill patients. **(G)** Correlation plot of selected parameters of patients with a critical disease course on day 1 showing Pearson correlation. Bordered squares show significant correlations. **(H)** IL10 titers in sera of patients with critical disease course. **(I)** Flow cytometry data corresponding to **(D)** applied to the critical cohort; non-filled points show cluster of patients with increased Ab titer. **(J)** Representative dot plot (left panel) and quantitative boxplot (right panel) of T follicular helper cells in patients with a critical SARS-CoV-2 course; non-filled points show cluster of patients with increased Ab titer. **(K)** Ratio of the frequencies of T follicular helper cells to T regulatory cells ($CD3^+CD4^+CD25^{\text{high}}CD127^-$); non-filled points show cluster of patients with increased Ab titer. Ctrl denotes a cohort of patients with similar symptoms but without a positive SARS-CoV-2 test. Blue line, mean concentration in healthy Ctrl; blue dashed line, 95% confidence interval; LLoQ, Lower Level of Quantification; Mann-Whitney U test, un-adjusted p -value (B, C, E, G, H, I, J); * p Val < 0.05, ** p Val < 0.01, *** p Val < 0.001.

2.1.2. Critical Cohort

To investigate whether α -Spike-Ab concentrations between mild and critical COVID-19 patients differ and hypothetically could predict the severe forms of COVID-19, titers of α -Spike-Ab were monitored from admission to the ICU until discharge from the hospital, death, or at least up to 15 days of hospitalization (Figure 1E). There was a significant difference in α -Spike-Ab concentrations between mild and critically infected COVID-19 patients who died from SARS-CoV-2 infection ($p_{d1} = 0.005$, $p_{d8} = 0.0006$, $p_{d15} = 0.001$, Figure 1E) and those patients who survived COVID-19 ($p_{d1} = 0.04$, $p_{d8} = 0.004$, $p_{d15} = 0.03$, Figure 1E). Similar to patients with mild forms of COVID-19, Ab titers for the alpha-, beta- and gamma variant of SARS-CoV-2 in patients with critical SARS-CoV-2 infection were reduced in comparison to α -Spike-Ab against the original Wuhan variant (Supplementary Figure S1F). Comparing the α -Spike-Ab concentrations between survivors and deceased patients, we did not find any significant differences over the duration of study (Figure 1E). Following the hypothesis that severe disease courses with poor outcome might be linked to low affinity of IgG antibodies against the Receptor Binding Domain of the Spike protein of SARS-CoV-2, we performed neutralization assays against the initial strain as well as alpha, beta and gamma variants of concern. In this assay, neutralizing antibodies in the sera of COVID-19 patients compete with human ACE2 protein standard for binding to SARS-CoV-2 RBD antigens (Wuhan, alpha, beta and gamma strains) immobilized on the plate surface. In contrast to the neglectable presence of neutralizing antibodies in the control group (mean and SEM for Ctrl Wuhan: $2 \pm 1\%$; alpha: $3 \pm 1\%$; beta: $3 \pm 2\%$; gamma: $10 \pm 2\%$), specific neutralizing antibodies were found in the group of severe COVID-19 patients with variable neutralizing capacity against four SARS-CoV-2 variants (Figure 1F, Supplementary Figure S1G). The neutralizing capacities varied not only between the virus strains, but also between the survivor and deceased patients, yet these differences were found to be not significant (mean and SEM for Wuhan Surv.: $93 \pm 1\%$, Dec.: $70 \pm 18\%$; alpha Surv.: $86 \pm 3\%$, Dec.: $65 \pm 18\%$; beta Surv.: $45 \pm 6\%$, Dec.: $36 \pm 15\%$; gamma Surv.: $59 \pm 6\%$, Dec.: $47 \pm 14\%$). Independent of the disease outcome, the capacity to neutralize SARS-CoV-2 Spike-RBD of the beta variant was the lowest among the analyzed strains (Supplementary Figure S1G). As observed by Garcia-Beltran et al. [25], the titers of α -Spike-RBD-Ab correlated positively to its percent of neutralization capacity of RBD-specific antibodies against the four tested SARS-CoV-2 variants (Supplementary Figure S1H). For the survivor group, we observed a separation into either high or low α -Spike-Ab titers at d1 of admission to the ICU ward. This was independent of the viral load, as we did not observe any differences in the N-protein concentrations in these patients' sera. In contrast, all patients in the deceased group showed high α -Spike-Ab throughout hospitalization. By Pearson correlation analysis, we integrated additional data on cytokine concentrations and blood immune cell frequencies of critically ill patients to investigate if the low α -Spike-Ab titers of COVID-19 survivors correlated to deviations in the immune response. The anti-inflammatory cytokine IL10 and the T cell counts correlate positively to low α -Spike-Ab titers of COVID-19 survivors (Figure 1G,H). Not distinguishing patient clusters, critically ill patients who survived the SARS-CoV-2 infection showed a trend to higher IL10 concentrations ($p = 0.28$, Figure 1H). This tendency for higher IL10 serum concentrations became significant when distinguishing the group of survivors by the α -Spike-Ab titer: Higher α -Spike-Ab titers correlated positively with high IL10 concentrations. Critically ill COVID-19 patients who died from SARS-CoV-2 infection showed a decreased frequency of mature B cells in the blood on the day of admission to the ICU (Supplementary Figure S1I), but higher frequencies of pro B cells (mean and SEM for Ctrl: $33 \pm 3\%$; Surv.: $17 \pm 3\%$; Dec.: $58 \pm 12\%$). The percentage of immature B cells was lower in the uninfected controls compared to deceased or survivors with similar rates (mean and SEM for Ctrl: $3 \pm 0\%$; Surv.: $15 \pm 6\%$; Dec.: $10 \pm 4\%$). Of note, deceased patients showed higher percentages of class-switched memory B cells compared to those who survived the infection (median, interquartile range for Surv.: 44 (37–51)%; Dec.: 66 (57–76%); Figure 1I). Yet, no significant differences were found for class-switched memory B cell frequencies between survivors

with high and low α -Spike-Ab titers ($p = 0.8$). Similar observations were made for Tfh cells (median, interquartile range for Surv.: 4 (3–10)%; Dec.: 17 (15–38)%; Figure 1J). In contrast, no significant differences in percentages of non-class switched B cells were observed (median, interquartile range for Surv.: 8 (5–12)%; Dec.: 8 (4–24)%; Supplementary Figure S1J). The ratio of Tfh and Treg cell frequencies indicates an ongoing inflammatory immune response and autoimmune diseases [26]. We observed that patients with a critical disease course who died from the infection had a 3.2-fold elevated ratio of Tfh/Treg cells compared to those who survived (Figure 1K). This observation was independent of the differences of α -Spike-Ab titers found in the group of survivors, which we interpret as part of a dysregulated immune response fostered on different levels, like lack of anti-inflammatory cytokines, like IL10 and dysregulation of Treg cells. Previously, a low ratio between IFN γ and IL10 has been associated with viral infection [27]. Calculating the IFN γ /IL10 ratio for critical patients, we did not observe any differences between non-infected control participants and critical patients who survived or died from SARS-CoV-2 infection. Therefore, we conclude that the usage of the IFN γ /IL10 ratio as a predictive marker for life-threatening SARS-CoV-2 outcomes is not adequate.

2.1.3. Long COVID

Neurath et al. [28] hypothesized a persistence of SARS-CoV-2 in unknown reservoirs after an acute, cured infection, causing an ongoing form of low-grade inflammation and/or neuronal damage. We asked: Does an ongoing immune response, as seen by a continuous production of antibodies against the Spike protein and production of cytokines by immune cells, could contribute to the development of Long-COVID? Our cohort of 20 Long-COVID patients suffered from long-term complications such as fatigue, tachycardia or high blood pressure (summarized under “cardiovascular system”), headaches and insomnia. (Figure 2A, Supplementary Figure S2A,B). We age-matched these Long-COVID patients with patients suffering from comparable symptoms (LC control, mean_{yrs}: 40; Long-COVID, mean_{yrs} = 39; Supplementary Figure S2A,B). Ab titers against Spike protein of different SARS-CoV-2 variants in Long-COVID patients were elevated up to eight months after infection and decreased over the observation period of 12 months (Figure 2B, Supplementary Figure S2C). In contrast, α -Spike-Ab concentrations in sera of LC controls were reduced 392-fold compared to Long-COVID_{0–4 m} (median, interquartile range for LC controls: 1 (1–39) BAU/mL; Long-COVID_{0–4 m}: 444 (278–600) BAU/mL) and did not differ in α -Spike-Ab titers to healthy-aged matched controls (median, interquartile range for Ctrl: 1 (0–1) BAU/mL), which further supports the lack of infection with SARS-CoV-2 in this control group (Figure 2B). Despite elevated α -Spike-Ab titers, we did not detect any SARS-CoV-2 N-protein in LC patients (means for Long-COVID_{0–12 m}: 594 pg/mL; LC control: 477 pg/mL; Figure 2C) in comparison to acutely infected patients (means for Mild_{t2–4}: 1072 pg/mL; Critical_{d1}: 6927 pg/mL). We tested the serum samples for classical inflammatory and anti-inflammatory cytokines as systemic markers for a prolonged immune response, and observed a trend for slightly elevated cytokine levels for IL8, TNF α , IL6, IL12p70, IL10, IL5 and IL4 in the first four months after the infection (Figure 2D). IL12p70 was significantly elevated in Long-COVID patients up to 4 months after infection (means for LC control: 0.00 pg/mL; Long-COVID_{0–4 m}: 0.13 pg/mL; Supplementary Figure S2D). Four months after the infection and later, we found significantly increased IL10 concentrations (means for Long-COVID_{0–4 m}: 0.84 pg/mL; Long-COVID_{4–8 m}: 0.38 pg/mL; Figure 2E). Further, we tested the serum for markers of neuroinflammation and -degeneration. There were no significant differences in A β 40, A β 42, GFAP and NF-light concentrations between the LC and LC controls (Supplementary Figure S2E). Therefore, we could not correlate neuroinflammation and -degeneration to Long-COVID symptoms.

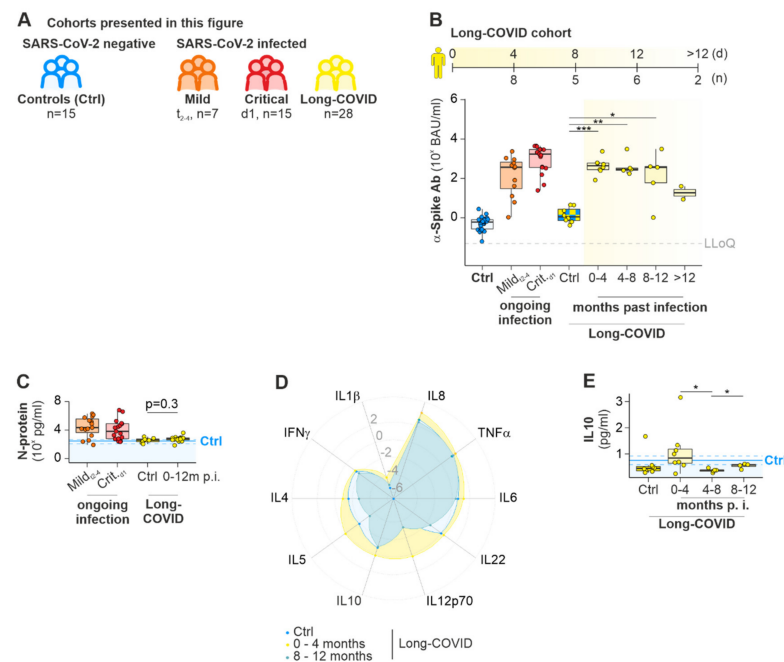


Figure 2. Dynamics of Ab titers against Wuhan SARS-CoV-2 Spike-protein and cytokines in Long-COVID. (A) Scheme of patient cohorts presented in the figure. (B) Comparison of α -Spike-Ab titers of included Long-COVID volunteers after various timepoints of infection to healthy controls, patients with a mild and critical COVID-19 disease course, as well as Long-COVID controls. (B–E) Characterization of the Long-COVID cohort by α -Wuhan-Spike-Ab (B), N-protein (C), normalized cytokine titers in a radar plot (D), and IL10 titers (E). Ctrl denotes a cohort of patients with similar symptoms but without a positive SARS-CoV-2 test. Blue line, mean concentration in healthy Ctrl; blue dashed line, 95% confidence interval; LLoQ, Lower Level of Quantification; Mann-Whitney U test; * p Val < 0.05, ** p Val < 0.01, *** p Val < 0.001.

In summary, we demonstrate that class-switched memory B cells increase from day seven after infection together with rising α -Spike-Ab titers. We observed that patients with mild symptoms, critically ill patients as well as Long-COVID patients, display comparable levels of α -Spike-Ab titers. Critically ill patients who survived COVID-19 and Long-COVID patients showed elevated levels of the anti-inflammatory cytokine IL10, which was independent of N-protein levels. In contrast, patients who died from SARS-CoV-2 infection showed reduced IL10 levels as well as a higher percentage of class-switched memory B cells and Tfh cells. The ratio for the cellular frequency of Tfh/Treg was elevated. This could indicate the induction of an autoimmune response by SARS-CoV-2 in those critically ill patients who died from the disease.

2.2. mRNA-Based COVID-19 Vaccines Lead to a Temporal Immunity against SARS-CoV-2

From December 2020 on, three COVID-19 vaccines were available in Europe: the vector-based vaccine ChAdOx1nCoV-19 by AstraZeneca (AZ), and two mRNA-based vaccines by Pfizer–BioNTech (BT) and Moderna (MO). We recruited 76 volunteers for three representative cohorts with slightly different vaccination strategies (Figure 3A, Supplementary Figure S3A) to study the timing and amount of α -Spike-Ab developed in response to each vaccination. After the first inoculation with AZ, titers of α -Spike-Ab against the Wuhan and to a lesser extent alpha-, beta- and gamma SARS-CoV-2 variants were increased and comparable to levels of patients with an ongoing SARS-CoV-2 infection (Figure 3B, Supplementary Figure S3B). Participants reported adverse events like, fever, chills, head and body aches. These flu-like symptoms are hypothetically caused by an activation of the immune system, leading to the production of pro- and anti-inflammatory cytokines. We quantified 10 classical cytokines participating in immune responses in the blood of AZ vaccinated participants 14 days after the first inoculation. IFN γ was the only investigated cytokine that increased significantly with AZ (means for Ctrl: 0.04 pg/mL; 1st

AZ: 0.44 pg/mL; Figure 3C,D). IFN γ is released by CD4⁺ T_H1 cells. Its serum levels can serve as an indicator for the induction of a broad T-cell response against the S antigen, as observed before for other replication-deficient adenoviral vectors [29].

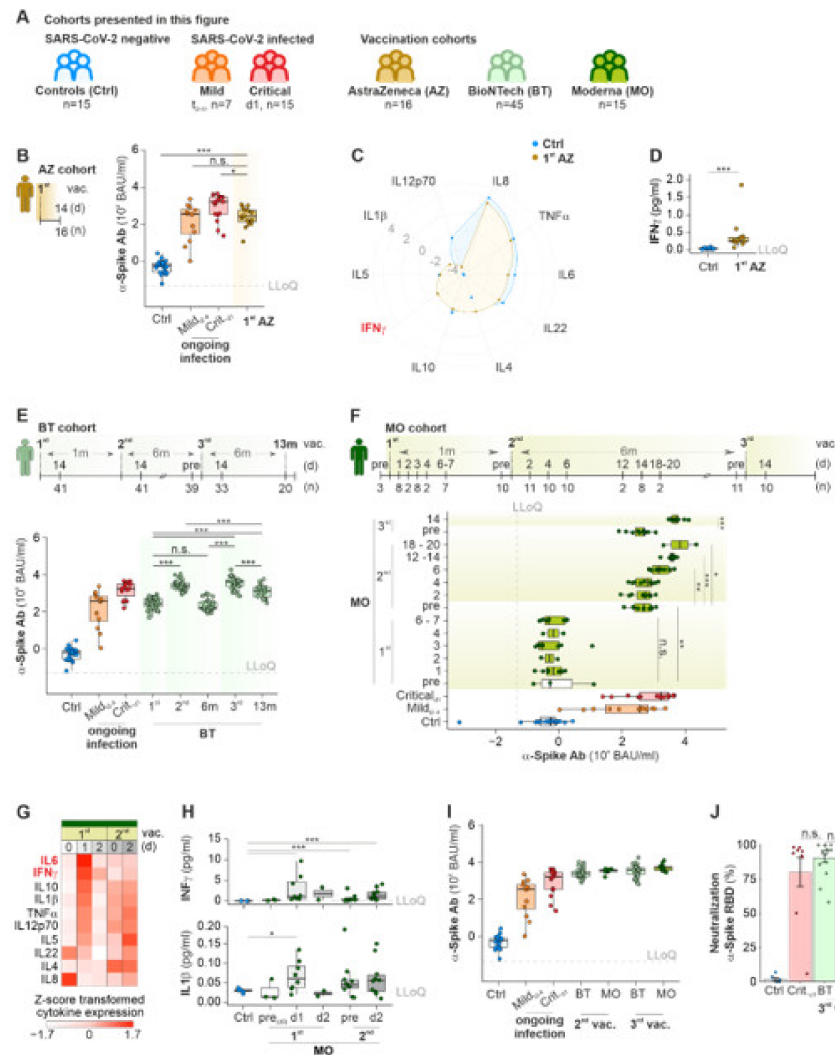


Figure 3. Dynamics of Ab titers against Wuhan SARS-CoV-2 Spike-protein in different vaccination regimens. (A) Scheme of vaccination cohorts and groups of SARS-CoV-2 infected patients. (B–D) Concentrations of α -Spike-Ab (B), cytokines (C) including IFN γ (D) in sera of participants 14 d after vaccination with AZ. (E,F) Scheme of vaccination strategy and longitudinal analysis of α -Spike-Ab titers in participants multiple times vaccinated with BT (E) or MO (F). (G) Heatmap of Z-score transformed cytokine concentrations in blood of participants vaccinated with MO before and shortly after the vaccination. (H) Cytokine concentrations for IFN γ (top) and IL1 β (bottom) before and after vaccination with MO. (I) Comparative analysis for α -Spike-Ab titers after multiple inoculations with mRNA vaccines. (J) Neutralization capacity of antibodies against α -Spike-RBD of SARS-CoV-2 in healthy non-vaccinated controls, critically ill COVID-19 patients, and vaccinated individuals with BT and MO six months after the second booster. LLoQ, Lower Level of Quantification; Mann–Whitney U test, un-adjusted p -value (A), adjusted p -value (B, E); * p Val < 0.05, ** p Val < 0.01, *** p Val < 0.001.

An initial vaccination with Comirnaty from Pfizer–BioNTech induced α -Spike-Ab titers in healthy participants comparable to COVID-19 patients with ongoing SARS-CoV-2 infection at early time points (medians for Mild_{t₂₋₄}: 369 BAU/mL; 1st BT: 272 BAU/mL; Figure 3E). Similar to the AZ-vaccination and active ongoing SARS-CoV-2 infections, α -Spike-Ab titers against SARS-CoV-2 variants were reduced by up to 50% (Supplementary Figure S3C). The second vaccination with BT led to a significant booster effect with increased concentrations

of α -Spike-Ab (median for 2nd BT: 2488 BAU/mL); albeit, the booster effect did not last very long: 6 months after the booster vaccination, α -Spike-Ab titers were reduced to levels lower than 2 weeks after the initial vaccination (median for BT_{6m}: 164 BAU/mL). A third vaccination was able to restore and moreover increase the α -Spike-Ab titers even beyond the concentrations achieved 14 days after the second vaccination with BT (median for 3rd BT: 3920 BAU/mL). Six months after the third vaccination, titers for α -Spike-Ab returned to lower yet potent levels (median for BT^{13m}: 1283 BAU/mL).

We observed similar dynamics of α -Spike-Ab titers for mRNA-1273 (Spikevax[®]) from Moderna (MO). Six days after the initial vaccination with MO, α -Spike-Ab were not yet detectable (median for MO_{d6-7}: 0 BAU/mL; Figure 3F). Yet, after four weeks, titers of α -Spike-Ab against the Wuhan variant of SARS-CoV-2 and to a lesser extent to other variants (Supplementary Figure S3D) were increased. Six to 20 days after the booster, titers increased rapidly (medians for 2nd MO_{pre}: 483 BAU/mL; 2nd MO_{d18-20}: 12,221 BAU/mL). Comparable to BT, α -Spike-Ab titers were reduced to basal immunization titers 6 months after the booster (median for 3rd MO_{pre}: 484 BAU/mL). Yet, a third vaccination enabled the α -Spike-Ab titers to be elevated again to levels comparable to the titers after the second vaccination (median for 3rd MO_{d14}: 5001 BAU/mL). Participants vaccinated with MO reported flu-like symptoms, similar to volunteers vaccinated with AZ. To investigate, if vaccination with MO leads to an inflammatory response, the presence of pro- and anti-inflammatory cytokines was quantified in the sera of participants before, on days one and two after the first inoculation, and before and two days after the second vaccination with MO (Figure 3G). Inflammatory cytokines like IL6, IFN γ , IL1 β and TNF α were induced 24 h after the first inoculation (Supplementary Figure S3E), of which only IFN γ (medians for Ctrl: 0.03 pg/mL; 1st MO_{d1}: 1.16 pg/mL) and IL1 β (medians for Ctrl: 0.03 pg/mL; 1st MO_{d1}: 0.06 pg/mL) were significantly upregulated by the initial vaccination (Figure 3H). This pro-inflammatory immune response was short-lived as the concentrations of pro-inflammatory cytokines were reduced to control levels at d2 after vaccination. We did not detect any significant increase in cytokine levels following the second inoculation in comparison to levels before the initial vaccination (pre_{d0}).

There was neither significant difference between Ab titers induced by BT or MO components 14 days after the second and third vaccination nor between the test regimes at the chosen time point (Figure 3I). We completed our analysis on the efficiency of COVID-19 vaccines by studying the neutralization capacity of α -Spike-Ab induced by BT or MO vaccines, six months after the second booster vaccination (3rd vac). Antibodies in the serum of vaccinated participants showed similar neutralization of Spike RBD of the Wuhan and alpha variant to critically ill COVID-19 patients (Figure 3J, Supplementary Figure S3F). Despite the reduced number of data points for the MO test cohort, we observed a significant stronger neutralization against the Spike RBD of beta and gamma SARS-CoV-2 strains by the antibodies developed after BT vaccination (Supplementary Figure S3F).

It can be concluded that both mRNA-based vaccines show similar efficiencies in the induction of Ab titers against SARS-CoV-2 variants. Additionally, we observed decreasing Ab titers against the Spike protein over a period of six months after the inoculation for all herein-investigated mRNA vaccines.

2.3. Cross-Vaccination with Different COVID-19 Vaccines Does Not Exceed Ab Titers against Spike-Protein Achieved with Mono-Vaccine Usage

Due to vaccine shortage and adverse events, including cerebral vein thrombosis after COVID-19 vaccination (summarized by Jaiswal et al. [30]), recommendations on target groups for AZ, JJ, BT or MO were revised. At the time of writing this manuscript (August 2022), the German council for vaccines (STIKO, Robert Koch Institute (RKI), Berlin, Germany) recommended combining AZ as a first inoculation with mRNA-based COVID-19 vaccines as a booster or two vaccinations with AZ for citizens over the age of 60 [31]. In total, 3 healthy participants initially vaccinated twice with AZ followed by one inoculation with BT were included in the study (Figure 4A, Supplementary Figure S4A). As

established before, a single vaccination with AZ led to a significant increase of α -Spike-Ab concentrations against the original Wuhan strain but also to other SARS-CoV-2 variants (Figure 3B, Supplementary Figure S2B). A booster vaccination with BT up to 28 days after the 2nd AZ lead to a 13-fold increase in levels of α -Spike-Ab from d7 (medians for BT_{pre}: 181 BAU/mL; BT_{d7}: 3153 BAU/mL; Figure 4A). These levels were comparable to those of BT controls after two inoculations. Additionally, we investigated the α -Spike-Ab titers of four participants whose vaccination schemes followed a different recommendation of the German Council for vaccines (Figure 4B). These participants were inoculated once with AZ and twice with BT. Their α -Spike-Ab titers were compared to controls of participants who received in total three inoculations with BT. Due to the short time between the first and second BT vaccination (<8 weeks), α -Spike-Ab concentrations before the second BT vaccination were already elevated (median for 2nd BT_{pre}: 2781 BAU/mL) to comparable levels of participants who received two or three inoculations with BT only (medians for BT_{2nd}: 2488 BAU/mL; BT_{3rd}: 3920 BAU/mL). No further increase of α -Spike-Ab concentrations was observed up to 21 d after the second BT vaccination (2nd BT_{d21}: 3468 BAU/mL).

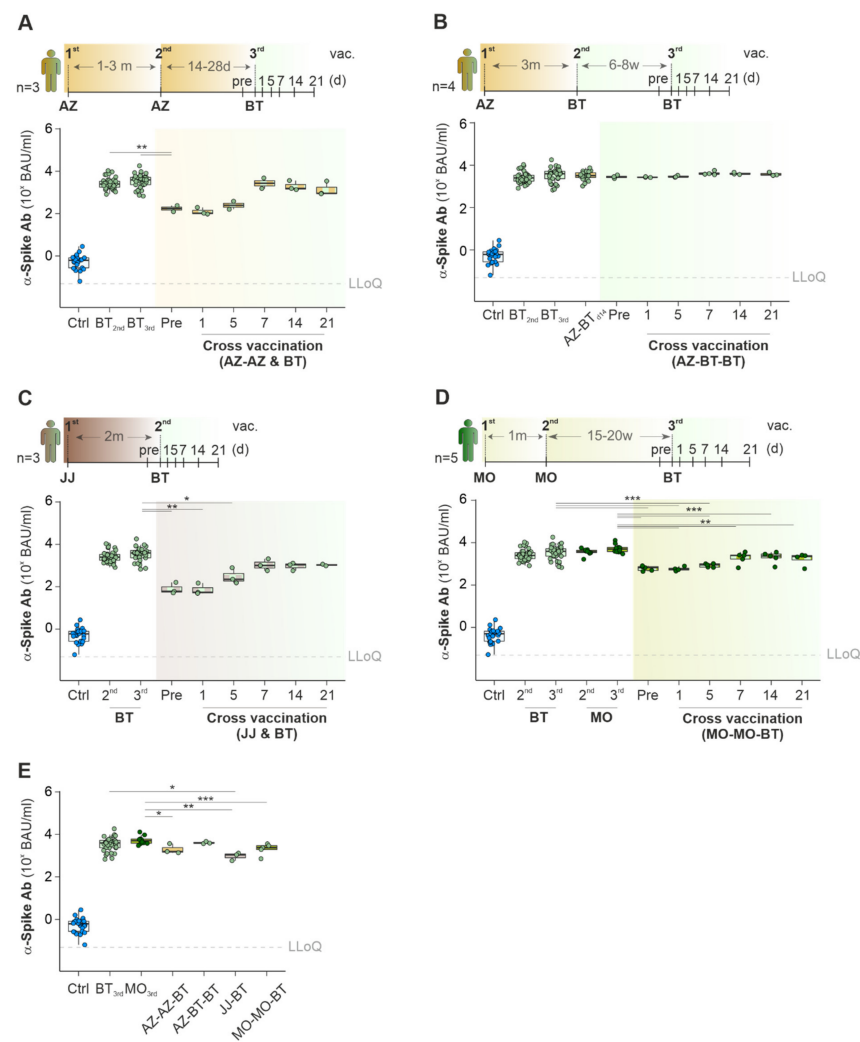


Figure 4. Comparative analysis of Ab titers against Wuhan SARS-CoV-2 Spike-protein in vaccination regimens with multiple vaccines. (A–E) Vaccination scheme (top) and concentrations of α -Spike-Ab over time (bottom) in cohorts vaccinated with various combinations (as indicated by the scheme) of AZ-AZ-BT (A), AZ-BT-BT (B), JJ-BT (C), and MO-MO-BT (D). (E) Comparison between the various vaccination schemes; LLoQ, Lower Level of Quantification; Man–Whitney U test, unadjusted p -value (A), adjusted p -value (C–E); * p Val < 0.05, ** p Val < 0.01, *** p Val < 0.001.

In contrast to the test group which followed the vaccination scheme AZ-BT-BT, three participants received only one inoculation with JJ. They showed significantly lower α -Spike-Ab titers after two months (median for JJ_{pre}: 61 BAU/mL; Figure 4C). One additional vaccination with BT increased the titers significantly to 1007 BAU/mL after seven days. These values were comparable to the BT controls (medians for BT_{2nd}: 2488 BAU/mL; BT_{3rd}: 3920 BAU/mL). In conclusion, participants vaccinated with a single JJ vaccination benefit from a booster vaccination with BT.

Finally, we observed that participants, who were initially vaccinated two times with MO and switched for the third vaccine to BT, did not benefit from this vaccination strategy (Figure 4D): their α -Spike-Ab titers were two-fold lower in comparison to participants who received three vaccinations with MO (medians for BT_{d14}: 2347 BAU/mL; MO_{3rd}: 5001 BAU/mL).

In summary, all investigated diverse vaccination strategies resulted in satisfactory α -Spike-Ab titers against Wuhan and other variants 14 days after the last booster (Figure 4E, Supplementary Figure S4B). Yet, we observed significant lower α -Spike-Ab titers between cohorts with a mixed vaccination scheme than the respective BT_{3rd} or MO_{3rd} controls.

2.4. Cured COVID-19 Patients Benefit from COVID-19 Vaccination from 6 Months on after the Infection

Infection with SARS-CoV-2 mounted a rapid generation of antibodies against the Spike protein during the initial phase of the immune response within the first seven days (Figure 1B). Data from Long-COVID patients showed that α -Spike-Ab titers started to diminish after eight months (Figure 1J). Moreover, they continued to decrease over a period of up to 12 months. To protect against re-infection with SARS-CoV-2, three patients with cured COVID-19 were inoculated twice with BT six months after SARS-CoV-2 infection (Figure 5A). These patients were categorized as healthy as they did not have any diagnosis of hypertension or diabetes, nor were they overweight (Figure 5B). Titers of α -Spike-Ab in sera of cured COVID-19 patients were significantly lower (median for 1st BT_{pre}: 148 BAU/mL; Figure 5C) 6 months after infection compared to titers of healthy volunteers vaccinated twice with BT (median for BT_{2nd}: 3488 BAU/mL). Interestingly, cured COVID-19 patients showed higher relative α -Spike-Ab titers against the alpha- and gamma-variant, similarly to patients with acute SARS-CoV-2 infection when contrasted to vaccinated participants (Supplementary Figures S1C,F, S3C,D and S5A). Inoculation of cured COVID-19 patients with one dose of BT led to a strong elevation of α -Spike-Ab concentrations in sera after seven days (median for BT_{7d}: 3008 BAU/mL) which were comparable to BT controls. A second vaccination after one month with BT did not increase the α -Spike-Ab titers beyond concentrations achieved by the first BT dose (median for 2nd BT_{d7}: 3918 BAU/mL). It is worth emphasizing that infection with SARS-CoV-2 and additional vaccination with BT did not lead to a long-lasting Ab production against the Spike protein: 183 days after the vaccination, α -Spike-Ab had decreased to a basal level of 544 BAU/mL (Figure 3F). Overall, our data support the current scientific opinion that even cured COVID-19 patients benefit from an mRNA-based COVID-19 vaccine six months after infection [32,33]. A single SARS-CoV-2 infection does not lead to longer-lasting nor higher levels of Ab titers than vaccination.

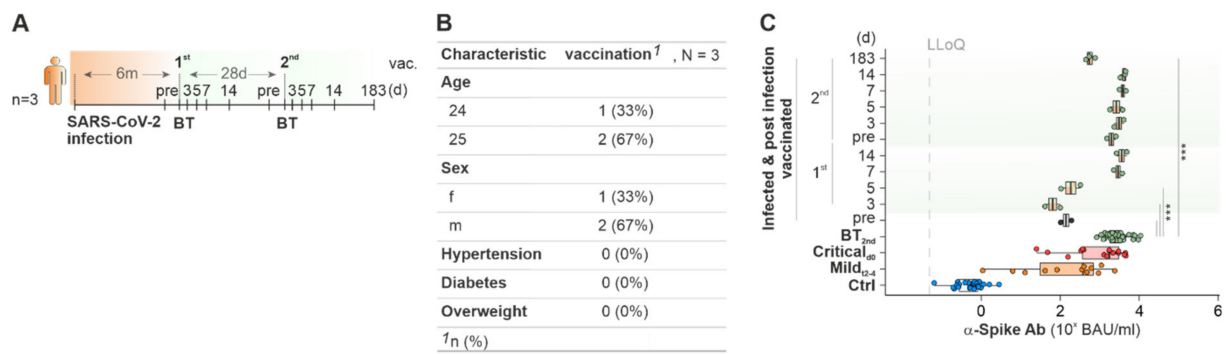


Figure 5. Ab titers against Wuhan SARS-CoV-2 Spike protein after infection and subsequent vaccination over time. (A) Vaccination scheme, (B) table of clinical characteristics and (C) Concentrations of α -Spike-Ab of patients after infection and subsequent vaccination at indicated timepoints. LLoQ, Lower Level of Quantification; Mann-Whitney U test; unadjusted p -value (C); *** p Val < 0.001.

3. Discussion

At the beginning of the SARS-CoV-2 pandemic there was an urgent need to prevent high incidences of critically ill COVID-19 patients because health care systems around the globe were flooded by intensive-care units requiring COVID-19 patients. The situation was dramatically worsened when medical health care workers became infected and had to temporarily resign from their duties. Intensive efforts to develop effective vaccine against SARS-CoV-2 were initiated, with the aim of raising a strong humoral immune response through the production of neutralizing antibodies against the Spike protein of SARS-CoV-2. On March 18 2020, the U.S Food and Drug Administration (FDA) and the European Medicines Agency (EMA) jointly chaired the first global regulators meeting to discuss regulatory strategies to facilitate the development of SARS-CoV-2 vaccines [34]. Through the US-funded Operation Warp Speed initiative, phases (phase 1–3) of a clinical approval study normally conducted sequentially were instead conducted in parallel. On December 10, 2020, the safety and efficacy of the BNT162b2 mRNA COVID-19 Vaccine were published [20]. On December 11, 2020, the FDA issued the first emergency use authorization (EUA) for BNT162b2 for the mitigation of COVID-19 caused by SARS-CoV-2 in individuals 16 years of age and older [35]. Vaccines by MO, AZ and JJ followed in this order, so that at the end of 2020, just one year after the initial outbreak, several vaccines were licensed for usage in the US and Europe. The approval studies had a mean follow up of only two months, leaving a number of unexplored questions about Ab dynamics. A number of subsequent studies have compared different vaccines [13,14,20,36,37]. Secondary to the generation of neutralizing antibodies against the Spike-protein [38], vaccination led to lower viral loads in previously vaccinated COVID-19 patients [39].

3.1. Antibodies

Obesity and related co-morbidities have been reported to correlate with negative disease outcomes [40,41]. We investigated how this correlation translates to antibody titers against SARS-CoV-2 in our study, but we were not able to find any significant correlations in our patient cohorts with regards to obesity, hypertension or diabetes and anti-spike antibody titers. Independent of the vaccine used or the disease stage of COVID-19, we observed a certain range of maximum IgG α -Spike-Ab titers generated (Figures 3–5), and these titers were comparable to patients vaccinated once with any kind of COVID-19 vaccine (Figure 3B,E,F). Similar results were found by Brochot et al. [42], who showed that Ab titers against Spike- and N-protein reached a plateau after 14 days of infection onset. Others observed a similar dynamic and plateau for IgM antibodies against the Spike-protein [36]. Due to the half-life of 184 days of α -Spike-Abs [43], a reduction of Ab titers was expected. Indeed, we observed that α -Spike-Abs titers were reduced in cured COVID-19 and Long-COVID patients 6 months after the infection (Figures 1K and 5C). A similar observation was made in a cohort study

that focused on the long-term health consequences of COVID-19 patients discharged from the hospital [44]. Post-infection vaccination with mRNA vaccines increased the Ab titers to those of the vaccine control groups (Figure 5C). These results suggest that even cured COVID-19 patients benefited from a mRNA vaccination 6 months after the infection, consistent with CDC, the recommendation for vaccination of all former COVID-19 patients several months after the infection [32,33]. We observed that three vaccine inoculations of BT led to the production of long-lasting (>6 months) α -Spike-RBD-Abs with high neutralizing potential, not only for the initial Wuhan SARS-CoV-2 strain but also against other variants of concern (alpha, beta and gamma; Supplementary Figure S3F). Moreover, we show that beta-specific antibody titers and their neutralizing capacity in vaccinated individuals (Supplementary Figure S3F) and severe COVID-19 patients (Supplementary Figure S1G) were lower than for the Wuhan, alpha and gamma strains. Similar observations were made in nonhuman primates. The beta variant was the most neutralization- and vaccine-resistant of the first four variants of concern, including the delta strain [45]. In contrast, Newman et al. observed no neutralizing capacity against the beta variant of SARS-CoV-2 in sera of elderly people vaccinated twice with BT [46]. The differences in neutralization potential of α -Spike-Ab between the studies might be explained on the one hand by the presence of younger participants in our study, and on the other, by a third inoculation with the mRNA vaccine after six months. We conclude from these results that a third vaccination or inoculation with adapted vaccines against newer variants might be necessary for a robust antibody response against SARS-CoV-2 variants of concern.

3.2. Cytokines

Despite the fact that the vast majority of COVID-19 vaccines were well tolerated, a minority of individuals who received a vaccination reported side effects, such as redness and swelling at the side of injection. Mild side effects included flu-like symptoms [47], but serious side effects were also reported, including myocarditis (reviewed by Ling et al. [48]) and thrombosis [49]. Of note, none of the participants in this study reported any serious side effects. The participants in our study reported common and mild side effects like pain at the site of vaccination, headache or fatigue, and in rare cases fever, which were temporary and disappeared after one day. Severe hyper-inflammatory reactions are rare but have also been reported after inoculation with mRNA and DNA vaccines against COVID-19 [50]. As abnormal cytokine concentrations are the driving factor behind hyper-inflammatory reactions, Arunchalam et al. [51] investigated cytokine titers following BT vaccination and found that especially IFN γ was increased after the second inoculation with BT. We can confirm this observation also for vaccinations with AZ (Figure 3A) and MO (Figure 3G,H). Moreover, we observed in participants' sera vaccinated with MO an increase in the highly pro-inflammatory cytokine IL1 β 24 h after the inoculation (Figure 3G,H). Cytokine concentrations were reduced back to normal ranges two days after the inoculation, suggesting that mRNA- and vector-based COVID-19 vaccines cause a temporal, short-lived inflammatory immune reaction in healthy participants. In case of hyper-inflammatory reactions due to COVID-19 vaccination, treatment with the IL1 receptor antagonist Anakinra was able to restrain the overshooting immune response to the vaccination [50]. COVID-19 vaccination has been associated with adverse reactions in response to certain treatments, e.g., dermal fillers, like hyaluronic acid, polymethyl-methacrylate and fluid silicone, in the facial region [52]. In this case study, 20 patients, who were injected with dermal fillers, reported swelling and redness as well as other inflammatory hyper-responsiveness at the side of dermal filler injection immediately after a COVID-19 vaccination. It can be hypothesized that the usage of dermal fillers sensitized the body for Polyethylene glycol (PEG) particles [53], which are used as stabilizers in mRNA COVID-19 vaccines and connected to anaphylaxis [54,55]. As PEG is used widely by pharmaceutical, cosmetics and food industries, allergic reactions are a potential source of concern [56,57] and might explain the adverse events after COVID-19 vaccination [58]. Another potential source for inflammatory immune reactions in response to an inoculation with mRNA-based vaccines might be lipid compounds, which are used to encapsulate the mRNA into vesicle for transfection of human cells. A recent study

presented evidence for membrane-destabilizing lipids leading to inflammasome activation and induction of pro-inflammatory cytokine secretion in murine bone marrow-derived macrophages and HEK cells [59].

Interestingly, we observed that patients with a critical disease course, who survived the infection (Figure 1F), showed significantly elevated levels of IL10 in their blood. Similar observations have been made by other researchers, who hypothesized that the elevated IL10 levels contribute to the pathogenesis of severe COVID-19 diseases by amplifying viral sepsis-related hyper-inflammation and induction of cytotoxic CD8⁺ T cells [60]. Except for the herein presented data, so far, there have not been published any studies to our knowledge that discriminate the critically ill COVID-19 patients into survived and deceased. Many different immune cells produce the immune suppressive cytokine IL10 contributing to the re-establishment of immune homeostasis after an infection [61]. While the present study did not establish the source of IL10 and limited flow cytometric analysis of the B cell compartment, we speculate that a specialized but heterogeneous subpopulation of B cells, called regulatory B cells (Bregs) contribute to the elevated IL10 levels in critical COVID-19 patients. Breg cells are able to produce IL10 and can be characterized by CD19⁺CD24^{hi}CD38^{hi}CD1d^{hi} and CD19⁺CD24^{hi}CD27⁺ [62].

One aspect of our study was to investigate the dynamics and expansion of class-switched memory B cells and circulating Tfh cells, which are central to the establishment of immunity against pathogens [63]. Similar to Hartley et al. [64], we observed that IgD⁻CD27⁺CD38^{low} class-switch B cells expanded rapidly after the first symptoms appeared and moreover, correlated to increasing α -Spike-Abs titers and numbers of Tfh cells during the initial stage of infection (Figure 1B–D). At later stages of uncleared SARS-CoV-2 infections, we observed higher frequencies of class-switched memory B cells and Tfh cells in deceased critically ill patients in comparison to survivors (Figure 1H,I), leading to an increased Tfh/Treg ratio (Figure 1J). An increase in Tfh/Treg ration has been previously associated with autoimmune diseases, like systemic lupus erythematosus [7]. One might speculate that the elevated Tfh/Treg ratio together with the presence of increased levels of IL10 are signs of the unrestrained immune reactions in severe COVID-19 disease courses which resemble ongoing autoimmune diseases.

The aim of our study was to understand the dynamics of Ab development against SARS-CoV-2 in different vaccination cohorts. These cohorts represent real-life scenarios. Given the fact that even today, infection-preventing Ab titers are not known, we went on to compare resulting Ab titers between different vaccination schemes. In addition, we monitored cytokines as potential inflammatory vaccine response. Despite the limited number of participants, we were able to describe a brought picture of several vaccination strategies and could demonstrate that even cured COVID-19 patients benefit from vaccination. In regard to potential side effects, we could demonstrate that COVID-19 vaccination led to a low-grade, barely detectable systemic inflammatory response, which was in a timely manner restrained and reverted. Through the present study, we hope to further encourage people all over the world to participate in vaccination campaigns to fight the still ongoing pandemic.

4. Material and Methods

4.1. Study Design and Patient Cohorts

Infection with SARS-CoV-2 was confirmed in all patients with qRT-PCR test or antigen-tests for SARS-CoV-2 in nasopharyngeal swabs, and quantification of SARS-CoV-2 N-protein concentrations and serum-anti-N Ab titers. Characterization of the virus strains was not performed. Samples from mild COVID-19 cases (collected from January to March 2020) and critically ill COVID-19 patients (collected from November 2020 to February 2021) were collected in Germany in the region of North-Rhine-Westphalia. This study was performed in line with the principles of the Declaration of Helsinki. Blood sampling of SARS-CoV-2 infected or recovered patients and healthy controls was approved by the local institutional research ethics board (University Hospital Bonn, ethics vote 468/20). We col-

lected comprehensive clinical and demographic information, medical history, comorbidities and vaccination schedules for all patients and participants.

We categorized patients in the mild cohort when their symptoms included fever, loss of smell and taste, headache and diarrhea, and when they recovered at their private residencies. The quarantine regulations required the help of the Medical Corps of the German Armed Forces to obtain samples of mildly infected patients in their households up to 6 times during the 21 days from inclusion into the study.

Patients with acute respiratory distress syndrome (ARDS) caused by SARS-CoV-2 infection were diagnosed according to the Berlin Definition [65] and categorized as “Critical”. They were included in the study upon admission to the ICU. These patients were also sampled up to six times during the 21 days from inclusion in the study. Treatment included invasive mechanical ventilation or extracorporeal membrane oxygenation (ECMO).

Patients with a history of SARS-CoV-2 infection clinically categorized as cured yet suffering from persisting COVID-19 symptoms at least eight weeks and up to 12 months after infection onset were classified as “Long-COVID”. Patients were recruited at the Long-COVID ambulance of the University Hospital Bonn (Germany) and through Long-COVID support groups on social media (Twitter and Facebook) (UK). Symptoms included fatigue, reduced resilience, cognitive dysfunction, headache, PoTS, tachycardia, palpitations, chest pain and shortness of breath.

Vaccinated volunteers were sampled at various timepoints before and after administration of the vaccine shots (BNT162b2, Sikevax mRNA-1273, Vaxzevria or Janssen) and followed up to one year after the first shot. Participants who did not undergo an active SARS-CoV-2 infection and without any history of prior COVID-19 were categorized as “Control” (Ctrl). Healthy controls were sampled up to 5 times within a fortnight.

4.2. Sample Generation and Storage

We used 7.5 mL Z-Gel S-Monovettes (Sarstedt, Nümbrecht, Germany) for peripheral blood. For flow-cytometry, 9 mL of blood was collected in K3E S-Monovettes (Sarstedt). Serum gel tubes were centrifuged at RT for 10 min at 2500× g. The cell-depleted serum fraction was transferred to sterile, barcoded polypropylene tubes (Azenta, Chelmsford, MA, USA) and frozen at −80 °C until needed.

4.3. Quantification of SARS-CoV-2 N-Protein, α -Spike-Antibodies Titers and Neutralization

SARS-CoV-2 N-protein concentrations in sera were quantified using the S-PLEX SARS-CoV-2 N Kit (Meso Scale Diagnostics, Rockville, MD, USA) according to the manufacturer’s protocol. Similarly, the concentrations of α -SARS-CoV-2 IgG antibodies and their neutralization capacity in sera were quantified using the SARS-CoV-2 Plate 7 (Meso Scale Diagnostics). Immune assays from Meso Scale were acquired via the MESO QuickPlex SQ 120 imager (Meso Scale Diagnostics) and analyzed with the MSD Discovery Workbench (Meso Scale Diagnostics).

4.4. Quantification of Cytokines and Markers for Neuroinflammation

We screened serum samples at chosen time points of the SARS-CoV-2 disease course for the expression of pro- and anti-inflammatory cytokines using the Simoa CorPlex Human Cytokine 10-plex Panel 1 assay (Quanterix, Billerica, MA, USA). We targeted the following analytes: IFN γ , IL1 β , IL4, IL5, IL6, IL8, IL10, IL12p70, IL22 and TNF α . In addition, markers for neuroinflammation were quantified using the Simoa Human Neurology 4-Plex E assay (Quanterix) for Abeta 40 (A β 40), Abeta 42 (A β 42), Glial Fibrillary Acidic Protein (GFAPTM) and Neurofilament light (Nf-L). Data for the 10 CorPlex were acquired and analyzed on the SP-X Imaging and Analysis SystemTM (Quanterix), whereas the Neurology 4-Plex E assay was analyzed on the Simoa[®] HD-X AnalyzerTM (Quanterix). Both kits were used according to the manufacturer’s instructions.

4.5. Quantification of B Cell Subtypes and T Follicular Helper Cells by Flow Cytometry

EDTA blood samples were centrifuged at $1200 \times g$ for 10 min, and the cell pellet was washed once with PBS and treated with ACK lysis buffer (Thermo Fisher, Waltham, MA, USA) for 5 min. The ACK reaction was stopped with an additional wash. Cells were subsequently resuspended in PBS. Up to 2×10^6 live PBMC (per sample) were stained. Viable and dead cells were discriminated by staining with the following Ab compositions for 30 min at 4°C : LIVE/DEAD™ Fixable Far Red Dead Cell Stain, FITC-conjugated anti-CD45 (HI30), eFluor™ 506-conjugated anti-CD19 (HIB19), PerCP-eFluor™ 710-conjugated anti-IgD (IA6-2), eFluor™ 450-conjugated anti-IgM (SA-DA4), PE-conjugated anti-CD38 (HB7), PE-eFluor610-conjugated anti-CD27 or Super Bright™-conjugated anti-CD24 (eBioSN3), PerCP-conjugated anti-CD4 (SK3), PE-Cyanine7-conjugated anti-CD25 (CD25-4E3) and Alexa Fluor™ 660-conjugated anti-CD127 (eBioRDR5), all from Invitrogen, FITC-conjugated anti-CD3 (OKT3), Brilliant Violet™ 650-conjugated anti-CD4 (RPA-T4), Brilliant Violet™ 421-conjugated anti-CXCR5 (J252D4) and FITC-conjugated anti-CD3 (OKT3) from Biolegend. After surface staining, cells were washed and fixed in 4% PFA for 10 min at room temperature (RT). Single-cell suspensions were acquired on Attune Next Generation (ThermoFisher) and analyzed with FlowJo (version 10.0.7, Tree star).

4.6. Software and Tools for Statistical Analysis

Statistical analysis was performed in R (v4.1.2; [66] by the rstatix (v.0.7.0; [67]). Tables were created using the gtsummary package (v1.5.2; [68]). Figures were created with the ggplot package (v3.3.5; [69] and ggpubr (v0.4.0; [70]). The Kruskal–Wallis and Mann–Whitney U tests were used to calculate p values. Adjusted p values less than 0.05 were considered statistically significant. Deviations are outlined in figure legends.

Supplementary Materials: The supporting information can be downloaded at: <https://www.mdpi.com/article/10.3390/ijms232012231/s1>.

Author Contributions: A.O., J.S., C.L. and S.V.S. designed the study and concept; patient recruitment; sample collection and transportation was performed by C.B.; F.S., C.P., R.M.S., G.W., E.S., N.T.M., F.R., L.K., M.W., K.v.B., T.P., G.M. and C.L.; the samples were processed by A.O., J.S., S.S. (Simon Schade), T.J.K., J.N., A.K., M.K. and U.S.; cytokine and Ab quantification was carried out by A.O., J.M.J., D.M., A.J.B., S.S. (Stefan Scory) and R.M.; flow cytometry on whole blood from the samples was performed with assistance from J.B.S. and Z.A.; data analysis and visualization was performed by A.O., J.S. and S.V.S.; for project supervision and administration were responsible S.V.S. and C.L.; S.V.S. accomplished the funding acquisition; the manuscript was written with input from all co-authors by A.O., J.S., C.L. and S.V.S. All authors have read and agreed to the published version of the manuscript.

Funding: This work was funded by the German Federal Ministry of Education and Research through the COVIMMUN project (grant number 01KI20343).

Institutional Review Board Statement: All experimental work was performed under protocols approved by the local Institutional Review Board (IRB) of the University Hospital Bonn (ethics vote 468/20), after written informed consent for publication of clinical and immunological information of the patients.

Informed Consent Statement: All participants provided informed consent to participate. All participants have consented to publication of their data.

Data Availability Statement: Data presented in this manuscript will be made available upon request.

Acknowledgments: The authors want to thank Andrea Rothballer for the help in the grant application and correspondence with the funding agency. Many thanks to the patients and their families who volunteered to donate blood. The authors express their gratitude to the University Hospital Bonn for providing infrastructure, and transportation possibilities during the phase of sample collection. We thank Meso Scale Diagnostics, Quanterix and IFM for providing the equipment to quantify Ab and cytokine titers. The authors thank Rolf von Uslar for interconnecting the project and the medical soldiers from the German Armed Forces. Further, we thank Jana Schulz and Nicole Alda, both from the Dardenne Eye Hospital, for the organization and serum collection of participants for the vaccination study.

Conflicts of Interest: Joseph M. Johnson, Dawn Mattoon and Andrew J. Ball work at Quanterix Corporation. Stefan Scory and Richard McGuire work at Meso Scale Diagnostics LLC. The remaining authors declare no competing interests.

References

- Liu, Y.-C.; Kuo, R.-L.; Shih, S.-R. COVID-19: The first documented coronavirus pandemic in history. *Biomed. J.* **2020**, *43*, 328–333. [[CrossRef](#)] [[PubMed](#)]
- World Health Organization. Tracking SARS-CoV-2 Variants. 2022. Available online: <https://www.who.int/activities/tracking-SARS-CoV-2-variants> (accessed on 29 July 2022).
- World Health Organization. (COVID-19) Homepage. WHO Coronavirus (COVID-19) Dashboard. 2022. Available online: <https://covid19.who.int/> (accessed on 29 July 2022).
- Diamond, M.S.; Kanneganti, T.-D. Innate immunity: The first line of defense against SARS-CoV-2. *Nat. Immunol.* **2022**, *23*, 165–176. [[CrossRef](#)] [[PubMed](#)]
- Hojo, S.; Uchida, M.; Tanaka, K.; Hasebe, R.; Tanaka, Y.; Murakami, M.; Hirano, T. How COVID-19 induces cytokine storm with high mortality. *Inflamm. Regen.* **2020**, *40*, 1–7. [[CrossRef](#)]
- van Paassen, J.; Vos, J.S.; Hoekstra, E.M.; Neumann, K.M.I.; Boot, P.C.; Arbous, S.M. Corticosteroid use in COVID-19 patients: A systematic review and meta-analysis on clinical outcomes. *Crit. Care* **2020**, *24*, 1–22. [[CrossRef](#)] [[PubMed](#)]
- Xu, B.; Wang, S.; Zhou, M.; Huang, Y.; Fu, R.; Guo, C.; Chen, J.; Zhao, J.; Gaskin, F.; Fu, S.M.; et al. The ratio of circulating follicular T helper cell to follicular T regulatory cell is correlated with disease activity in systemic lupus erythematosus. *Clin. Immunol.* **2017**, *183*, 46–53. [[CrossRef](#)]
- Cantini, F.; Niccoli, L.; Matarrese, D.; Nicastrì, E.; Stobbione, P.; Goletti, D. Baricitinib therapy in COVID-19: A pilot study on safety and clinical impact. *J. Infect.* **2020**, *81*, 318–356. [[CrossRef](#)]
- Yan, R.; Zhang, Y.; Li, Y.; Xia, L.; Guo, Y.; Zhou, Q. Structural basis for the recognition of SARS-CoV-2 by full-length human ACE2. *Science* **2020**, *367*, 1444–1448. [[CrossRef](#)]
- Hoffmann, M.; Kleine-Weber, H.; Schroeder, S.; Krüger, N.; Herrler, T.; Erichsen, S.; Schiergens, T.S.; Herrler, G.; Wu, N.H.; Nitsche, A.; et al. SARS-CoV-2 cell entry depends on ACE2 and TMPRSS2 and is blocked by a clinically proven protease inhibitor. *Cell* **2020**, *181*, 271–280. [[CrossRef](#)]
- Long, Q.X.; Liu, B.Z.; Deng, H.J.; Wu, G.C.; Deng, K.; Chen, Y.K.; Liao, P.; Qiu, J.F.; Lin, Y.; Cai, X.F.; et al. Antibody responses to SARS-CoV-2 in patients with COVID-19. *Nat. Med.* **2020**, *26*, 845–848. [[CrossRef](#)]
- Juno, J.A.; Tan, H.X.; Lee, W.S.; Reynaldi, A.; Kelly, H.G.; Wragg, K.; Esterbauer, R.; Kent, H.E.; Batten, C.J.; Mordant, F.L.; et al. Humoral and circulating follicular helper T cell responses in recovered patients with COVID-19. *Nat. Med.* **2020**, *26*, 1428–1434. [[CrossRef](#)]
- Sadoff, J.; Gray, G.; Vandebosch, A.; Cárdenas, V.; Shukarev, G.; Grinsztejn, B.; Goepfert, P.A.; Truyers, C.; Fennema, H.; Spiessens, B.; et al. Safety and efficacy of single-dose Ad26. COV2. S vaccine against COVID-19. *N. Engl. J. Med.* **2021**, *384*, 2187–2201. [[CrossRef](#)] [[PubMed](#)]
- Voysey, M.; Clemens, S.A.C.; Madhi, S.A.; Weckx, L.Y.; Folegatti, P.M.; Aley, P.K.; Angus, B.; Baillie, V.L.; Barnabas, S.L.; Borat, Q.E.; et al. Safety and efficacy of the ChAdOx1 nCoV-19 vaccine (AZD1222) against SARS-CoV-2: An interim analysis of four randomised controlled trials in Brazil, South Africa, and the UK. *Lancet* **2021**, *397*, 99–111. [[CrossRef](#)]
- Hung, I.F.N.; Poland, G.A. Single-dose Oxford–AstraZeneca COVID-19 vaccine followed by a 12-week booster. *Lancet* **2021**, *397*, 854–855. [[CrossRef](#)]
- World Health Organization. The Janssen Ad26.COV2.S COVID-19 Vaccine: What You Need to Know. 2022. Available online: <https://www.who.int/news-room/feature-stories/detail/the-j-j-covid-19-vaccine-what-you-need-to-know> (accessed on 29 July 2022).
- World Health Organization. The Moderna COVID-19 (mRNA-1273) Vaccine: What you Need to Know. 2022. Available online: <https://www.who.int/news-room/feature-stories/detail/the-moderna-covid-19-mrna-1273-vaccine-what-you-need-to-know> (accessed on 29 July 2022).
- World Health Organization. Interim Recommendations for Use of the Pfizer–BioNTech COVID-19 Vaccine, BNT162b2, under Emergency Use Listing. 2022. Available online: https://www.who.int/publications/i/item/WHO-2019-nCoV-vaccines-SAGE_recommendation-BNT162b2-2021.1 (accessed on 29 July 2022).
- Jackson, L.A.; Anderson, E.J.; Roupheal, N.G.; Roberts, P.C.; Makhene, M.; Coler, R.N.; McCullough, M.P.; Chappell, J.D.; Denison, M.R.; Stevens, L.J.; et al. An mRNA vaccine against SARS-CoV-2—Preliminary report. *N. Engl. J. Med.* **2020**, *383*, 1920–1931. [[CrossRef](#)] [[PubMed](#)]
- Polack, F.P.; Thomas, S.J.; Kitchin, N.; Absalon, J.; Gurtman, A.; Lockhart, S.; Perez, J.L.; Marc, G.P.; Moreira, E.D.; Zerbini, C.; et al. Safety and efficacy of the BNT162b2 mRNA COVID-19 vaccine. *N. Engl. J. Med.* **2020**, *283*, 2603–2615. [[CrossRef](#)]
- Heinz, F.X.; Stiasny, K. Distinguishing features of current COVID-19 vaccines: Knowns and unknowns of antigen presentation and modes of action. *NPJ Vaccines* **2021**, *6*, 1–13. [[CrossRef](#)]
- Turner, J.S.; O’Halloran, J.A.; Kalaidina, E.; Kim, W.; Schmitz, A.J.; Zhou, J.Q.; Lei, T.; Thapa, M.; Chen, R.E.; Case, J.B.; et al. SARS-CoV-2 mRNA vaccines induce persistent human germinal centre responses. *Nature* **2021**, *596*, 109–113. [[CrossRef](#)]

23. Takahashi, T.; Ellingson, M.K.; Wong, P.; Israelow, B.; Lucas, C.; Klein, J.; Silva, J.; Mao, T.; Oh, J.E.; Tokuyama, M.; et al. Sex differences in immune responses that underlie COVID-19 disease outcomes. *Nature* **2020**, *588*, 315–320. [CrossRef]
24. Shan, D.; Johnson, J.M.; Fernandes, S.C.; Suib, H.; Hwang, S.; Wuelfing, D.; Mendes, M.; Holdridge, M.; Burke, E.M.; Beauregard, K.; et al. N-protein presents early in blood, dried blood and saliva during asymptomatic and symptomatic SARS-CoV-2 infection. *Nat. Commun.* **2021**, *12*, 1–8. [CrossRef]
25. Garcia-Beltran, W.F.; Lam, E.C.; Astudillo, M.G.; Yang, D.; Miller, T.E.; Feldman, J.; Hauser, B.M.; Caradonna, T.M.; Clayton, K.L.; Nitido, A.D.; et al. COVID-19-neutralizing antibodies predict disease severity and survival. *Cell* **2021**, *184*, 476–488. [CrossRef]
26. Ding, T.; Su, R.; Wu, R.; Xue, H.; Wang, Y.; Su, R.; Gao, C.; Li, X.; Wang, C. Frontiers of autoantibodies in autoimmune disorders: Crosstalk between Tfh/Tfr and regulatory B cells. *Front. Immunol.* **2021**, *12*, 641013. [CrossRef] [PubMed]
27. Shabrish, S.; Desai, M.; Saxena, V.; Kelkar, M.; Madkaikar, M. IFN-g: IL-10 ratio: A putative predictive biomarker to discriminate HLH from severe viral infections. *J. Clin. Immunol.* **2019**, *39*, 135–137. [CrossRef] [PubMed]
28. Neurath, M.F.; Überla, K.; Ng, S.C. Gut as viral reservoir: Lessons from gut viromes, HIV and COVID-19. *Gut* **2021**, *70*, 1605. [CrossRef] [PubMed]
29. Sadoff, J.; Le Gars, M.; Shukarev, G.; Heerwegh, D.; Truyers, C.; de Marit Groot, A.; Stoop, J.; Tete, S.; Van Damme, W.; Leroux-Roels, I.; et al. Safety and immunogenicity of the Ad26. COV2. S COVID-19 vaccine candidate: Interim results of a phase 1/2a, double-blind, randomized, placebo-controlled trial. *MedRxiv* **2020**. [CrossRef]
30. Jaiswal, V.; Nepal, G.; Dijamco, P.; Ishak, A.; Dagar, M.; Sarfraz, Z.; Shama, N.; Sarfraz, A.; Lnu, K.; Mitra, S.; et al. Cerebral Venous Sinus Thrombosis Following COVID-19 Vaccination: A Systematic Review. *J. Prim. Care Community Health* **2022**, *13*, 21501319221074450. [CrossRef]
31. Impfkommision, S. Beschluss der STIKO zur 20. Aktualisierung der COVID-19-Impfempfehlung. *Epidemiol. Bull.* **2022**, *21*, 3–19.
32. Centers for Disease Control and Prevention. Interim Clinical Considerations for Use of COVID-19 Vaccines Currently Approved or Authorized in the United States. 2022. Available online: <https://www.cdc.gov/vaccines/covid-19/clinical-considerations/interim-considerations-us.html#infection> (accessed on 29 July 2022).
33. Centers for Disease Control and Prevention. Science Brief: SARS-CoV-2 Infection-Induced and Vaccine-Induced Immunity. 2021. Available online: <https://www.cdc.gov/coronavirus/2019-ncov/science/science-briefs/vaccine-induced-immunity.html> (accessed on 29 July 2022).
34. U.S. Food and Drug Administration. Summary of FDA & EMA Global Regulators Meeting on Data Requirements Supporting First-in-Human Clinical Trials with SARS-CoV-2 Vaccines. 2020. Available online: <https://www.fda.gov/news-events/fda-meetings-conferences-and-workshops/summary-fda-ema-global-regulators-meeting-data-requirements-supporting-first-human-clinical-trials> (accessed on 29 July 2022).
35. U.S. Food and Drug Administration. FDA Takes Key Action in Fight against COVID-19 by Issuing Emergency Use Authorization for First COVID-19 Vaccine. 2020. Available online: <https://www.fda.gov/news-events/press-announcements/fda-takes-key-action-fight-against-covid-19-issuing-emergency-use-authorization-first-covid-19> (accessed on 29 July 2022).
36. Bao, Y.; Ling, Y.; Chen, Y.-Y.; Tian, D.; Zhao, G.-P.; Zhang, X.-H.; Hang, H.; Li, Y.; Su, B.; Lu, H.-Z.; et al. Dynamic anti-spike protein antibody profiles in COVID-19 patients. *Int. J. Infect. Dis.* **2021**, *103*, 540–548. [CrossRef]
37. Baden, L.R.; El Sahly, H.M.; Essink, B.; Kotloff, K.; Frey, S.; Novak, R.; Diemert, D.; Spector, S.A.; Rouphael, N.; Creech, C.B.; et al. Efficacy and safety of the mRNA-1273 SARS-CoV-2 vaccine. *N. Engl. J. Med.* **2020**, *384*, 403–416. [CrossRef]
38. Favresse, J.; Gillot, C.; Di Chiaro, L.; Eucher, C.; Elsen, M.; Van Eeckhoudt, S.; David, C.; Morimont, L.; Dogné, J.-M.; Douxfils, J. Neutralizing antibodies in COVID-19 patients and vaccine recipients after two doses of BNT162b2. *Viruses* **2021**, *13*, 1364. [CrossRef] [PubMed]
39. Thompson, M.G.; Burgess, J.L.; Naleway, A.L.; Tyner, H.; Yoon, S.K.; Meece, J.; Olsho, L.E.W.; Caban-Martinez, A.J.; Fowlkes, A.L.; Lutrick, K.; et al. Prevention and Attenuation of Covid-19 with the BNT162b2 and mRNA-1273 Vaccines. *N. Engl. J. Med.* **2021**, *385*, 320–329. [CrossRef]
40. Huang, R.; Zhu, L.; Xue, L.; Liu, L.; Yan, X.; Wang, J.; Zhang, B.; Xu, T.; Ji, F.; Zhao, Y.; et al. Clinical findings of patients with coronavirus disease 2019 in Jiangsu province, China: A retrospective, multi-center study. *PLoS Negl. Trop. Dis.* **2020**, *14*, e0008280. [CrossRef] [PubMed]
41. Chen, T.; Wu, D.; Chen, H.; Yan, W.; Yang, D.; Chen, G.; Ma, K.; Xu, D.; Yu, H.; Wang, H.; et al. Clinical characteristics of 113 deceased patients with coronavirus disease 2019: Retrospective study. *BMJ* **2020**, *368*, m1091. [CrossRef] [PubMed]
42. Brochot, E.; Demey, B.; Touzé, A.; Belouzard, S.; Dubuisson, J.; Schmit, J.L.; Duverlie, G.; Francois, C.; Castelain, S.; Helle, F. Anti-spike, anti-nucleocapsid and neutralizing antibodies in SARS-CoV-2 inpatients and asymptomatic individuals. *Front. Microbiol.* **2020**, *11*, 2468. [CrossRef] [PubMed]
43. Wei, J.; Matthews, P.C.; Stoesser, N.; Maddox, T.; Lorenzi, L.; Studley, R.; Bell, J.I.; Newton, J.N.; Farrar, J.; Diamond, I.; et al. Anti-spike antibody response to natural SARS-CoV-2 infection in the general population. *Nat. Commun.* **2021**, *12*, 1–12. [CrossRef]
44. Huang, C.; Huang, L.; Wang, Y.; Li, X.; Ren, L.; Gu, X.; Kang, L.; Guo, L.; Liu, M.; Zhou, X.; et al. 6-month consequences of COVID-19 in patients discharged from hospital: A cohort study. *Lancet* **2021**, *397*, 220–232. [CrossRef]
45. Corbett, K.S.; Gagne, M.; Wagner, D.A.; O’Connell, S.; Narpala, S.R.; Flebbe, D.R.; Andrew, S.F.; Davis, R.L.; Flynn, B.; Johnston, T.S.; et al. Protection against SARS-CoV-2 Beta variant in mRNA-1273 vaccine-boosted nonhuman primates. *Science* **2021**, *374*, 1343–1353. [CrossRef]

46. Newman, J.; Thakur, N.; Peacock, T.P.; Bialy, D.; Elrefaey, A.M.; Bogaardt, C.; Horton, D.L.; Ho, S.; Kankeyan, T.; Carr, C.; et al. Neutralizing antibody activity against 21 SARS-CoV-2 variants in older adults vaccinated with BNT162b2. *Nat. Microbiol.* **2022**, *7*, 1180–1188. [[CrossRef](#)]
47. El-Shitany, N.A.; Harakeh, S.; Badr-Eldin, S.M.; Bagher, A.M.; Eid, B.; Almukadi, H.; Alghamdi, B.S.; Alahmadi, A.A.; Hassan, N.A.; Sindi, N.; et al. Minor to moderate side effects of Pfizer-BioNTech COVID-19 vaccine among Saudi residents: A retrospective cross-sectional study. *Int. J. Gen. Med.* **2021**, *14*, 1389. [[CrossRef](#)]
48. Ling, R.R.; Ramanathan, K.; Tan, F.L.; Tai, B.C.; Somani, J.; Fisher, D.; MacLaren, G. Myopericarditis following COVID-19 vaccination and non-COVID-19 vaccination: A systematic review and meta-analysis. *Lancet Respir. Med.* **2022**, *10*, 679–688. [[CrossRef](#)]
49. Higgins, H.; Andrews, N.; Stowe, J.; Amirthalingam, G.; Ramsay, M.; Bahra, G.; Hackett, A.; Breen, K.A.; Desborough, M.; Khan, D.; et al. Risk of thrombosis with thrombocytopenia syndrome after COVID-19 vaccination prior to the recognition of vaccine-induced thrombocytopenia and thrombosis: A self-controlled case series study in England. *Res. Pract. Thromb. Haemost.* **2022**, *6*, e12698. [[CrossRef](#)]
50. Bindoli, S.; Giollo, A.; Galozzi, P.; Doria, A.; Sfriso, P. Hyperinflammation after anti-SARS-CoV-2 mRNA/DNA vaccines successfully treated with anakinra: Case series and literature review. *Exp. Biol. Med.* **2022**, *247*, 338–344. [[CrossRef](#)] [[PubMed](#)]
51. Arunachalam, P.S.; Scott, M.K.D.; Hagan, T.; Li, C.; Feng, Y.; Wimmers, F.; Grigoryan, L.; Trisal, M.; Edara, V.V.; Lai, L.; et al. Systems vaccinology of the BNT162b2 mRNA vaccine in humans. *Nature* **2021**, *596*, 410–416. [[CrossRef](#)] [[PubMed](#)]
52. Alijotas-Reig, J.; Imenez, V.G.; Velthuis, P.J.; Niessen, F.B.; Decates, T.S. Inflammatory immune-mediated adverse reactions induced by COVID-19 vaccines in previously injected patients with soft tissue fillers: A case-series of 20 patients. *J. Cosmet. Dermatol.* **2022**, *21*, 3181–3187. [[CrossRef](#)] [[PubMed](#)]
53. Zerbinati, N.; Esposito, C.; Cipolla, G.; Calligaro, A.; Monticelli, D.; Martina, V.; Golubovic, M.; Binic, I.; Sigova, J.; Gallo, A.L.; et al. Chemical and mechanical characterization of hyaluronic acid hydrogel cross-linked with polyethylen glycol and its use in dermatology. *Dermatol. Ther.* **2020**, *33*, e13747. [[CrossRef](#)]
54. Sellaturay, P.; Nasser, S.; Islam, S.; Gurugama, P.; Ewan, P.W. Polyethylene glycol (PEG) is a cause of anaphylaxis to the Pfizer/BioNTech mRNA COVID-19 vaccine. *Clin. Exp. Allergy* **2021**, *51*, 861. [[CrossRef](#)]
55. Sellaturay, P.; Gurugama, P.; Harper, V.; Dymond, T.; Ewan, P.; Nasser, S. The Polysorbate containing AstraZeneca COVID-19 vaccine is tolerated by polyethylene glycol (PEG) allergic patients. *Clin. Exp. Allergy* **2022**, *52*, 12–17. [[CrossRef](#)]
56. Cox, F.; Khalib, K.; Conlon, N. PEG that reaction: A case series of allergy to polyethylene glycol. *J. Clin. Pharmacol.* **2021**, *61*, 832–835. [[CrossRef](#)]
57. Wylon, K.; Dölle, S.; Worm, M. Polyethylene glycol as a cause of anaphylaxis. *Allergy Asthma Clin. Immunol.* **2016**, *12*, 1–3. [[CrossRef](#)]
58. Mortz, C.G.; Kjaer, H.F.; Rasmussen, T.H.; Rasmussen, H.M.; Garvey, L.H.; Bindslev-Jensen, C. Allergy to polyethylene glycol and polysorbates in a patient cohort: Diagnostic work-up and decision points for vaccination during the COVID-19 pandemic. *Clin. Transl. Allergy* **2022**, *12*, e12111. [[CrossRef](#)]
59. Forster, J.; Nandi, D.; Kulkarni, A. mRNA-Carrying Lipid Nanoparticles that Induce Lysosomal Rupture Activate NLRP3 Inflammasome and Reduce mRNA Transfection Efficiency. *Biomater. Sci.* **2022**, *10*, 5566–5582. [[CrossRef](#)]
60. Lu, L.; Zhang, H.; Dauphars, D.J.; He, Y.-W. A potential role of interleukin 10 in COVID-19 pathogenesis. *Trends Immunol.* **2021**, *42*, 3–5. [[CrossRef](#)] [[PubMed](#)]
61. Rojas, J.M.; Avia, M.; Martín, V.; Sevilla, N. IL-10: A multifunctional cytokine in viral infections. *J. Immunol. Res.* **2017**, *2017*, 6104054. [[CrossRef](#)] [[PubMed](#)]
62. Hagn, M.; Jahrsdörfer, B. Why do human B cells secrete granzyme B? Insights into a novel B-cell differentiation pathway. *Oncoimmunology* **2012**, *1*, 1368–1375. [[CrossRef](#)] [[PubMed](#)]
63. Akkaya, M.; Kwak, K.; Pierce, S.K. B cell memory: Building two walls of protection against pathogens. *Nat. Rev. Immunol.* **2020**, *20*, 229–238. [[CrossRef](#)]
64. Hartley, G.E.; Edwards, E.S.; Aui, P.M.; Varese, N.; Stojanovic, S.; McMahon, J.; Peleg, A.Y.; Boo, I.; Drummer, H.E.; Hogarth, P.M.; et al. Rapid generation of durable B cell memory to SARS-CoV-2 spike and nucleocapsid proteins in COVID-19 and convalescence. *Sci. Immunol.* **2020**, *5*, eabf8891. [[CrossRef](#)]
65. Force, A.D.T.; Ranieri, V.M.; Rubenfeld, G.D.; Thompson, B.; Ferguson, N.; Caldwell, E.; Fan, E.; Camporota, L.; Slutsky, A.S. Acute respiratory distress syndrome. *JAMA* **2012**, *307*, 2526–2533.
66. R. C. Team. *R: A Language and Environment for Statistical Computing*; R Foundation for Statistical Computing: Vienna, Austria, 2013; Available online: <http://www.R-project.org/> (accessed on 1 April 2022).
67. Kassambara, A. *rstatix: Pipe-Friendly Framework for Basic Statistical Tests*, R package version 0.7.0. 2021. Available online: <http://www.R-project.org/> (accessed on 25 May 2022).
68. Sjöberg, D.D.; Whiting, K.; Curry, M.; Lavery, J.A.; Larmarange, J. Reproducible Summary Tables with the gtsummary Package. *R J.* **2021**, *13*, 570–594. [[CrossRef](#)]
69. Wickham, H. Data analysis. In *ggplot2*; Springer: Berlin/Heidelberg, Germany, 2016; pp. 189–201.
70. Kassambara, A. *ggpubr: 'ggplot2' based Publication Ready Plots*; Github: San Francisco, CA, USA, 2020.

3.2 Publication 2: Interferon-induced IL-10 drives systemic T-cell dysfunction during chronic liver injury

Interferon-induced IL-10 drives systemic T-cell dysfunction during chronic liver injury

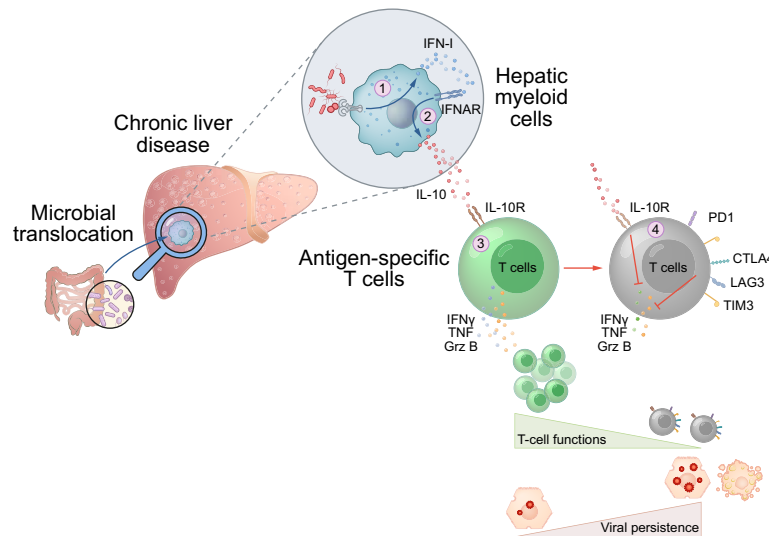
Authors

Carl-Philipp Hackstein, Jasper Spitzer, Konstantinos Symeonidis, ..., Susanne V. Schmidt, Percy A. Knolle, Zeinab Abdullah

Correspondence

zeinab.abdullah@uni-bonn.de (Z. Abdullah).

Graphical abstract



Highlights

- During chronic liver injury, antigen-specific T cells feature hallmarks of T-cell exhaustion.
- IFN-I/IL-10 signaling axis is a determinant of impaired systemic T-cell responses in chronic liver injury and cirrhosis.
- IFN-I-induced by translocated gut microbiota hampers systemic T-cell immunity via IL-10 release by myeloid cells.
- IL-10 suppresses T-cell immunity by directly acting on antigen-specific T cells.
- IL-10R blockade promotes the reconstitution of T-cell functions in virus infected mice and vaccinated patients.

Impact and implications

Chronic liver injury and cirrhosis are associated with enhanced susceptibility to viral infections and vaccine hyporesponsiveness. Using different preclinical animal models and patient samples, we identified that impaired T-cell immunity in BDL- and CCL₄-induced prolonged liver injury is driven by sequential events involving microbial translocation, IFN signaling leading to myeloid cell-induced IL-10 expression, and IL-10 signaling in antigen-specific T cells. Given the absence of immune pathology after interference with IL-10R, our study highlights a potential novel target to reconstitute T-cell immunity in patients with CLD that can be explored in future clinical studies.

Interferon-induced IL-10 drives systemic T-cell dysfunction during chronic liver injury

Carl-Philipp Hackstein^{1,12,†,‡}, Jasper Spitzer^{2,†,‡}, Konstantinos Symeonidis¹, Helena Horvatic¹, Tanja Bedke³, Babett Steglich³, Sabine Klein⁴, Lisa M. Assmus¹, Alexandru Odainic², Jennifer Szlapa¹, Nina Kessler¹, Marc Beyer⁵, Ricarda Schmithausen⁶, Eicke Latz², Richard A. Flavell⁷, Natalio Garbi¹, Christian Kurts¹, Beate M. Kümmerer^{8,9}, Jonel Trebicka⁴, Axel Roers¹⁰, Samuel Huber³, Susanne V. Schmidt², Percy A. Knolle^{11,13,‡}, Zeinab Abdullah^{1,*,‡}

Journal of Hepatology 2023. vol. 79 | 150–166



Background & Aims: Patients with chronic liver disease (CLD), including cirrhosis, are at increased risk of intractable viral infections and are hyporesponsive to vaccination. Hallmarks of CLD and cirrhosis include microbial translocation and elevated levels of type I interferon (IFN-I). We aimed to investigate the relevance of microbiota-induced IFN-I in the impaired adaptive immune responses observed in CLD.

Methods: We combined bile duct ligation (BDL) and carbon tetrachloride (CCl₄) models of liver injury with vaccination or lymphocytic choriomeningitis virus infection in transgenic mice lacking IFN-I in myeloid cells (LysM-Cre IFNAR^{flox/flox}), IFNAR-induced IL-10 (MX1-Cre IL10^{flox/flox}) or IL-10R in T cells (CD4-DN IL-10R). Key pathways were blocked *in vivo* with specific antibodies (anti-IFNAR and anti-IL10R). We assessed T-cell responses and antibody titers after HBV and SARS-CoV-2 vaccinations in patients with CLD and healthy individuals in a proof-of-concept clinical study.

Results: We demonstrate that BDL- and CCL₄-induced prolonged liver injury leads to impaired T-cell responses to vaccination and viral infection in mice, subsequently leading to persistent infection. We observed a similarly defective T-cell response to vaccination in patients with cirrhosis. Innate sensing of translocated gut microbiota induced IFN-I signaling in hepatic myeloid cells that triggered excessive IL-10 production upon viral infection. IL-10R signaling in antigen-specific T cells rendered them dysfunctional. Antibiotic treatment and inhibition of IFNAR or IL-10Ra restored antiviral immunity without detectable immune pathology in mice. Notably, IL-10Ra blockade restored the functional phenotype of T cells from vaccinated patients with cirrhosis.

Conclusion: Innate sensing of translocated microbiota induces IFN-/IL-10 expression, which drives the loss of systemic T-cell immunity during prolonged liver injury.

© 2023 The Author(s). Published by Elsevier B.V. on behalf of European Association for the Study of the Liver. This is an open access article under the CC BY-NC-ND license (<http://creativecommons.org/licenses/by-nc-nd/4.0/>).

Introduction

Chronic liver diseases (CLD) such as liver fibrosis and cirrhosis are associated with barrier dysfunction and enhanced microbial translocation into the liver, leading to tonic and chronic type I interferon (IFN-I) signaling, release of pro-inflammatory cytokines and chronic immune cell activation.^{1,2} As the disease progresses, systemic inflammation and structural distortion of liver tissue are believed to determine progressive loss of immune surveillance known as cirrhosis-associated immune dysfunction (CAID).³ Enhanced susceptibility to infections^{4–6} and poor response to vaccination against influenza, hepatitis A and hepatitis B constitute major factors contributing to patients' morbidity and mortality.^{3,7–9} We have previously shown that IFN-I acting on hepatic myeloid cells in the context of bacterial infection during liver damage is responsible for

impaired innate immunity in mouse and man.¹ Interestingly, excessive IFN-I signaling has also been shown to be involved in loss of T-cell functionality in chronic viral infections,¹⁰ rendering the immune system unable to contain infection.

Herein, we report that tonic IFN-I signaling during prolonged liver injury (hereafter referred to as pLI) and cirrhosis determines the loss of systemic CD8 and CD4 T-cell-mediated immunity through induction of the immune-regulatory cytokine IL-10. In preclinical models of bile duct ligation (BDL)- and carbon tetrachloride (CCL₄)-induced pLI and patients with cirrhosis, we identified IL-10 as the key mediator of T-cell dysfunction during chronic liver injury and provide evidence that blocking IL-10 rescues T-cell function and allows for control of viral infection without immune pathology in mice. Given the importance of CD8 and CD4 T-cell responses for immune surveillance, our findings contribute to the understanding of failing immune

Keywords: Chronic liver disease; fibrosis; cirrhosis; T-cell immunity; viral infection; vaccination.

Received 10 August 2022; received in revised form 8 February 2023; accepted 13 February 2023; available online 2 March 2023

* Corresponding author. Address: Venusberg Campus 1, University Hospital Bonn, 53127 Bonn, Germany; Tel.: +49 228 287 11138, fax: +49 228 287 51204.

E-mail address: zeinab.abdullah@uni-bonn.de (Z. Abdullah).

† Contributed equally as first authors

‡ These authors contribute equally

<https://doi.org/10.1016/j.jhep.2023.02.026>



responses in patients with cirrhosis and identify the IL-10Ra signaling pathway as a potential molecular target to improve immune control and vaccination efficacy in these patients.

Materials and methods

Patients and blood samples

Blood and serum samples as well as questionnaire-based assessment of donor characteristics and disease stage were collected from patients with cirrhosis and healthy volunteers before vaccination with TWINRIX (HAV and HBsAg) at the University Hospital Bonn and general practices in Bonn (healthy individuals, $n = 16$; patients with cirrhosis, $n = 16$). All enrolled participants had never been exposed to HBV or vaccinated against HBV or HAV, as proven by the absence of anti-HBs antibodies on serological testing before vaccination. Informed consent was obtained from all patients and healthy individuals enrolled in the trial in accordance with the Declaration of Helsinki protocol. The study was approved by and performed according to the guidelines of the local ethics committees of the University of Bonn (310/16). All enrolled participants received four doses of the vaccine on day 1, 7, 21 and after 6 months. Sample collection was performed 4 to 5 weeks after the last injection. Peripheral blood mononuclear cells (PBMCs) were isolated by Ficoll-Hypaque (PromoCell, Germany) density gradient centrifugation and stored at -80°C until further use. Serum was separated by centrifugation for 10 min and supernatant was stored at -80°C . Detailed characteristics of healthy donors and patients with CLD and the study design are provided in [Table S1 and S2](#) and [Fig. S1E,F](#).

HBs-specific T-cell activation

Forty-three (80-90% purity) 15-mer synthetic peptides, overlapping by 10 amino acids (Xaia Custom Peptides, Sweden) and covering the sequence of the HBV surface antigen (HBsAg) protein according to the Galibert sequence, were generated ([Table S3](#)). Peptides were pooled and used for detection of HBs-specific T cells and their function. After isolation from peripheral blood, untouched CD3 T cells were labelled with CellTrace Violet (0.5 μM ; Thermo Fisher Scientific) and cultured in round-bottom 96-well plates at 5×10^4 /well, in the presence of autologous irradiated (4,000 rads) PBMCs (10^5 /well), HBs peptides and recombinant human IL-2 (50 U/ml; PeproTech). After 5 days of incubation, proliferation and cytokine production in HBs-specific T cells were assessed by flow cytometry.

Anti-RBD (S) SARS-CoV-2 antibodies assay

Serum samples were analyzed for anti-S-RBD IgG titers using the SARS-CoV-2 Plate 7 V-PLEX Serology Kit from MSD (Meso Scale Diagnostics, LLC). Antibody concentrations were quantified via the MESO SECTOR S 600. Raw data was analyzed with the MSD Discovery Workbench tool (V 4.0.13), that quantifies anti-RBD IgG. All assays were performed by trained laboratory technicians according to the manufacturer's standard procedures.

SARS-CoV-2 neutralization assay

Heat-inactivated sera were serially twofold diluted starting with 1:5 dilutions. 120 μl of each serum dilution was mixed with

120 μl of OptiPRO™ SFM cell culture media (Gibco) containing 80 plaque-forming units (PFUs) of SARS-CoV-2 (isolate B.3). After 1 h at 37°C , 200 μl of each mixture was added to wells of a 24 well plate seeded the day before with 1.5×10^5 Vero E6 cells/well. After incubation at 37°C for 1 h, the inoculum was removed and cells were overlaid with a 1:1 mixture of 1.5% carboxymethylcellulose (Sigma) in 2x MEM (Biochrom) with 4% FBS (Gibco). After a 3-day incubation at 37°C , cells were fixed with 6% formaldehyde and stained with 1% crystal violet in 20% ethanol.

In vitro activation and proliferation assay of human T cells

PBMCs were labelled with CellTrace Violet (0.5 μM ; Thermo Fisher Scientific) and cultured in RPMI supplemented with 10% FCS at 1×10^6 cells/well in 96-well plates (Corning) coated with anti-CD3 (clone HIT3a, BioLegend), anti-CD28 (clone L293, BD Biosciences) (each at 3 $\mu\text{l}/\text{ml}$) and IL-2 (10 IU/ml; PeproTech). T-cell proliferation and intracellular cytokine expression, as well mitochondrial assays, were assessed by flow cytometry.

In vitro IL-10Ra blockade on human T cells

PBMCs were cultured in RPMI supplemented with 10% FCS at 1×10^6 cells/well in 96-well plates (Corning) coated with anti-CD3 (clone HIT3a, BioLegend) and anti-CD28 (clone L293, BD Biosciences) (each at 3 $\mu\text{l}/\text{ml}$) and IL-2 (10 IU/ml; PeproTech). 5 $\mu\text{g}/\text{ml}$ of the blocking anti-IL-10Ra antibody (3F9; BioLegend) was added 12 h later.

ELISA for detection of cytokine expression

Human IFN γ , TNF and IL-2 in the supernatant of *in vitro*-activated cells and murine IL-10 in the serum were detected using ELISA MAX Deluxe Set (BioLegend) according to the manufacturer's instructions.

Quantification of mitochondrial membrane potential, mitochondrial mass and mitochondrial superoxide production

Mitochondrial studies in human T cells were performed after anti-CD3 stimulation. Cells were incubated with 50 nM MitoTracker Green (MTG) and/or 25 nM MitoTracker DeepRed (MTDR) for 30 min at 37°C before cell surface staining. Mitochondrial superoxide levels in human T cells were determined, after cell surface staining, by incubation (15 min at 37°C) of overnight anti-CD3 stimulated and unstimulated cells in the presence of MitoSOX Red (5 μM ; Molecular Probes).

Mice

6-9-week-old mice C57BL/6J (B6) were purchased from Janvier (Le Genest-Saint-Isle, France). LysM^{Cre}-IFNAR^{fl/fl} (previously described¹⁸), OT-I, OT-II, CD45.1-B6 (B6.SJL-Ptprca Pepcb/BoyJ), 6C2.36 and P14 mice were originally purchased from The Jackson Laboratory and maintained in the House of Experimental Therapy, University Clinic Bonn. Mx1^{Cre}-Il10^{fl/fl} x Mx1^{Cre} ((Il10^{tm1Roer}) x (C.Cg-Tg(Mx1-Cre)1Cgn/J)) were kindly provided by Axel Roers. IL10Ra^{DN} mice⁴³ were kindly provided by Samuel Huber. All mice were maintained under specific pathogen-free (SPF) conditions and were handled according to the guidelines of the institutional animal guidelines of the animal

IL-10 drives T-cell dysfunction in chronic liver disease

facilities of the University of Bonn. Experimental procedures were approved by the Animal Ethics Committee of the state of North Rhine-Westphalia, Germany. For antibiotic treatment, mice were given a combination of vancomycin (1 g/L), ampicillin (1 g/L), kanamycin (1 g/L), and metronidazole (1 g/L) in drinking water⁷². All antibiotics were obtained from Sigma Aldrich. Colonization of germ-free (GF) mice with caecal microbiota of SPF mice was performed as previously described⁷³. Briefly GF mice received a suspension of the cecum content from wild-type (WT) mice (who had undergone a sham operation or BDL) by oral gavage on 3 consecutive days, and underwent BDL 1 week after the last transfer.

Murine liver injury models

Liver injury was induced in 8–9-week-old male mice via BDL or treatment with CCl₄ following established protocols⁷⁵. In brief, to induce BDL, the animals were treated with painkillers and anaesthetized before the peritoneal cavity was opened along the *linea alba*. Two ligatures were placed around the common bile duct in order to obstruct it, the incisions in the peritoneum and the skin were then closed and the mice were allowed to recover. During the first 5 days after the operation all animals received additional injections of painkillers and liver injury was allowed to develop for 10 days before experiments were performed. Alternatively, mice received 0.5 µl CCl₄/g body weight for 12 weeks intraperitoneally. CCl₄ was dissolved 1:7 in olive oil and was administered at 3-day intervals. After the final injection, mice were allowed to recover for 10 days before further experiments were performed. Control mice underwent a sham operation (no ligation of the bile duct) or received olive oil (i.p.) injections respectively. During all experiments, animals were monitored closely on a daily basis. To inhibit the IFN alpha receptor (IFNAR) or interleukin 10 receptor-alpha (IL-10Ra) signaling *in vivo*, mice were treated intraperitoneally with 250 µg/mouse of blocking antibodies targeting TGFBR-II (clone: 1D11.16.8), IFNAR1 (clone: MAR1-5A3), or IL-10Ra (clone: 1B1.3A) from BioXcell. Control animals received injections containing the HPRN and MOPC-21 antibodies respectively.

LCMV infection

Mice were infected with 2x10⁴ PFUs of lymphocytic choriomeningitis virus (LCMV) strain WE or Armstrong diluted in sterile PBS intravenously.

Irradiation and adoptive cell transfers

Mice were subjected to sublethal irradiation (6 Gy) one day before transfer. T cells were isolated from the spleens and lymph nodes of donor mice and 4x10⁶ CD3⁺ T cells (1:1 of WT and transgenic [TG] cells) per recipient were transferred intravenously. Before any subsequent experiment, recipient mice were allowed to recover for 12 days in order to ensure proper engraftment. For all other infection or vaccination studies, Naïve P14, OT-I and OT-II cells were isolated from the spleens of mice and 2.5x10⁵ cells were transferred 1 day before vaccination.

Murine in vitro T-cell proliferation assay

48-well plates were coated with antibodies directed against murine CD3 (clone: 500A.2, BD Biosciences) and CD28 (clone:

37.51, Biolegend) at a concentration of 0.5 µg/ml and 10 µg/ml, respectively, incubated at 37 °C for 2 h and washed. T cells isolated from the spleens of sham-operated or BDL mice were stained with CellTrace Violet (Thermo Fisher Scientific) and added at a concentration of 2x10⁶ cells/ml. T-cell proliferation was measured after 3 days by flow cytometry.

Flow cytometry and antibodies

Single-cell suspensions were acquired on a FACSCanto II or LSRII Fortessa (DFG ID 216372401) and analyzed with FlowJo (version 10.0.7, Tree star). In order to determine the expression of surface molecules, cells were stained on ice for 20 min. The LIVE/DEAD fixable Near-IR Dead Cell Stain kit (Life Technologies) was used in all staining to detect dead cells, also, an in-house antibody (clone: 2.4G2) directed against the epitopes shared by Fc-gamma receptors was added. Single-cell suspensions from spleen or liver were stimulated with 100 ng/ml or 200 ng/ml PMA, in the presence of Brefeldin A and monensin for 3 h, before collection and intracellular staining for flow cytometry. To block unspecific staining, cytokines were stained after fixation with 4% PFA and permeabilization with 1x Permeabilization buffer (FoxP3/Transcription Factor Staining Buffer Set, eBioScience) and transcription factors with the FoxP3/Transcription Factor Staining Buffer Set according to the manufacturer's instructions. Antibodies directed against the following targets in mice were purchased from Biolegend, eBioScience or Miltenyi: anti-CD3e (145-2C11), anti-CD4 (GK1.5 or RM4-5), anti-CD8a (53-6.7), anti-CD11b (M1/70), anti-CD11c (N418), anti-CD44 (1M7), anti-CD45.1(A20), anti-CD45.2(104), anti-CD146 (ME-9F1), anti-CD210a (1B1.3a), anti-CTLA-4 (UC10-4B9), anti-Eomes (Dan11mag), anti-F4/80 (BM8), anti-GzmB (GB11), anti-IFNγ (XMG1.2), anti-IL-2 (JES6-5H4), anti-IL-21 (FFA2), anti-LAG3 (C9B7W), anti-PD-1 (29F.1A12), anti-T-bet (4B10), anti-IRF4 (IRF4.3E4), anti-TOX (TXRX10), anti-TCF-1 (S33-966), anti-TCRb (H57.597), anti-TIM3 (RMT3-23) and anti-TNF (MP6-XT22), anti-phospho-STAT3 (Stat3Y705-B12) and anti-phospho-SMAD2 (Ser250 (SD207-1)). CD8 and CD4 T-cell tetramers specific for the LCMV epitopes gp33-41 and gp66-77, respectively, were purchased from Immudex (gp33-dextramer) or provided by the NIH Tetramer Core Facility (Emory University). The following antibodies were used to detect protein expression on human cells: anti-CD3 (SK3), anti-CD62L (DREG-56), anti-CD8 (PRA-T8), anti-CD45RA (HI100), anti-CD45 (HI30) from ThermoFisher, and anti-CD4 (PRA-T4), anti-PD1 (EH12.2H7), anti-CTLA4 (BNI3), anti-CD3 (OKT3), anti-IFNγ (4S.B3), anti-IL-21 (3A3-N2), anti-IL-10Ra (3F9) from BioLegend.

Immunofluorescence microscopy

Liver tissue samples were fixed in a 0.05 M phosphate buffer containing, 0.1 M L-lysine, 2 mg/ml NaO₄, and 10 mg/ml paraformaldehyde at pH7.4 overnight. Subsequently, samples were washed in phosphate buffer and dehydrated in 30% sucrose overnight. Finally, samples were placed in Tissue TEK (Sakura Finetek), snap-frozen and stored at -80 °C. 20 µm sections were acquired on a CM3050S cryostat, rehydrated and stained with antibodies in buffer containing 1% normal mouse serum. Pictures were acquired on an LSM 710 confocal Microscope (Zeiss). A BV421-conjugated antibody directed against F4/80 (BM8) was purchased from Biolegend; for detection of the LCMV nucleoprotein, an unconjugated rat-anti-

LCMV antibody (VL4) was purchased from BioXCell; expression was detected via an AF647-conjugated goat-anti-rat antibody (Invitrogen).

RNA extraction, cDNA-synthesis and RT-PCR

Small samples of liver tissue were homogenized in 1 ml Quiazol and total RNA was isolated using the RNeasy Lipid Tissue Kit (Qiagen, 74804). Afterwards, 2–5 µg of RNA was reverse transcribed into cDNA at 37 °C for 2 h using the High-Capacity cDNA Reverse Transcription Kit (Applied Biosystems, 4368814). cDNA was stored at -20 °C and real-time PCR was performed using Taqman primers and probes for *Il10*, *Irf1*, *Mx1*, *Hprt* and *Gapdh* in murine samples and *PDCD1*, *CTLA4*, *CD244*, *EOMES*, *BATF*, *GAPDH* and *HPRT* in human samples. The relative mRNA expression was calculated with the $\Delta\Delta C_t$ -method.

RNA sequencing and data analysis

Transcriptomic differences in isolated T cells from BDL and sham-operated mice were determined by QuantSeq 3'mRNA sequencing (Lexogen). FACS (Aria Fusion DFG ID 387333827) sorted cells were lysed in 700 µl Trizol and stored until RNA extraction was performed with the RNeasy micro kit (Qiagen). Library production for 3'-mRNA sequencing was performed with up to 160 ng purified RNA according to the manufacturers' protocol and sequenced on a HiSeq2500 (Illumina) with a sequencing depth of 15 Mio reads per sample (NGS Core Facility, University Hospital, Bonn, Germany). The alignment was performed with STAR (v2.5.3a) against the murine reference genome mm10. Transcripts were quantified with the Partek E/M algorithm and further processed for normalization in R (v3.5.0) with the DESeq2 algorithm (v1.20.0). The data set was further optimized by flooring transcripts with minimal gene counts at least to ≤ 1 and the exclusion of transcripts with a mean expression ≤ 10 in every test condition. Differentially expressed genes were identified in the Partek Genomics Suite (v7.18.0402) for T cells isolated from BDL vs. sham-operated mice using a one-way-ANOVA (fold-change ≥ 1.5), false discovery rate-adjusted p value ≤ 0.05). Data visualization and biological interpretation were performed with the Partek Genomics Suite, ClueGo plugin (v2.5.2) for Cytoscape (v3.7.2) and R packages ggplot2 (v3.2.1), Enhanced Volcano (v1.6) and tidy (v1.0.2). Heatmaps of two groups were created using means across the two groups, with expression being centered around 0 and visualized with Maya (v2.14).

16S qPCR for quantification of bacterial DNA

DNA was extracted from samples using MoBio PowerSoil kit (Qiagen). DNA concentration was calculated using a standard curve of known DNA concentrations from *E. coli* K12. 16S qPCR with primers identifying different regions of the V6 16S gene was performed using Kappa SYBR fast mix. The absolute number of bacteria in the samples was then approximated as DNA amount in a sample/DNA molecule mass of bacteria. Liver tissue of GF mice was used as an internal control.

Statistical analysis

To determine statistical differences, a two-tailed unpaired or paired Student's t test was used when two groups were

compared; a repeated-measurements one-way ANOVA was used when three groups were compared. For non-parametric data, the Mann-Whitney test was used when comparing two groups and the Kruskal-Wallis test when comparing three or more groups, respectively. Analysis was performed with Prism 8. Statistical significance was set at $p < 0.05$.

Results

Failure of T-cell immunity to control viral infection in mice with CLD

To explore the impact of CLD on T cell-mediated antiviral immune responses, we combined two different mouse models of pLI (*i.e.*, BDL and CCl₄ treatment) with LCMV-WE and LCMV-Armstrong strain infections, which are rapidly cleared by the T-cell response in healthy mice. While healthy mice successfully controlled LCMV replication by day 12 at the latest (Fig. 1A-C, Fig. S1A-D, data not shown), BDL and CCl₄-treated mice failed to clear LCMV-WE from blood, liver and spleen and viral replication persisted for at least 30 days post infection (*p.i.*), indicating a systemic loss of antiviral immune surveillance, rather than a local attenuation of antiviral immunity selectively in the liver. At the peak of the immune response, *i.e.* day 8 *p.i.*, pLI mice showed significantly lower numbers of LCMV-specific CD8 T cells recognizing the gp33 epitope of LCMV compared to healthy mice (Fig. 1D,E and Fig. S1E,F). Moreover, fewer LCMV-specific CD8 T cells were present (and a lower percentage were IFN γ /TNF-producing) in pLI mice (Fig. 1F,G, Fig. S1G), indicating loss of antiviral immune surveillance during pLI independent of its aetiology. Of note, we observed reduced numbers of LCMV-specific CD4 T cells in BDL mice (Fig. 1H,I), that had diminished effector cytokine production with only few cells co-expressing IFN γ , TNF and IL-2 (Fig. S1H,I). To study the defect in virus-specific CD8 T cells in more detail, we transferred TCR-TG P14 CD8 T cells, which express a T-cell receptor specific for the LCMV-gp33 epitope, into BDL mice 1 day before LCMV infection. BDL mice showed reduced frequencies and numbers of IFN γ /TNF-producing T cells compared to sham mice (Fig. S1J-M), confirming the results observed in endogenous T cells. Together, these experiments demonstrated a broad and severe dysfunction of virus-specific T-cell immunity in pLI mice that was associated with failure to control LCMV infection.

Defective T-cell responses to vaccination in patients and mice with liver injury

To assess whether the observations made in the mouse models of BDL- and CCl₄-induced prolonged liver injury recapitulate the phenotype of T cells from patients, we stimulated PBMC-derived T cells from healthy individuals and patients with cirrhosis (Table S1) with anti-CD3/CD28 antibodies to induce antigen-mediated T-cell activation. T cells from patients with CLD produced significantly lower levels of IL-2, IFN γ and TNF (Fig. 2A) which were associated with enhanced apoptosis (AnnexinV^{positive}), lower mitochondrial membrane potential, higher numbers of depolarized mitochondria, and higher levels of reactive oxygen species that failed to increase upon stimulation (Fig. S2A-D). To explore the mechanisms of CLD-associated T-cell dysfunction, we studied the responses of patients with cirrhosis and healthy individuals (Table S1) to

IL-10 drives T-cell dysfunction in chronic liver disease

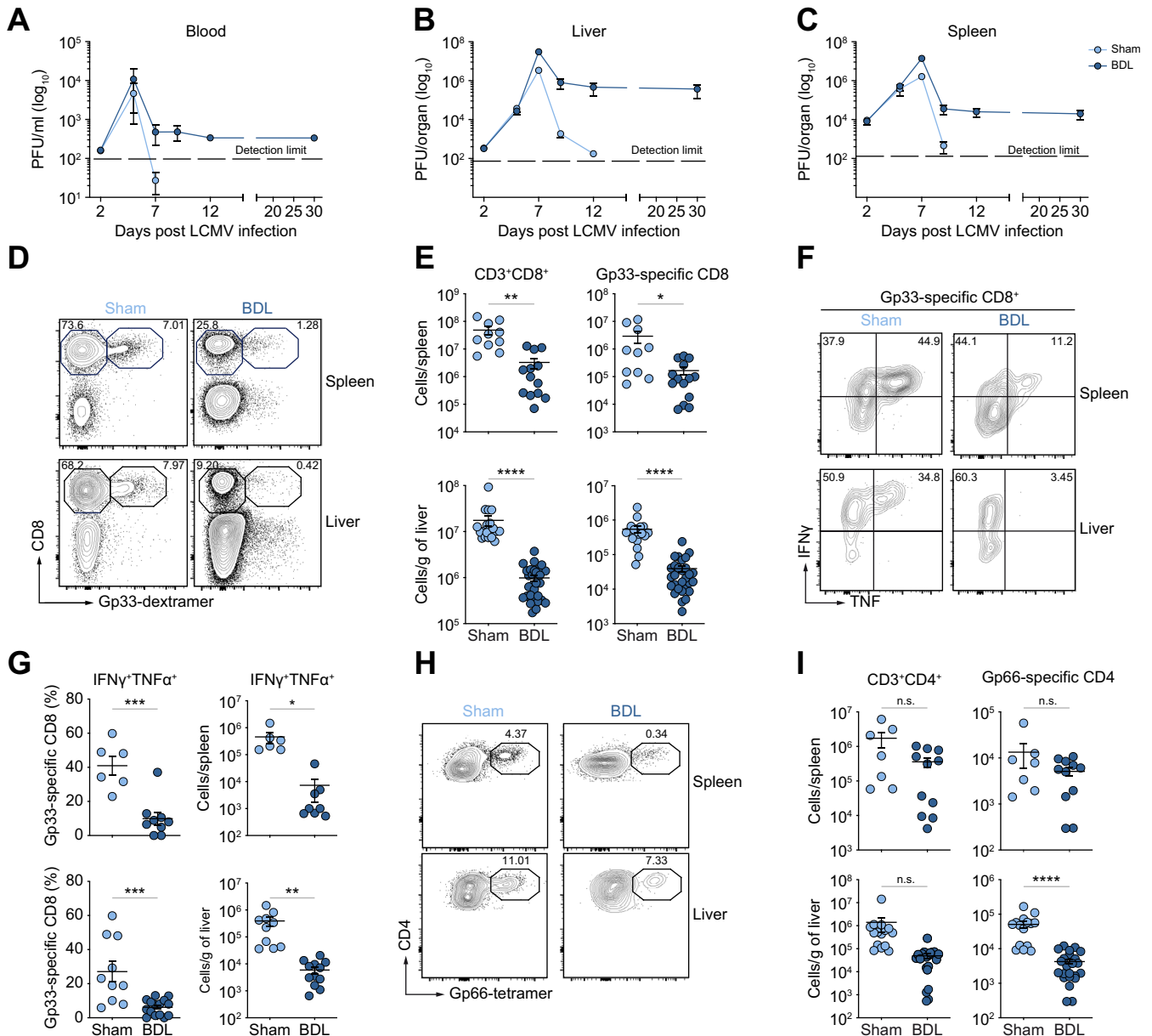


Fig. 1. Impaired antiviral T-cell responses in mice with pLI. BDL- or sham-operated mice were infected with LCMV (2×10^4 PFU) on day 9 post-operation. (A-C) LCMV titers (PFU) in the blood, liver and spleen. (D,E) Total and gp33-specific CD8 T cells from spleen and liver on day 8. (F,G) IFN γ /TNF production by LCMV-specific CD8 T cells. (H,I) Frequencies of total and LCMV-specific CD4 T cells on day 8. (A-C) Data representative of ≥ 3 independent experiments; (E,G,I) pooled data from ≥ 3 independent experiments; statistical analysis by unpaired *t* test. BDL, bile duct ligation; gp33, glycoprotein 33; PFU, plaque forming unit.

HBV vaccination in a proof-of-concept clinical study (Fig. S2E). In line with previous studies,¹¹ 94% of the healthy vaccinees had anti-HBs antibody titers >100 IU/L (strong responders) after vaccination, while only 38% of patients with cirrhosis had a titer >100 IU/L, and 62% had titers between 10-100 IU/L (weak responders) (Fig. 2B). Furthermore, HBs-specific blood-derived CD8 and CD4 T cells from patients with cirrhosis failed to proliferate and to produce IFN γ and IL-21 after stimulation with HBs-specific peptides (Fig. 2C-F). Additionally, we assessed the response to SARS-CoV-2 vaccination in naïve patients with cirrhosis and healthy individuals (Table S2) who received two doses of mRNA (BNT162b2) vaccine (Fig. S2F). Blood samples were obtained before and 7-10 days after the second

vaccination. RBD IgG binding to WT virus – as well as variants of concern, such as B.1.351 (beta), B.1.1.7(alpha) and P.1(gamma) – and neutralization capacity were significantly lower in patients with cirrhosis compared to healthy individuals (Fig. 2G,H, Fig. S2G). Likewise, CD4 and CD8 T cells from patients with cirrhosis produced significantly lower levels of IFN γ upon *in vitro* stimulation with spike protein peptides (Fig. 2I). Together, these results indicate impaired antigen-specific B- and T-cell immunity after vaccination in patients with cirrhosis.

To characterize impaired T-cell immunity after vaccination *in vivo*, we transferred naïve HBs-specific (6C2.36) or ovalbumin-specific CD45.1⁺CD8 (OT-I) and CD4 (OT-II) TG T

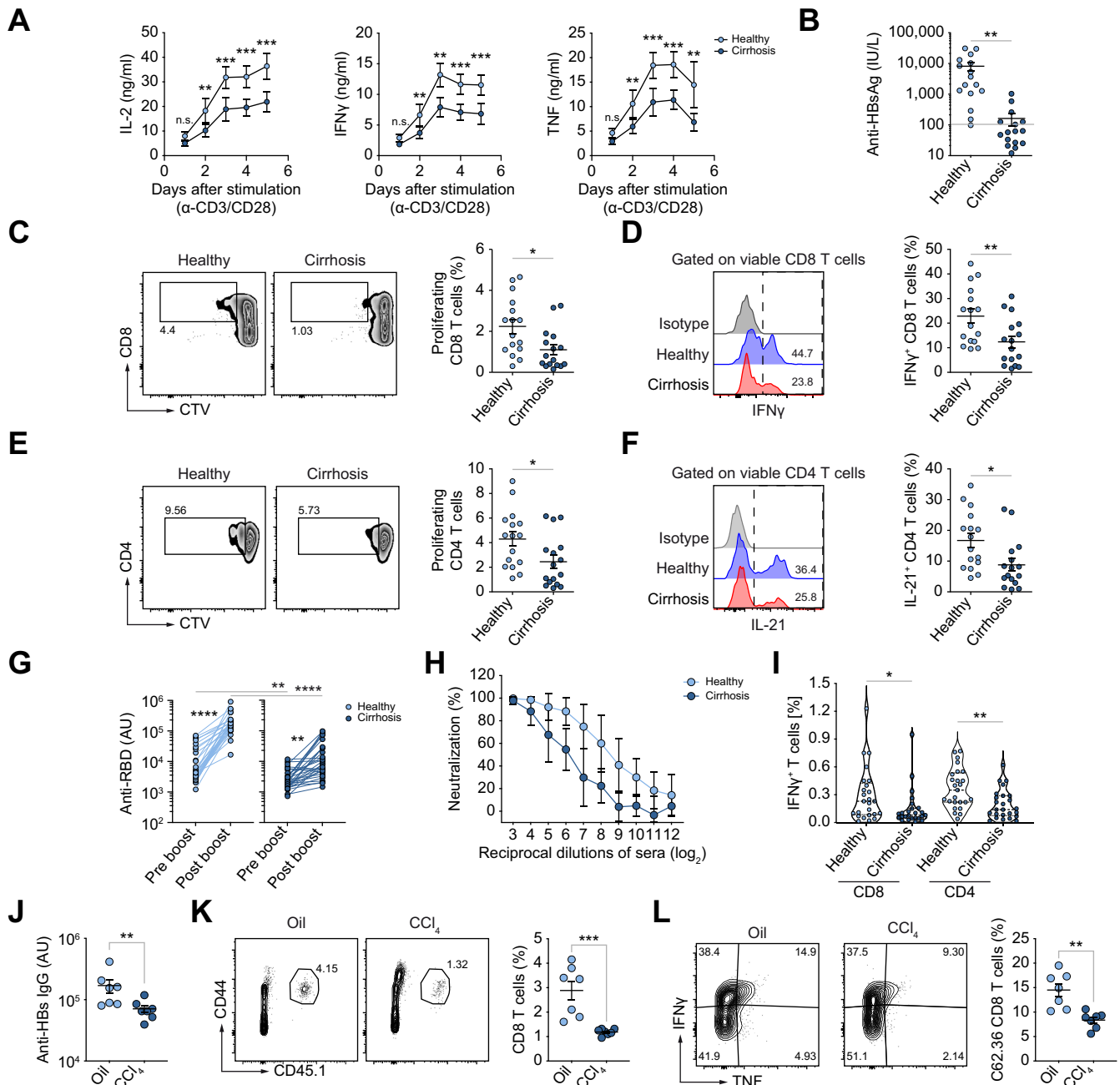


Fig. 2. Poor immune responses to vaccination in patients and mice with cirrhosis. (A) IL-2, IFN γ /TNF-release from anti-CD3/CD28-stimulated T cells from healthy donors or patients with cirrhosis. (B) anti-HBs IgG titers in the sera of healthy donors (n = 16) and patients with cirrhosis (n=16) vaccinated against HBs Ag. (C-F) Frequencies of proliferating and IFN γ -producing CD8 T cells or IL-21-producing CD4 T cells after *ex vivo* stimulation with HBsAg peptides. (G) Serum IgG binding to RBD of SARS-CoV-2 at day 7-10 after the second SARS-CoV-2 mRNA vaccination (BNT162b2). (H) Neutralization of wild-type SARS-CoV-2 by the sera of healthy (n = 7) or cirrhosis (n = 9) vaccinees. (I) Frequencies of IFN γ -producing CD8 and CD4 T cells after *in vitro* stimulation with SARS-CoV-2 spike protein. (J-L) Oil- or CCl₄-treated (12 weeks) mice were vaccinated with HBsAg/polyI:C. (J) Anti-HBs IgG titer on day 7. (K) Percentages of splenic CD45.1+ HBs-specific (6C2.36) CD8 T cells. (L) Frequency of IFN γ /TNF-producing CD8 T cells. Data representative of three (A) or two (H,J,K,L) independent experiments. (A-F, I-L) Statistical analysis by unpaired *t* test, (G) paired Wilcoxon. BNT, Pfizer BioNTech; CCl₄, carbone tetrachloride; HBsAg, hepatitis B virus surface antigen; RBD, receptor binding domain.

cells into CCl₄-treated and BDL mice, respectively, 1 day before vaccination with HBs antigen or ovalbumin with polyI:C as an adjuvant. In line with the results from patients with CLD, we detected significantly lower titers of anti-HBs antibodies (Fig. 2J) as well as lower frequencies of 6C2.36 (Fig. 2K,L), and lower frequencies of OT-I and OT-II cells and reduced

frequencies of IFN γ -, TNF- and IL-2- producing specific T cells (Fig. S2H-K) in the spleen of pLI mice, which suggest reduced T-cell expansion and effector function. Together, these findings suggest that systemic antigen-specific T-cell responses to vaccination were impaired during chronic liver disease and cirrhosis.

IL-10 drives T-cell dysfunction in chronic liver disease

Liver injury renders virus-specific T cells dysfunctional

To fine-map the transcriptional profile of antigen-specific CD8 T cells during pLI, we performed bulk RNA-seq analysis of sorted P14 cells from BDL or sham-operated mice at day 8 post LCMV infection and identified 2,153 differentially expressed genes (Fig. S3A). Gene ontology enrichment analysis and network visualization revealed differences in processes associated with lymphocyte activation, immune effector functions, metabolic and signal transduction processes (Fig. 3A). Genes encoding inhibitory receptors (*Havrc2*, *Pdcd1*, *Ctla4*, and *Lag3*) and inflammation-associated cytokines like *Tnf* and *Il10* were upregulated in T cells from BDL mice, whereas transcription factors associated with effector T-cell functions, namely *Tbet*, *Tcf7*, *Eomes* and *Bcl6*,¹² were downregulated (Fig. 3B,C). P14 T cells from BDL mice showed increased expression of transcription factors associated with T-cell exhaustion, such as *Tox*, *Batf*, *Irf4* and *Id3*^{13,14} (Fig. 3C). Further, gene set enrichment analysis (GSEA) for genes found in T-cell exhaustion in cancer and chronic viral infections¹⁴ showed enrichment for these genes in P14 T cells from pLI mice (Fig. 3D,E). Flow cytometric analysis confirmed expression of these genes at the protein level in both transferred P14 (Fig. 3F) and endogenous LCMV-specific CD8 T cells in BDL mice (Fig. S3B,C). We further detected increased expression of PD1, TIM3 and LAG3 in virus-specific CD8 and CD4 T cells from the liver and spleen of both BDL and CCl₄-treated mice (Fig. S3D-F). To assess whether T-cell dysfunction in pLI coincided with expression of TOX, BATF and IRF4, we determined the expression of IFN γ /TNF and these transcription factors in T cells on day 5 p.i., when precursors of exhausted T cells are known to emerge.¹⁵ Although P14 T cells already lost their effector function by day 5 p.i. in BDL mice, no increased expression of TOX or BATF was detected at this time point (Fig. 3G). These results indicated that T-cell dysfunction during pLI was distinct from TOX-dependent exhausted T cells.

CD4 and CD8 T-cell dysfunction during liver injury is associated with IFN-I signaling

Chronic liver injury is associated with elevated expression of immune regulatory molecules,^{1,16,17} which may curtail T cell-mediated immunity. GSEA revealed enrichment of 148 genes associated with TGF β signaling in P14 T cells from BDL mice (Fig. 4A and Fig. S4A). Consistently, we detected increased levels of TGF β expression in the liver (Fig. 4B) and enhanced levels of phospho-SMAD2 (Fig. 4C), a key downstream effector of TGF β -receptor signaling in LCMV-specific CD8 T cells from BDL mice. To test the relevance of TGF β -receptor signaling on T-cell dysfunction during pLI, we treated BDL mice with TGF β RII-blocking antibodies during LCMV infection. However, 60% of BDL mice succumbed after infection when TGF β -receptor signaling was blocked (Fig. 4D), without evidence for increased viral clearance (Fig. 4E), suggesting a non-redundant and specific function of TGF β in tissue-protection but not immune surveillance during liver injury.

Besides TGF β , we also detected enhanced expression of IFN-I and the interferon-stimulated gene *Mx1* in livers of BDL mice that further increased after LCMV infection (Fig. 4F). GSEA indicated significant enrichment of 230 IFNAR signaling-associated genes¹⁸ in P14 T cells from BDL mice (Fig. 4G, Fig. S4B). Among the top 20 upregulated genes, we found *Irf4*,

Nr4a2, *Mt2*, *Egr2*, *Lclat1* and *Frm4a* (Fig. 4H), which have been associated with T-cell dysfunction in cancer and chronic viral infections,¹⁹ suggesting a potential role of IFN-I in T-cell dysfunction under pLI conditions. As reported before,¹ we found that translocation of gut microbiota in mice with BDL- and CCl₄-induced pLI- and patients with CLD (Fig. S4C,D) induced tonic IFNAR signaling in hepatic myeloid cells (Fig. S4E,F). Interestingly, colonization of BDL GF mice with the microbiome of sham-operated or BDL mice (Fig. S4G) led to comparable levels of IFN-I (Fig. S4H,I), suggesting that chronic IFNAR signaling during pLI was triggered by sensing translocated gut microbiota independent of its composition. More importantly, reduction of intestinal microbial burden by antibiotic treatment led to a reduction of IFN-I expression in the liver and intestine of BDL mice, improved expansion and effector cytokine production by LCMV-specific CD8 T cells and consequently enhanced viral clearance (Fig. S4J and Fig. 4I-K). These results demonstrated a critical role of microbial translocation in IFN-I production and T-cell dysfunction during chronic liver injury.

High IFN-I expression during pLI drives loss of T-cell immunity

Next, we investigated the relevance of IFN-I signaling for loss of T-cell immunity during liver injury. Antibody-mediated blockade of IFNAR in LCMV-infected pLI mice led to significant reduction of IFNAR-induced genes (Fig. S5A). Strikingly, inhibition of IFNAR signaling increased the numbers of total (Fig. S5B) and LCMV-specific CD8 and CD4 T cells in BDL as well as CCl₄-treated mice (Fig. 5A,C, Fig. S5B-H). Blockade of IFNAR signaling led to enhanced expression of IFN γ /TNF in T cells and pronounced reduction of the viral load in pLI mice (Fig. S5A-E, Fig. S5D-H). Further we observed a reduction in PD1, TIM3 and LAG3 and TOX, IRF4 and BATF expression (Fig. S5F-I) in LCMV-specific CD8 T cells. Of note, IFNAR blockade induced higher numbers of TCF1⁺P14 T cells and TCF1⁺TIM3⁻ progenitor exhausted cells (Fig. 5G,I). Thus, tonic IFNAR signaling in pLI mice determined T-cell dysfunction and viral persistence in a similar manner as in chronic LCMV infection with clone 13 and HIV infection.^{10,20}

To explore the relevance of T cell-specific IFNAR signaling in their dysfunction during pLI, we generated CD4-Cre^{ERT2} x IFNAR^{fl/fl} mice, in which tamoxifen injection deleted IFNAR selectively in ~60% of T cells (Fig. S6A). Tamoxifen application from day 3 after LCMV infection, neither restored T-cell function (Fig. S6B,C) nor improved viral clearance (Fig. S6D). Although this does not rule out a direct effect of IFN-I signaling on LCMV-specific CD8 T cells, it rather suggests a role of IFNAR signaling on other immune cell populations that then cause T-cell dysfunction. We therefore ablated IFNAR signaling in myeloid cells (i.e., macrophages, monocytes and neutrophils), using LysM-Cre x IFNAR^{fl/fl} mice. Strikingly, BDL LysM-Cre x IFNAR^{fl/fl} mice showed a better control of LCMV infection compared to IFNAR^{fl/fl} littermates (Cre^{negative}), had higher numbers of total and LCMV-specific CD8 T cells that produced more IFN γ /TNF (Fig. 6A-G) and expressed lower levels of PD1, LAG3 and TIM3 (Fig. S6E,F). This suggests that IFNAR signaling in myeloid immune cells plays a key role in T-cell dysfunction during pLI. Furthermore, we detected elevated IL-10 levels in the blood of pLI mice after LCMV infection that were reduced by anti-IFNAR or antibiotic treatment (Fig. 6H). Likewise, we observed higher levels of phosphorylated-STAT3, the canonical downstream

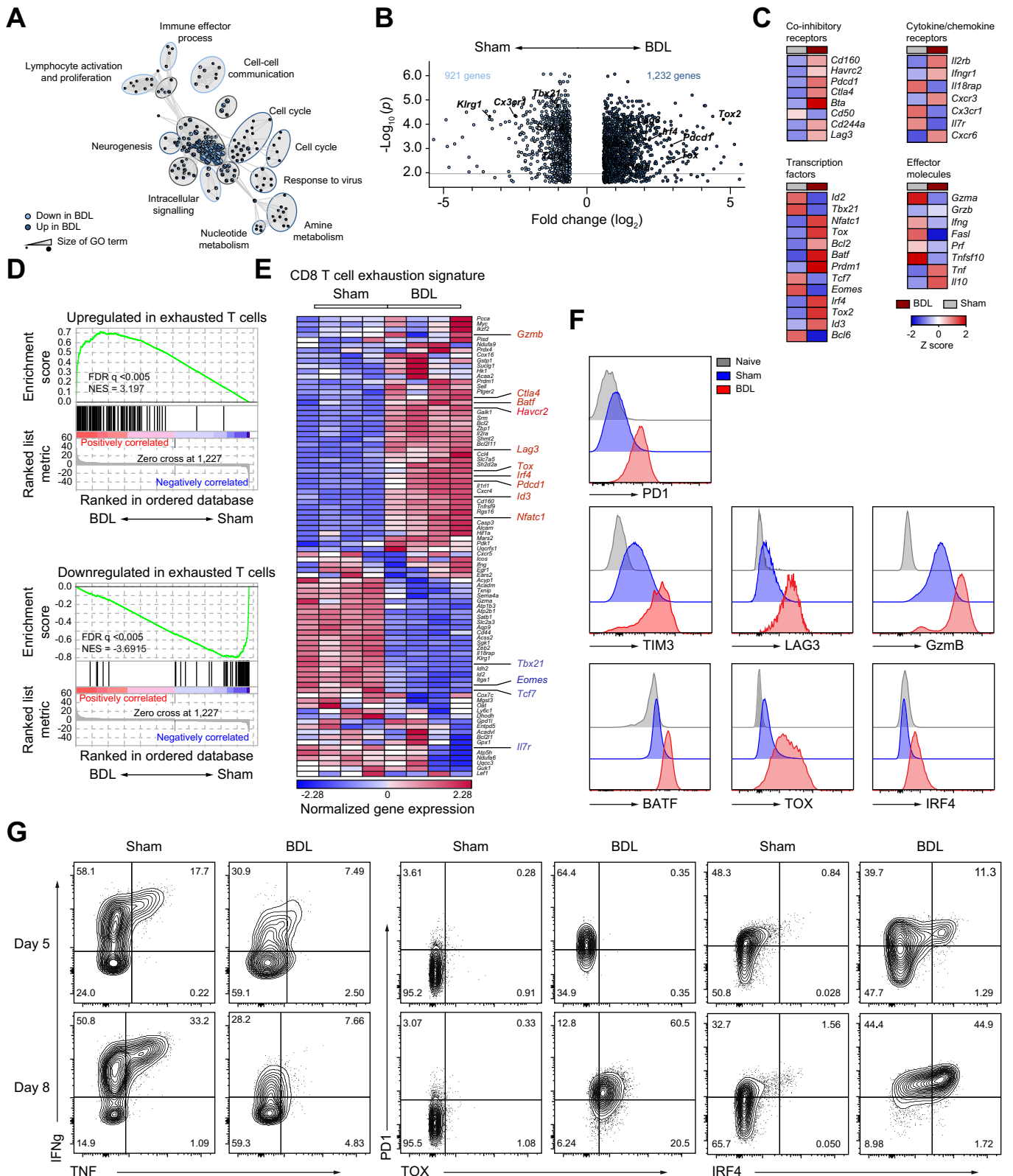


Fig. 3. T-cell exhaustion signature in antigen-specific T cells during pLI. (A-C) Gene-enrichment network (A), volcano plot (B) heatmap of centered mean expression (C) of DE genes in P14 T cells on day 8. (D) GSEA for exhausted T cell-associated genes. (E) Heatmap for DE genes in P14 T cells. (F,G) expression of inhibitory receptors and transcription factors in P14 T cells. (G) IFNg/TNF production, inhibitory receptors and transcription factor expression on day 5 or day 8. (F,G) Data representative of two independent experiments. DE, differentially expressed; GSEA, gene set enrichment analysis.

IL-10 drives T-cell dysfunction in chronic liver disease

signaling molecule of IL-10R, upon anti-IFNAR treatment (Fig. 6I). GSEA showed enrichment of IL-10R-stimulated genes in P14 T cells from BDL mice (Fig. 6J), indicating a role for IFNAR-induced IL-10 in T-cell dysfunction during pLI. To prove

this hypothesis, we generated MX1-Cre x IL-10^{fl/fl} mice, in which *I170* gene is deleted upon expression of the IFNAR-stimulated gene MX1.¹ LCMV-specific CD8 and CD4 T-cell numbers were higher in BDL MX1-Cre x IL-10^{fl/fl} mice (Fig. 6K,L

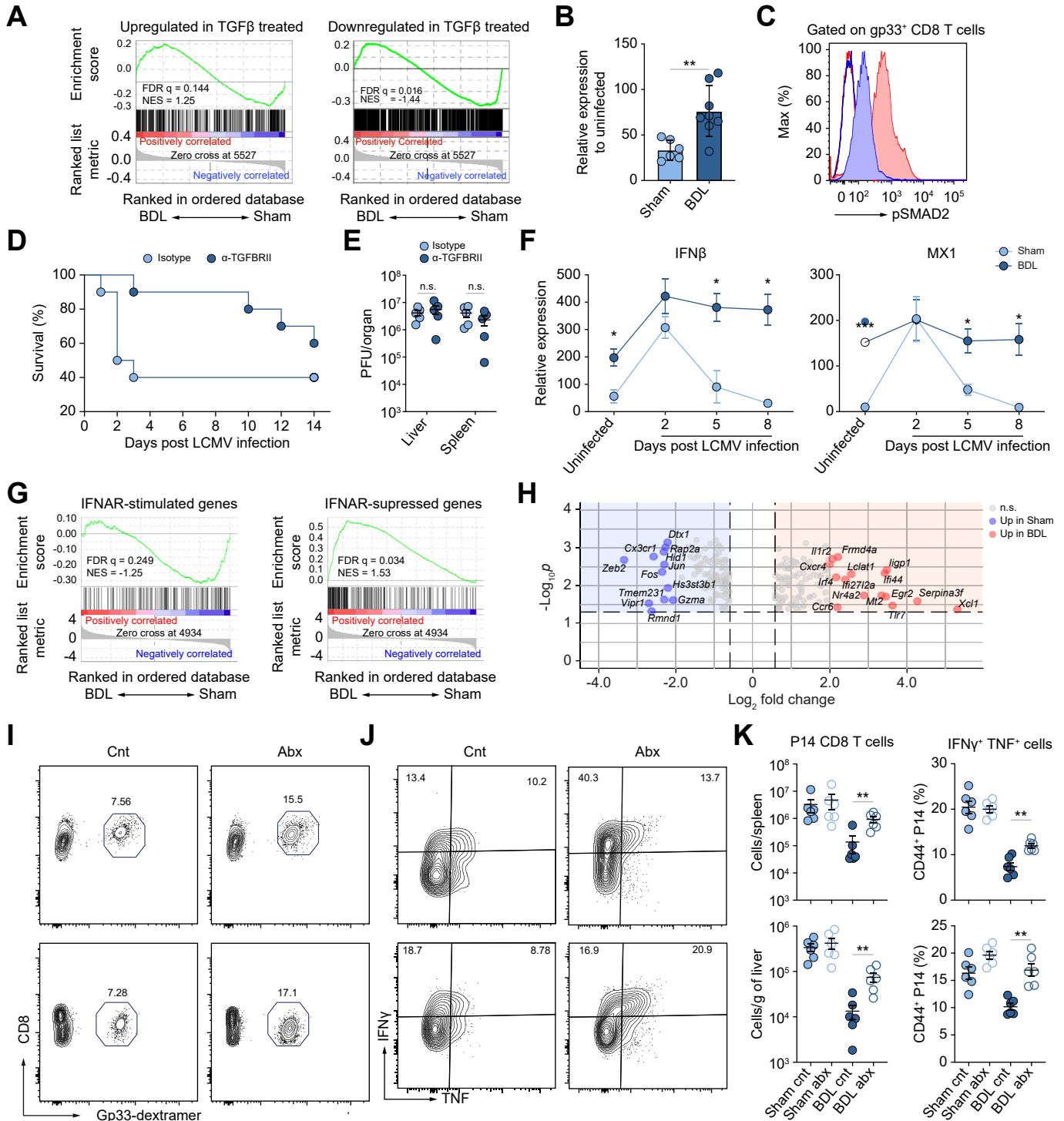


Fig. 4. Microbiota-induced IFN-I drives T-cell dysfunction during pLI. (A) GSEA of TGFβ-associated genes in P14 T cells on day 8 post infection. (B) Expression of TGFβ mRNA in the liver of mice in (A). (C) Phospho-Smad2 in LCMV-specific CD8 T cells. (D) Kaplan-Meier survival curves for LCMV-infected BDL mice receiving anti-TGFβR-II or isotype control. (E) Liver and spleen LCMV titers in mice in (D). (F) IFNβ or Mx1 mRNA expression in the liver. (G,H) GSEA (G) and volcano plot (H) of IFNAR-associated genes in P14 T cells. (I–K) Numbers and frequency of IFNγ/TNF-producing P14 T cells in antibiotic (Abx)-treated BDL mice. (A) One-way ANOVA, (B–F, I–K) Data from ≥2 independent experiments. (B,E,F,K) Statistics were assessed by unpaired t test, (I,K) one-way ANOVA with Dunnett's multiple comparisons test. GSEA, gene set enrichment analysis; TGFβR-II, TGFβ receptor II.

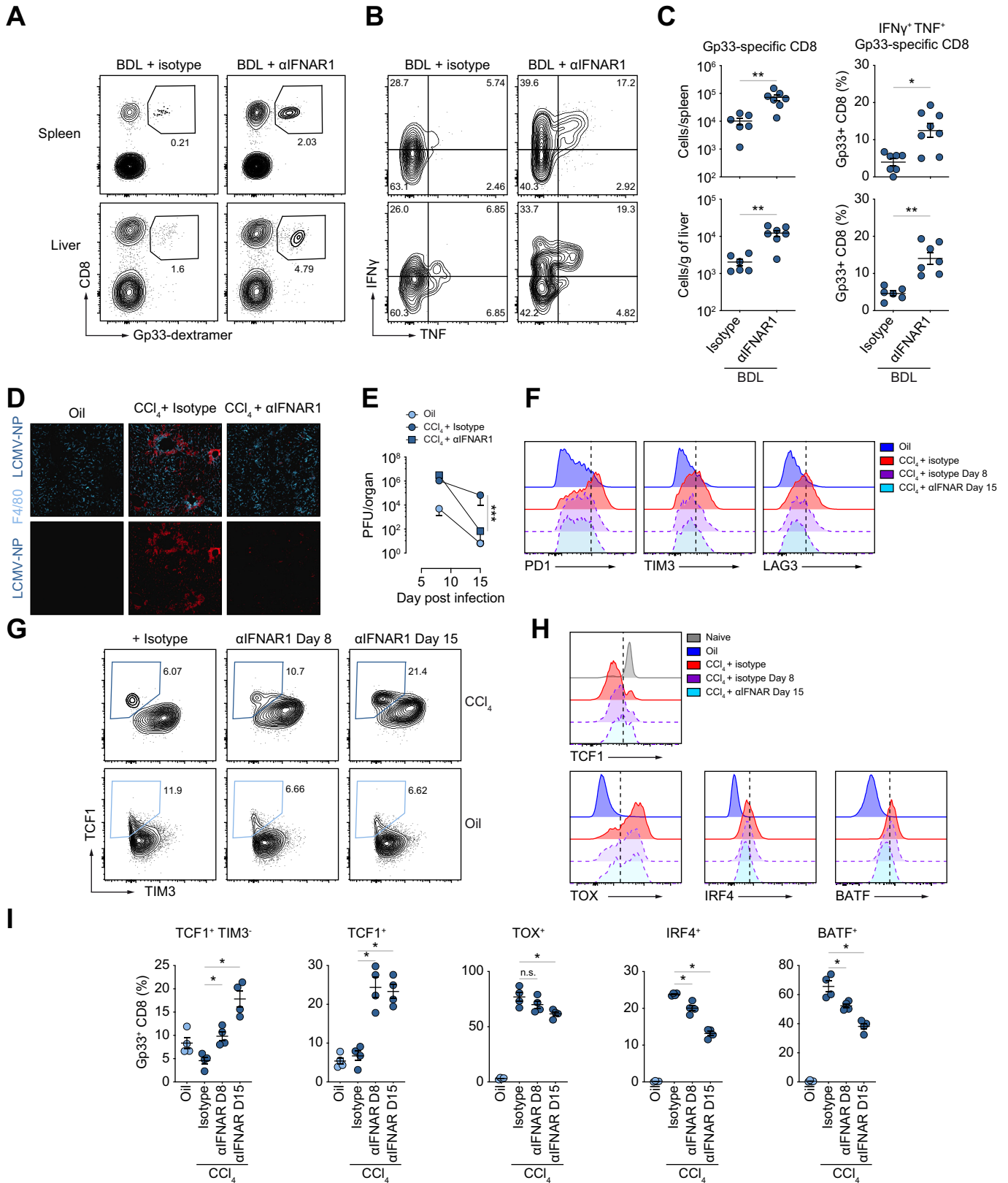
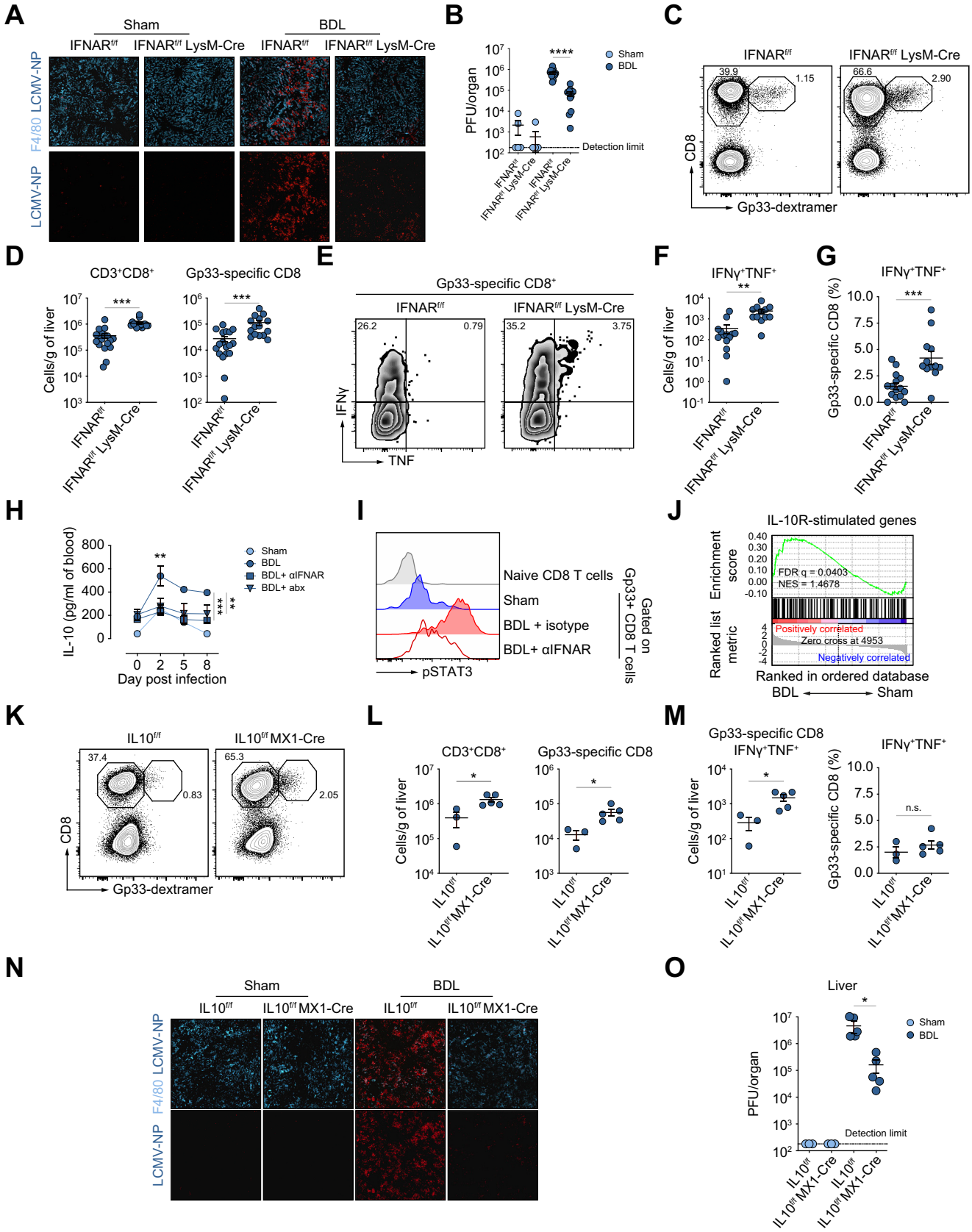


Fig. 5. Abrogation of IFNAR signaling improves LCMV-specific T-cell responses in pLI mice. pLI was induced by BDL or CCl_4 treatment before LCMV infection. Mice were treated with IFNAR1-blocking or isotype antibodies every second day starting at day 5 p.i. (A-C) Numbers of virus-specific and cytokine-producing LCMV-specific CD8 T cells on day 8 (A) and day 15 (B). (D) Liver immunofluorescence on day 15. (E) Quantification of LCMV titers in mice from (E). (F) expression of inhibitory receptors on LCMV-specific CD8⁺ T cells. (G-I) Co-expression of the indicated marker in LCMV-specific CD8 T cells on day 15. (C,E,I) Statistics assessed by unpaired *t* test. BDL, bile duct ligation; CCl_4 , carbon tetrachloride.

IL-10 drives T-cell dysfunction in chronic liver disease



and Fig. S6G,H), with higher levels of IFN γ /TNF production (Fig. 6M, Fig. S6I,J) and a reduced viral load (Fig. 6N,O) compared to littermate control mice. Overall, these data strongly indicate that IFNAR-induced IL-10 expression in myeloid cells contributed to T-cell dysfunction and failure to control viral infection during BDL- and CCL₄-induced pLI.

IL-10 acts directly on antigen-specific T cells during liver injury

To identify cell types on which IL-10 exerts its inhibitory effect, we determined IL-10Ra expression in different immune cell populations. While antigen-experienced (CD44⁺) CD8, CD4 and LCMV-specific T cells in BDL mice expressed higher IL-10Ra levels (Fig. 7A,B, Fig. S7A), no changes in IL-10Ra expression were observed in myeloid immune cells or CD44⁻ T cells (Fig. S7B-D). Importantly, we also detected elevated surface expression levels of IL-10Ra on CD45RA^{neg} T cells in patients with cirrhosis compared to healthy individuals (Fig. 7C), suggesting a higher sensitivity to IL-10 signaling in activated T cells during pLI. To assess the relevance of IFNAR signaling, we treated murine T cells with IFN-I for 48 h before T-cell receptor stimulation *in vitro* or induced IFN-I production *in vivo* by administering polyI:C for 1-3 days. Pre-exposure of T cells to IFN-I upregulated IL-10Ra expression in a time- and dose-dependent manner (Fig. 7D,E).

To investigate whether IL-10 was acting directly on T cells, we co-transferred equal numbers of WT (CD45.2⁺) or CD4-dominant-negative IL-10Ra TG (CD45.1/2⁺) T cells, which over-expressed a dominant-negative IL-10Ra and therefore had impaired IL-10 signaling,²¹ into irradiated WT mice. After induction of liver injury, chimeric mice (Fig. S7E) were infected with LCMV and T cells were analyzed on day 8 p.i. Strikingly, total numbers of activated TG CD8 T cells in the liver were significantly higher compared to WT cells (Fig. 7F). More importantly, CD4 and CD8 T cells with impaired IL-10Ra signaling were more prevalent among LCMV-specific T cells and had superior effector cytokine production compared to WT cells (Fig. 7G,H). Consistently, mice that received IL-10Ra-impaired T cells showed significantly lower viral load compared to their counterparts that received WT T cells (Fig. 7I). Thus, T cells with low responsiveness to IL-10 showed an improved proliferative capacity and effector cytokine production during pLI. Of note, TG LCMV-specific T cells had lower expression levels of PD-1, LAG-3 or TIM3 but no differences in expression of IRF4, TOX or BATF (Fig. 7J, Fig. S7F). Collectively, these results suggested that elevated levels of IL-10 during liver injury were responsible for T-cell dysfunction and impaired viral clearance.

Therapeutic targeting and inhibition of IL-10 signaling restores T-cell responses during liver injury

Next, we investigated whether therapeutic interference with IL-10R downstream signaling restores antiviral T-cell immune

surveillance during liver injury. Efficient IL-10Ra blockade, as indicated by reduced pSTAT3 expression (Fig. S8A), in LCMV-infected BDL and CCL₄-treated mice led to increased numbers of LCMV-specific CD8 T cells with higher IFN γ /TNF production and reduced PD-1, LAG-3 and TIM3 expression (Fig. 8A-D, Fig. S8B-E). Consistently, IL-10Ra blockade reconstituted clearance of viral infection in BDL and CCL₄-treated mice similar to healthy mice by day 15 p.i. (Fig. 8E-G). Moreover, IL-10Ra blockade enhanced the frequencies of TCF1⁺TIM3^{neg} T cells (Fig. S8F) and reduced TOX, IRF4 and BATF expression (Fig. 8H,I). Likewise, we observed a significant increase in the frequency of HBs-specific CD8 T cells, as well IFN γ /TNF CD8 T cells in HBs-vaccinated pLI mice upon treatment with anti-IL-10R antibodies (Fig. S8G,H). Next, we wondered whether interference with IL-10Ra signaling would also restore dysfunctional T cells from patients with CLD. Antibody-mediated blockade of the IL-10Ra in α CD3/CD28-stimulated T cells from patients with cirrhosis reduced PD-1 and CTLA-4 expression (Fig. 8J and Fig. S8I). More importantly, IL-10Ra blockade enhanced the proliferation, as well as IL-21 and IFN γ production (Fig. 8K,L, Fig. S8J,K), of T cells from vaccinated patients with cirrhosis upon stimulation with HBs peptides. Together, these data revealed that therapeutic blockade of IL-10Ra-signaling restored T-cell immune surveillance during BDL- and CCL₄-induced pLI in mice and in patients with cirrhosis.

Discussion

CAID is linked to poor responses to vaccination and occurrence of infections that can cause loss-of-function of remaining liver tissue and thereby trigger life-threatening liver failure,^{7,22-24} against which no specific therapeutic intervention exists. While intractable bacterial infections pose the most prominent threat to patients with cirrhosis,²³ viral infections also cause liver failure and difficult-to-treat infections in these patients.^{25,26} Herein, we identified the IFN-I/IL-10 signaling axis as a determinant of CAID, through which liver damage is linked to suppression of systemic T-cell immunity in response to acute LCMV infection in preclinical models of pLI and to vaccination in pLI mice and patients with cirrhosis.

The outcome of immunity to viral infection is determined by both virus-intrinsic properties and host factors. Virus-intrinsic properties and their contribution to the development of persistent viral infection have been extensively studied, such as LCMV clone 13 infection overcoming antiviral immunity by inducing T-cell exhaustion,¹³⁻¹⁵ HIV achieving persistence through viral integration into the host genome of T cells,²⁶ or HBV establishing robust viral latency in hepatocytes and exploiting the liver's tolerogenic properties.^{27,28} On the other side, host factors^{7,29,30} such as age, inflammation and comorbidities, amongst which antiviral immune responses develop, also shape the outcome of infection.³¹ In patients with COVID-19 and cardiovascular, lung or metabolic diseases, overshooting immune responses that cause organ pathology

Fig. 6. Abrogation of IFNAR/IL-10 axis restores T-cell immunity in pLI. (A-G) IFNAR^{flox/flox} and IFNAR^{flox/flox} × Lysm-Cre mice were infected with LCMV after BDL and analyzed on day 8. (A) Liver immunofluorescence for LCMV nucleoprotein and macrophages, (B) liver LCMV titers. (C,D) Quantification of virus-specific CD8 T cells and (E-G) cytokine-producing T cells. (H) IL-10 levels in blood of BDL mice treated with anti-IFNAR antibodies or antibiotic (Abx). (I) Phospho-STAT3 in LCMV-specific CD8 T cells at day 8 p.i. and after IFNAR-blockade. (J) GSEA of IL-10R-associated genes in LCMV-specific P14 T cells. (K-O) IL10^{fl/fl} Mx1-Cre⁺ or IL10^{fl/fl} (Cre-) littermates were infected with LCMV after the BDL operation. (K-M) Frequencies and numbers of hepatic CD8⁺ T cells, LCMV-specific CD8 T cells and IFN γ /TNF-producing LCMV-specific CD8 T cells. (M) Liver immunofluorescence of LCMV nucleoprotein and macrophages. (O) Liver LCMV titers. Data obtained from three (A-G), or two (K-O) independent experiments. (B,D,F,G,J,N,O) Statistics assessed by unpaired *t* test, (H) one-way ANOVA with Dunnett's multiple comparisons test. BDL, bile duct ligation.

IL-10 drives T-cell dysfunction in chronic liver disease

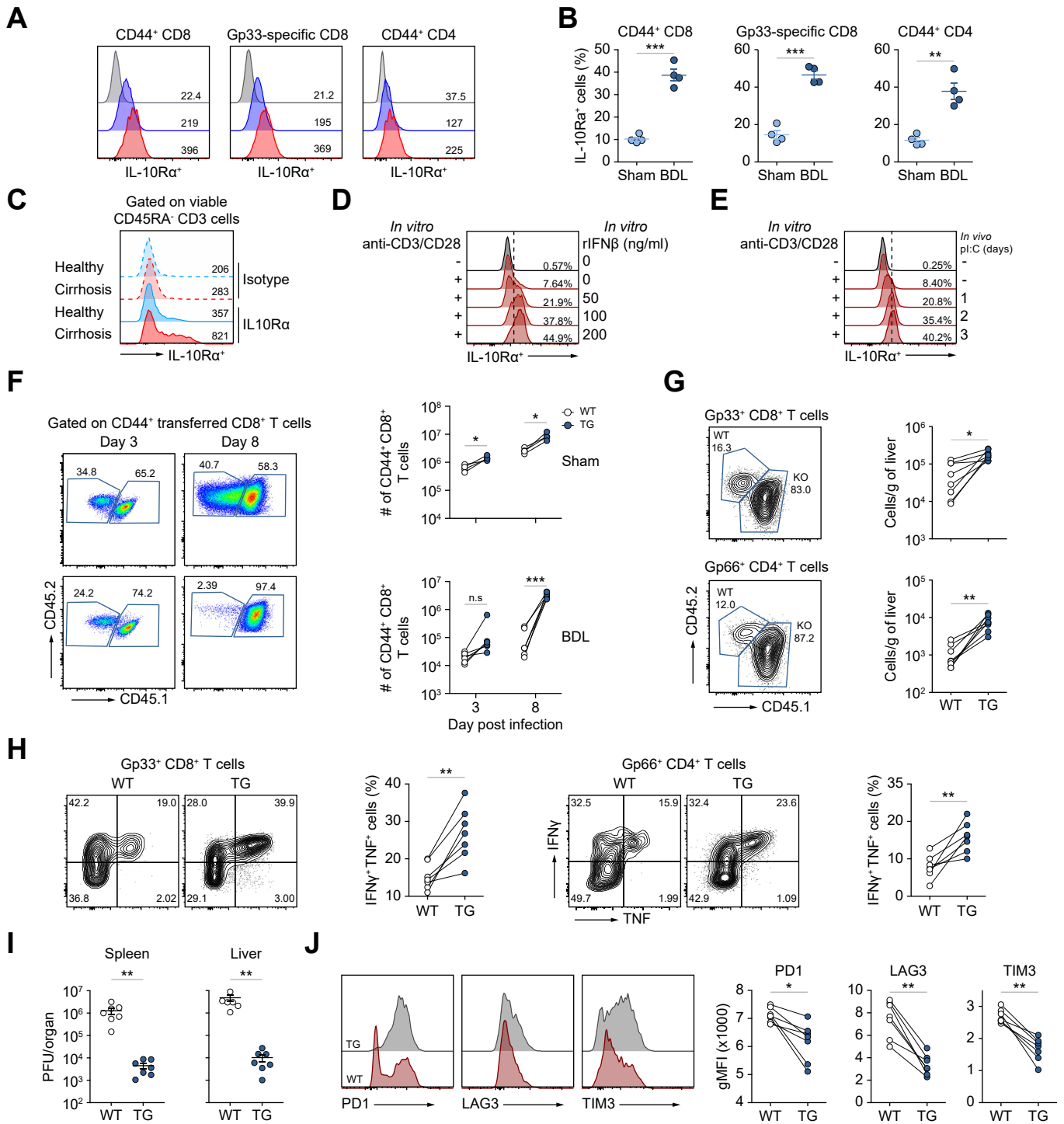


Fig. 7. T-cell-specific IL-10Ra-signaling hampers anti-LCMV immune responses. (A,B) Expression level and percentage of IL-10Ra-expressing T cells from BDL- or sham-operated mice at day 8. (C) IL10Ra expression on peripheral blood CD3⁺CD45RA^{int} T cells of healthy donors or patients with cirrhosis. (D) IL10Ra expression of murine T cells stimulated *ex vivo* with α CD3/CD28 in the presence of increasing IFN β concentrations. (E) IL10Ra expression after *ex vivo* stimulation with α CD3/CD28 in murine T cells isolated 3 days after pl:C application. (F–K) Sub-lethally irradiated B6 mice (CD45.1) received 1:1 mixture of naive WT (CD45.2⁺) and TG (CD45.1/2⁺) T cells. 4 weeks later mice underwent sham operation or BDL and were infected with LCMV. (F–H) Abundance of TG and WT CD8 T cells, (F) LCMV-specific CD8 T cells or LCMV-specific CD4 T cells, (G) IFN γ /TNF production in LCMV-specific T cells (H). (I) Liver and spleen LCMV-titer in BDL mice receiving either WT or TG T cells. (J) Expression of inhibitory receptors in LCMV-specific CD8 T cells. Data from three independent experiments (A–J) and (C) with individual donors. (B,I) Statistics assessed by unpaired *t* tests, and (F–J) two-tailed paired Student's *t* test. BDL, bile duct ligation; TG, transgenic; WT, wild type.

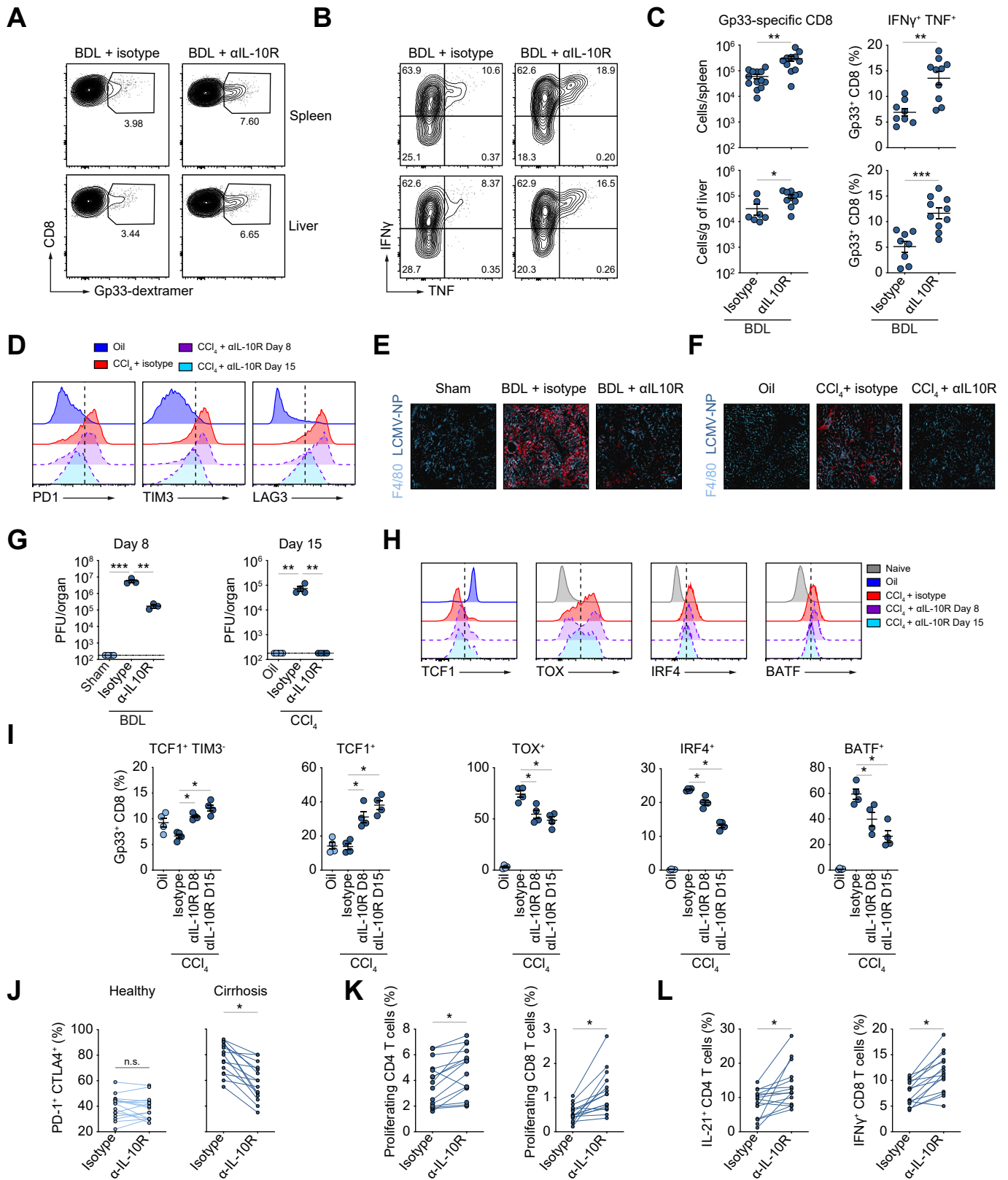


Fig. 8. IL-10Ra blockade restores T-cell immunity during pILI. BDL- or CCI₄-treated mice received anti-IL-10Ra antibody every second day during LCMV infection. (A-C) Frequencies and numbers of LCMV-specific and IFN γ /TNF-producing T cells. (D) Expression of inhibitory receptors by LCMV-specific CD8 T cells (D). (E-G) Liver immunofluorescence and liver LCMV titers. (H,I) Expression of indicated marker in LCMV-specific CD8 T cells. (J) Co-expression of PD1 and CTLA4 in CD8 T cells from PBMCs of healthy controls or patients with cirrhosis after stimulation with anti-CD3/CD28 in the presence of anti-IL10Ra or isotype control. (K,L) T cells from HBsAg-vaccinated healthy controls (n = 4) and patients with cirrhosis (n = 4) stimulated with HBsAg peptides in the presence of anti-IL10Ra or isotype control. (K) Frequencies of proliferating, (l) cytokine-producing CD4 and CD8 T cells. (A-G) Data from three independent experiments and (J-L) one experiment with individual donors. (C,G,I)

IL-10 drives T-cell dysfunction in chronic liver disease

Statistics assessed by unpaired *t* tests. (J-L) two-tailed paired Student's *t* test. n.s., not significant, **p* ≤ 0.05, ***p* ≤ 0.01, ****p* ≤ 0.001, *****p* ≤ 0.0001. HBsAg, hepatitis B virus surface antigen.

are more frequently observed.^{25,32} However, during CLD and cirrhosis patients suffer from an attenuated and dysfunctional immune response, largely driven by loss of tissue architecture and systemic chronic inflammation.^{7,24}

The liver serves as a firewall that eliminates intestinal microbiota that have gained access to portal venous blood.³³ In patients with CLD, increased microbial translocation is believed to cause systemic inflammation.^{34,35} Our results demonstrated that enhanced microbial translocation after liver injury caused increased tonic IFNAR signaling in liver myeloid cells and that abrogation of IFNAR signaling in these cells prevented loss of systemic T-cell immunity. It is well established that intestinal microbiota play a key role in the pathology and progression of liver diseases.^{36,37} Interestingly, reconstitution of GF mice with gut microbiota from either healthy mice or mice with liver injury led to similar levels of IFN-I and similar loss of systemic T-cell immunity. This suggests that IFNAR-induced loss of systemic T-cell immunity during pLI is rather driven by the innate sensing of translocated gut bacteria, and raised the question of how IFN signaling in myeloid cells might regulate T-cell function.

Genome-wide transcriptional and protein profiling of LCMV-specific T cells from pLI mice revealed gene signatures characteristic of exhausted T cells found in cancer or chronic infection. However, loss of T-cell effector function in pLI mice preceded the upregulation of exhaustion-associated transcription factors; TOX, BATF and IRF4, corroborating our assumption that loss of T-cell immunity during liver injury is not a cell-intrinsic process but is driven in a paracrine fashion. Of note, we detected gene signatures for TGFβ, IFN and IL-10 signaling among others. It was previously shown that blockade of TGFβ signaling does not lead to control of persistent viral infection under healthy conditions.³⁸ Our experiments confirmed these findings in the context of pLI and revealed a non-redundant role of TGFβ in organ protection during pLI as its blockade led to severe liver immune pathology. Importantly, after LCMV infection of mice with liver injury we detected increased IL-10 expression in monocytes/macrophages that depended on IFN-I signaling, which is unexpected because IFN-I is considered to be involved in self-perpetuating inflammation.³⁹ In contrast to the immune pathology-promoting effect of

blocking TGFβ, inhibition of IL-10 by antibodies or T cell-specific ablation of IL-10R signaling rescued effector function of LCMV-specific T cells in pLI mice and promoted viral clearance in the absence of notable immune pathology. Likewise, elimination of intestinal microbiota and reducing gut microbial translocation to the liver and blockade of IFN-I signaling in myeloid cells all prevented the excessive production of IL-10 and rescued antiviral T-cell function. Translating these results from preclinical models of liver injury to patients with CLD, our data suggest that inhibition of IL-10R signaling rescued vaccination-induced antigen-specific T cells from their dysfunction.

Although our data provides *in vitro*, *in vivo* and human evidence of this particular mechanism, the study may still have some limitations. First, none of the current mouse models faithfully reflect all etiological and pathophysiological characteristics of chronic liver disease and cirrhosis in humans. The BDL and CCl₄ models used in this study mainly induce prolonged liver injury, which indeed recapitulates several relevant aspects and complications observed in patients with cirrhosis, namely microbial translocation, chronic IFNAR signaling and immune dysfunction. It remains unclear whether acute liver injury or changes in the liver architecture occurring in cirrhosis patients further contribute to the mechanisms described here, such as enhanced gut bacterial translocation, or whether cirrhosis-associated ultrastructural changes themselves may influence hepatic or systemic immunity. Second, IL-10 signaling is a key regulator of immune effector functions and tissue integrity,⁴⁰ and its blockade may therefore carry the risk of inducing immunopathology or autoimmunity. Therefore, future studies aiming at overcoming the limitations of IL-10 signaling in CAID will need to fine-tune the duration, timing and levels of IL-10 inhibition before this approach can be used to increase vaccination efficacy in patients with CLD.

Taken together, our work provides a mechanistic understanding of the loss of systemic T-cell immunity during chronic liver injury, discriminates organ-protective TGFβ-signaling from T-cell suppressing IL-10 signaling and identifies IFN-I and IL-10 as molecular targets for immune interventions that reconstitute T-cell immunity.

Affiliations

¹Institute of Molecular Medicine and Experimental Immunology, University Hospital Bonn, Germany; ²Institute of Innate Immunity, University Hospital Bonn, Germany; ³Medizinische Klinik und Poliklinik, Hamburg Center for Translational Immunology (HCTI), Universitätsklinikum Hamburg-Eppendorf, 20246 Hamburg, Germany; ⁴Medizinische Klinik 1, Universitätsklinikum Frankfurt. Goethe Universität I. Medizinische Klinik und Poliklinik, Germany; ⁵Molecular Immunology in Neurodegeneration, German Center for Neurodegenerative Diseases (DZNE), Bonn, Germany; ⁶Institute for Hygiene and Public Health, University Hospital Bonn, Germany; ⁷Department of Immunobiology, Yale University School of Medicine, New Haven, CT, USA; ⁸Institute of Virology, University Hospital Bonn, Germany; ⁹German Center for Infection Research, Bonn-Cologne site; ¹⁰Institute of Immunology, University of Heidelberg, Germany; ¹¹Institute of Molecular Immunology and Experimental Oncology, Technical University of Munich, Germany; ¹²current address: Peter Medawar Building for Pathogen Research, Nuffield Department of Medicine, University of Oxford, UK; ¹³German Center for Infection Research, Munich site.

Abbreviations

BDL, bile duct ligation/bile duct ligated; CAID, cirrhosis-associated immune dysfunction; CCl₄, carbon tetrachloride; CLD, chronic liver disease; GSEA, gene set-enrichment analysis; IFN, interferon; IFNRA, type I interferon receptors; IL-10, interleukin-10; LCMV, lymphocytic choriomeningitis virus; PBMCs, peripheral blood mononuclear cells; PFUs, plaque-forming units; pLI, prolonged liver injury; TG, transgenic; WT, wild-type.

Financial support

ZA, PAK, SVS were supported by the German Research Foundation (DFG) projects: Excellence Cluster EXC 2151 (ID: 390873048). ZA, PAK were supported by SFBTR57 ((2)-P32 and -P11) (ID: 36842431). ZA, was supported by the GRK 2168 (ID: 272482170), SFB1454 (P10) (ID: 432325352), SFBTR237 (B15) (ID: 369799452), and by the German Federal Ministry of Education and Research (BMBF) for the COVIMMUNE project. CPH was supported by the DFG (project

number 403193363) and the Wellcome Trust (WT109965MA). PAK was supported by the European Union's Horizon 2020 research and innovation programme TherVacB, by the SFB-TRR179 and the German Center for Infection Research, Munich site. The DFG funded equipment used for flow cytometry (project numbers 21637201, 471514137, 387333827, and 216372545).

Conflict of interest

The authors declare that they have no conflict of interest.

Please refer to the accompanying ICMJE disclosure forms for further details.

Authors' contributions

Acquisition of data (CPH, JS, LMA, HH, SVS, RS, SK, TB, JS, BMK, ZA, BS, NK); study concept and design (CPH, CK, JT, NG, BMK, AR, SVS, ZA, PAK); analysis and interpretation of data (CPH, JS, SVS, ZA, KS, NG, AR, EL, JT, PAK); drafting the manuscript (ZA, PAK, CPH, AR, SVS).

Data availability statement

All data from this study are provided in the source data. RNA-seq expression data are available at NCBI GEO under the accession number: GSE158261. Primary data from flow cytometry or immunohistochemistry are available upon reasonable request.

Acknowledgments

We thank Alisa Ismaili, Maike Kreutzenbeck, Janett Wieseler, Sven Kröcker and Rebecca Balduf for technical assistance. We thank Dr. Michael Brinkmann and Lisa Brinkmann for the excellent support of the vaccination studies. We would like to acknowledge the support by the Flow Cytometry and Next Generation Sequencing Core Facilities at the Medical Faculty at the University of Bonn. The DFG funded equipment used for flow cytometry (project numbers 21637201, 471514137, 387333827, and 216372545).

Supplementary data

Supplementary data to this article can be found online at <https://doi.org/10.1016/j.jhep.2023.02.026>.

References

Author names in bold designate shared co-first authorship

- [1] **Hackstein CP, Assmus LM**, Welz M, Klein S, Schwandt T, Schultze J, et al. Gut microbial translocation corrupts myeloid cell function to control bacterial infection during liver cirrhosis. *Gut* 2017;66:507–518.
- [2] Wiest R, Lawson M, Geuking M. Pathological bacterial translocation in liver cirrhosis. *J Hepatol* 2014;60:197–209.
- [3] Albillos A, Lario M, Alvarez-Mon M. Cirrhosis-associated immune dysfunction: distinctive features and clinical relevance. *J Hepatol* 2014;61:1385–1396.
- [4] Chou AL, Huang WW, Lin MN, Su CC. Human herpesvirus type 8 in patients with cirrhosis independent of thrombocytopenia. *J Clin Pathol* 2010;63:254–258.
- [5] Premkumar M, Devurgowda D, Dudha S, Maiwall R, Bihari C, Grover S, et al. A/H1N1/09 influenza is associated with high mortality in liver cirrhosis. *J Clin Exp Hepatol* 2019;9:162–170.
- [6] Schutte A, Ciesek S, Wedemeyer H, Lange CM. Influenza virus infection as precipitating event of acute-on-chronic liver failure. *J Hepatol* 2019;70:797–799.
- [7] Albillos A, Martin-Mateos R, Van der Merwe S, Wiest R, Jalan R, Alvarez-Mon M. Cirrhosis-associated immune dysfunction. *Nat Rev Gastroenterol Hepatol* 2022;19:112–134.
- [8] Alter MJ. Vaccinating patients with chronic liver disease. *Gastroenterol Hepatol (N Y)* 2012;8:120–122.
- [9] Arvaniti V, D'Amico G, Fede G, Manousou P, Tsochatzis E, Pleguezuelo M, et al. Infections in patients with cirrhosis increase mortality four-fold and should be used in determining prognosis. *Gastroenterology* 2010;139:1246–1256. 1256 e1241-1245.
- [10] Zhen A, Rezek V, Youn C, Lam B, Chang N, Rick J, et al. Targeting type I interferon-mediated activation restores immune function in chronic HIV infection. *J Clin Invest* 2017;127:260–268.
- [11] Roni DA, Pathapati RM, Kumar AS, Nihal L, Sridhar K, Tumkur Rajashekar S. Safety and efficacy of hepatitis B vaccination in cirrhosis of liver. *Adv Virol* 2013;2013:196704.
- [12] Intlekofer AM, Takemoto N, Wherry EJ, Longworth SA, Northrup JT, Palanivel VR, et al. Effector and memory CD8+ T cell fate coupled by T-bet and eomesodermin. *Nat Immunol* 2005;6:1236–1244.
- [13] Khan O, Giles JR, McDonald S, Manne S, Ngo SF, Patel KP, et al. TOX transcriptionally and epigenetically programs CD8(+) T cell exhaustion. *Nature* 2019;571:211–218.
- [14] **Man K, Gabriel SS**, Liao Y, Gloury R, Preston S, Henstridge DC, et al. Transcription factor IRF4 promotes CD8(+) T cell exhaustion and limits the development of memory-like T cells during chronic infection. *Immunity* 2017;47:1129–1141 e1125.
- [15] **Utzscheider DT, Gabriel SS**, Chisanga D, Gloury R, Gubser PM, Vasanthakumar A, et al. Early precursor T cells establish and propagate T cell exhaustion in chronic infection. *Nat Immunol* 2020;21:1256–1266.
- [16] **Beyer M, Abdullah Z, Chemnitz JM**, Maisel D, Sander J, Lehmann C, et al. Tumor-necrosis factor impairs CD4(+) T cell-mediated immunological control in chronic viral infection. *Nat Immunol* 2016;17:593–603.
- [17] Seki E, De Minicis S, Osterreicher CH, Kluwe J, Osawa Y, Brenner DA, et al. TLR4 enhances TGF-beta signaling and hepatic fibrosis. *Nat Med* 2007;13:1324–1332.
- [18] Rusinova I, Forster S, Yu S, Kannan A, Masse M, Cumming H, et al. Interferome v2.0: an updated database of annotated interferon-regulated genes. *Nucleic Acids Res* 2013;41:D1040–D1046.
- [19] Williams MA, Bevan MJ. Immunology: exhausted T cells perk up. *Nature* 2006;439:669–670.
- [20] Teijaro JR, Ng C, Lee AM, Sullivan BM, Sheehan KC, Welch M, et al. Persistent LCMV infection is controlled by blockade of type I interferon signaling. *Science* 2013;340:207–211.
- [21] **Kamanaka M, Huber S, Zenewicz LA**, Gagliani N, Rathinam C, O'Connor Jr W, et al. Memory/effector (CD45RB(lo)) CD4 T cells are controlled directly by IL-10 and cause IL-22-dependent intestinal pathology. *J Exp Med* 2011;208:1027–1040.
- [22] Arroyo V, Moreau R, Kamath PS, Jalan R, Ginès P, Nevens F, et al. Acute-on-chronic liver failure in cirrhosis. *Nat Rev Dis Primers* 2016;2:16041.
- [23] Moreau R, Jalan R, Gines P, Pavesi M, Angeli P, Cordoba J, et al. Acute-on-chronic liver failure is a distinct syndrome that develops in patients with acute decompensation of cirrhosis. *Gastroenterology* 2013;144:1426–1437. 1437.e1421-e1429.
- [24] Hasa E, Hartmann P, Schnabl B. Liver cirrhosis and immune dysfunction. *Int Immunol* 2022;34:455–466.
- [25] Brodin P. Immune determinants of COVID-19 disease presentation and severity. *Nat Med* 2021;27:28–33.
- [26] Cohn Lillian B, Silva Israel T, Oliveira Thiago Y, Rosales Rafael A, Parrish Erica H, Learn Gerald H, et al. HIV-1 integration landscape during latent and active infection. *Cell* 2015;160:420–432.
- [27] **Limmer A, Ohl J**, Kurts C, Ljunggren HG, Reiss Y, Groettrup M, et al. Efficient presentation of exogenous antigen by liver endothelial cells to CD8+ T cells results in antigen-specific T-cell tolerance. *Nat Med* 2000;6:1348–1354.
- [28] Protzer U, Maini MK, Knolle PA. Living in the liver: hepatic infections. *Nat Rev Immunol* 2012;12:201–213.
- [29] Lebosse F, Gudd C, Tunc E, Singanayagam A, Nathwani R, Triantafyllou E, et al. CD8(+) T cells from patients with cirrhosis display a phenotype that may contribute to cirrhosis-associated immune dysfunction. *EBioMedicine* 2019;49:258–268.
- [30] Wasmuth HE, Kunz D, Yagmur E, Timmer-Stranghoner A, Vidacek D, Siewert E, et al. Patients with acute on chronic liver failure display “sepsis-like” immune paralysis. *J Hepatol* 2005;42:195–201.
- [31] Virgin HW, Wherry EJ, Ahmed R. Redefining chronic viral infection. *Cell* 2009;138:30–50.
- [32] Cao X. COVID-19: immunopathology and its implications for therapy. *Nat Rev Immunol* 2020;20:269–270.
- [33] Balmer ML, Slack E, de Gottardi A, Lawson MA, Hapfelmeier S, Miele L, et al. The liver may act as a firewall mediating mutualism between the host and its gut commensal microbiota. *Sci Transl Med* 2014;6:237ra266.
- [34] Hartmann P, Chu H, Duan Y, Schnabl B. Gut microbiota in liver disease: too much is harmful, nothing at all is not helpful either. *Am J Physiol Gastrointest Liver Physiol* 2019;316:G563–G573.
- [35] Trebicka J, Macnaughtan J, Schnabl B, Shawcross DL, Bajaj JS. The microbiota in cirrhosis and its role in hepatic decompensation. *J Hepatol* 2021;75(Suppl 1):S67–S81.
- [36] Wang R, Tang R, Li B, Ma X, Schnabl B, Tilg H. Gut microbiome, liver immunology, and liver diseases. *Cell Mol Immunol* 2021;18:4–17.

IL-10 drives T-cell dysfunction in chronic liver disease

- [37] Trebicka J, Bork P, Krag A, Arumugam M. Utilizing the gut microbiome in decompensated cirrhosis and acute-on-chronic liver failure. *Nat Rev Gastroenterol Hepatol* 2021;18:167–180.
- [38] Boettler T, Cheng Y, Ehrhardt K, von Herrath M. TGF-beta blockade does not improve control of an established persistent viral infection. *Viral Immunol* 2012;25:232–238.
- [39] Crow YJ, Lebon P, Casanova JL, Gresser I. A brief historical perspective on the pathological consequences of excessive type I interferon exposure *in vivo*. *J Clin Immunol* 2018;38:694–698.
- [40] O'Garra A, Barrat FJ, Castro AG, Vicari A, Hawrylowicz C. Strategies for use of IL-10 or its antagonists in human disease. *Immunol Rev* 2008;223:114–131.

3.3 Publication 3: CD4+ T cell calibration of antigen-presenting cells optimizes antiviral CD8+ T cell immunity



CD4⁺ T cell calibration of antigen-presenting cells optimizes antiviral CD8⁺ T cell immunity

Received: 8 November 2021

Accepted: 13 April 2023

Published online: 15 May 2023

 Check for updates

Elise Gressier ^{1,16}✉, Jonas Schulte-Schrepping ^{2,3,16}, Lev Petrov⁴, Sophia Brumhard⁵, Paula Stubbemann⁵, Anna Hiller⁵, Benedikt Obermayer ⁶, Jasper Spitzer ⁷, Tomislav Kostevc⁴, Paul G. Whitney¹, Annabell Bachem¹, Alexandru Odainic ^{1,7}, Carolien van de Sandt ¹, Thi H. O. Nguyen ¹, Thomas Ashhurst ⁸, Kayla Wilson ¹, Clare V. L. Oates¹, Linden. J. Gearing ^{9,10}, Tina Meischel ¹, Katharina Hochheiser¹, Marie Greyer¹, Michele Clarke¹, Maike Kreutzenbeck⁷, Sarah S. Gabriel ¹, Wolfgang Kastenmüller ¹¹, Christian Kurts¹², Sarah L. Londrigan ¹, Axel Kallies ¹, Katherine Kedzierska ¹, Paul J. Hertzog^{9,10}, Eicke Latz ⁷, Yu-Chen E. Chen¹³, Kristen J. Radford ¹³, Michael Chopin¹⁴, Jan Schroeder¹, Florian Kurth ⁵, Thomas Gebhardt ¹, Leif E. Sander ⁵, Birgit Sawitzki⁴, Joachim L. Schultze^{2,3,15}, Susanne V. Schmidt^{7,17} & Sammy Bedoui ^{1,12,17}✉

Antiviral CD8⁺ T cell immunity depends on the integration of various contextual cues, but how antigen-presenting cells (APCs) consolidate these signals for decoding by T cells remains unclear. Here, we describe gradual interferon- α /interferon- β (IFN α / β)-induced transcriptional adaptations that endow APCs with the capacity to rapidly activate the transcriptional regulators p65, IRF1 and FOS after CD4⁺ T cell-mediated CD40 stimulation. While these responses operate through broadly used signaling components, they induce a unique set of co-stimulatory molecules and soluble mediators that cannot be elicited by IFN α / β or CD40 alone. These responses are critical for the acquisition of antiviral CD8⁺ T cell effector function, and their activity in APCs from individuals infected with severe acute respiratory syndrome coronavirus 2 correlates with milder disease. These observations uncover a sequential integration process whereby APCs rely on CD4⁺ T cells to select the innate circuits that guide antiviral CD8⁺ T cell responses.

Antigen-presenting cells (APCs) depend on capturing and presenting viral antigens through major histocompatibility complex (MHC) molecules to prime naive T cells and restimulate antigen-experienced T cells during virus infections^{1–3}. Effective T cell responses also hinge on a variety of non-antigenic signals that are relayed from APCs to T cells by co-stimulatory molecules and soluble mediators. It is well established that such contextual cues broadly reflect the exposure of APCs to inflammatory cytokines, such as interferon- α /interferon- β (IFN α / β) and danger signals that stimulate the NF- κ B pathway^{3,4}. Yet, the number of co-stimulatory molecules and soluble mediators that APCs use to convey these cues to T cells is discrete, and the expression of many of these factors continues

to change as the APCs interact with T cells. For example, CD4⁺ T cells responding to antigen rapidly increase the expression of CD40L and provide stimulation back to the APC via CD40 and the NF- κ B pathway⁵. Such ‘T cell help’ involves cooperation with innate stimuli^{6,7}, but how APCs integrate these different signals at the cellular level and whether such cooperation requires prolonged interactions with CD4⁺ T cells or follows more dynamic patterns is currently unclear. Resolving how APCs integrate and relay these different signals to CD8⁺ T cells is important for our general understanding of how the innate–adaptive cross-talk regulates T cell responses and will provide key insights required to improve CD8⁺ T cell responses during infection and vaccination.

A full list of affiliations appears at the end of the paper. ✉ e-mail: elise.gressier07@gmail.com; sbedoui@unimelb.edu.au

Here, we systematically dissected how APCs integrate stimulation through IFN α/β and CD40 from CD4⁺ T cells. We identified an iterative process whereby APCs require IFN α/β -dependent rewiring of the signaling cascade downstream of CD40 that enables the subsequent partition of NF- κ B-, IRF1- and FOS-dependent genes into distinct patterns of co-stimulatory molecule expression and mediator provision. This carefully sequenced integration process is critical for antiviral CD8⁺ T cell responses in a mouse virus infection model, and its activity in APCs from individuals infected with severe acute respiratory syndrome coronavirus 2 (SARS-CoV-2) correlates with CD8⁺ T cell responses and milder forms of coronavirus disease 2019 (COVID-19).

Results

IFN α/β and CD40 induce distinct responses by dendritic cells

To dissect how APCs integrate signals from IFN α/β and CD40 stimulation, we initially focused on type I conventional dendritic cells (cDC1s), known platforms for T cell help^{8,9}. We exposed bone marrow-derived CD24^{hi}CD11b^{lo} cDC1s (hereafter, BMDC1s) to IFN α and an antibody that mimics T cell help by cross-linking CD40⁶. RNA sequencing (RNA-seq) revealed that CD40 induced some changes in BMDC1s, but this response was limited compared to >1,000 differentially expressed (false discovery rate (FDR) > 0.05, 1.5-fold change) genes induced by IFN α (Fig. 1a and Supplementary Table 1). Most IFN-stimulated genes (ISGs)¹⁰ remained unaffected by additional CD40 stimulation (Fig. 1a, 'CD40-unresponsive genes'). However, a subgroup of genes, which included *Ccl4* and *Il15*, was further increased when IFN α and CD40 antibody were applied together (Fig. 1a, 'amplified genes'). We also observed genes that could not be induced by either stimulus alone but were strongly increased in BMDC1s exposed to both IFN α and CD40 antibody (Fig. 1a, 'combinatorial genes'). This response included *Ccl5* and *Tnf* and other genes with known roles in the interplay between APCs and T cells, such as *Cd83* and *Cxcl16* (Fig. 1a). We validated these distinct response patterns in separate experiments, focusing on interleukin-15 (IL-15) and CCL4 as examples for the amplified response and tumor necrosis factor- α (TNF- α) and CCL5 for the combinatorial synergy between IFN α and CD40 stimulation (Fig. 1b,c and Extended Data Fig. 1a). Comparable responses could also be elicited when CD40 synergized with IFN β (Extended Data Fig. 1b) or other innate stimuli, such as polyinosinic–polycytidylic acid (poly(I:C)), lipopolysaccharide (LPS) or cytosine–phosphate–guanine (CpG), which triggered Toll-like receptor 3 (TLR3), TLR4 and TLR9, respectively (Extended Data Fig. 1c). These findings indicate that CD40 synergizes with various innate stimuli in inducing 'amplified' and 'combinatorial' responses in BMDC1s.

cDC1s require *in vivo* stimulation from both IFN α/β and CD4⁺ T cells through CD40 to 'amplify' their capacity to provide IL-15 to herpes simplex virus (HSV)-specific CD8⁺ T cells⁶. To investigate whether priming of HSV-specific CD8⁺ T cells requires mediators that can only be induced by the synergy between IFN α/β and CD40 (such as CXCL16 and CCL5), we transferred *Cxcr6*^{+/+} and *Cxcr6*^{-/-} bone marrow cells into irradiated hosts and infected them 6–8 weeks later with HSV-1 on the skin. Seven days later, splenic HSV-specific *Cxcr6*^{-/-} CD8⁺ T cells produced less IFN γ in response to *ex vivo* antigen restimulation than their *Cxcr6*^{+/+} counterparts (Fig. 1d). CCL5-competent transgenic HSV-specific CD8⁺ T cells transferred into *Ccl5*^{-/-} mice also had a significant, albeit more subtle, defect in IFN γ production in response to *ex vivo* antigen restimulation compared to wild-type recipients of HSV-specific transgenic CD8⁺ T cells (Fig. 1e), indicating that multiple genes required stimulation through both IFN α/β and CD40 for optimal helper-dependent DC–CD8⁺ T cell interactions *in vivo*.

IFN α/β change transcription downstream of CD40

Next, we tested whether IFN α/β and CD40 antibody acted concurrently or in sequence. To first investigate whether CD40 stimulation conditioned a more efficient response of BMDC1s to IFN α/β , we stimulated BMDC1s with CD40 antibody for 4 h and added IFN α for the last 15,

30, 60, 120 or 180 min of the stimulation. *Il15* expression increased after 1–2 h of IFN α stimulation, and this expression increased more than twofold in the presence of CD40 antibody (Fig. 2a). *Tnf*, *Cxcl16* and *Cd83* were also induced in BMDC1s after 2–3 h of IFN α stimulation (Fig. 2a), indicating that BMDC1s required ~2 h of IFN α/β exposure before they responded to CD40 triggering. We then determined whether IFN α/β conditioned the BMDC1s for CD40 responses by exposing BMDC1s to IFN α/β over 4 h and adding CD40 antibody for the last 15, 30, 60, 120 or 180 min. *Tnf*, *Cxcl16* and *Cd83* increased after 30–60 min (Fig. 2a), which showed that BMDC1s responded rapidly to CD40 stimulation if exposed to IFN α/β for ~2 h and suggested that BMDC1 need to be exposed to IFN α/β prior to CD40 stimulation. IFN α/β conditions the dendritic cells (DCs) to become receptive to T cell help. We also tested this requirement *in vivo* using HSV-1 skin infection⁶. CD8⁺ cDC1s residing in the brachial lymph nodes of wild-type mice increased MHC class II expression 2 days after infection, but this increase was absent in *Ifnar2*^{-/-} mice (Extended Data Fig. 1d). Because lack of CD4⁺ T cells does not impact MHC class II expression by CD8⁺ cDC1s in the brachial lymph nodes of wild-type mice infected 2 days earlier with HSV-1 on the skin⁶, these findings indicate that IFN α/β signals also need to precede CD40-mediated T cell help *in vivo*.

Next, we tested whether IFN α/β prepared DCs for T cell help by increasing CD40 expression⁷. IFN α -stimulated and unstimulated BMDC1s increased the expression of CD40 over time similarly (Extended Data Fig. 1e), indicating that surface CD40 expression was not rate limiting in these responses. To investigate whether the 'amplified' and 'combinatorial' responses resulted from the effect of IFN α/β on the pathways downstream of CD40, we performed RNA-seq of BMDC1s stimulated with IFN α for 4 h (BMDC1-IFN- α) and compared gene expression to BMDC1s additionally stimulated with CD40 antibody for the last 15 min (BMDC1-IFN α + CD40-15min) or 30 min (BMDC1-IFN α + CD40-30min) or over the entire 4-h period (BMDC1-IFN α + CD40-4h). Overall, BMDC1s changed expression of 341 genes over the 15-min, 30-min and 4-h time points compared to BMDC1-IFN α , BMDC1-CD40 or unstimulated BMDC1s (Fig. 2b). Unsupervised self-organizing maps (SOMs) of these 341 genes identified smaller groups of genes appearing transiently at 15 min and 30 min (that is, *Ifi44*, *Ifit3* and *Fos*), while different and larger sets of genes clustered at 4 h (that is, *Cd83*, *Il15*, *Cxcl16*, *Il27* and *Cd80*) (Fig. 2c and Supplementary Table 2). General cellular processes, such as 'enhanced survival' and 'increased mRNA stability', were enriched in BMDC1-IFN α + CD40-30min, while more specific responses, including 'regulation of cytokine production', characterized BMDC1-IFN α + CD40-4h (Fig. 2d). We also performed coexpression analysis¹¹ to identify similarly expressed groups of genes ('modules') independently of fold change cutoffs used to define differentially expressed genes across all time points (Fig. 2e and Supplementary Table 3). Genes in modules 1 and 3, such as *Cxcl16* and *Tnf*, responded to the combination of IFN α and CD40 antibody at 30 min and 4 h (Extended Data Fig. 2a). Modules 2 and 4 grouped genes that were induced by IFN α (that is, *Oas1l*, *Isg20* and *Il2rg*) or CD40 antibody (that is, *Cxcr4*, *Apol7c* and *Il12b*), respectively, while modules 5 and 6 contained genes with little responsiveness to either stimulation (that is, *Itga3*, *Sox4* and *Irak1*) (Fig. 2e). These modules also differed in GO term enrichments (Fig. 2d). Together, these analyses indicate that IFN α/β changed how BMDC1s responded at the transcriptional level to CD40 stimulation.

IFN α enable CD40 to activate p65, FOS and IRF1

Next, transcription factor binding motif prediction analysis of the 'amplified' genes suggested the involvement of overlapping transcriptional regulators, including members of the IRF and STAT families (Fig. 3a). More specifically, BMDC1-IFN α + CD40-30min and BMDC1-IFN α + CD40-4h were enriched for binding sites for NF- κ B, including NFKB1, REL, RELA (p65 subunit) and RELB (Fig. 3a). To test these predictions, we examined canonical and non-canonical NF- κ B

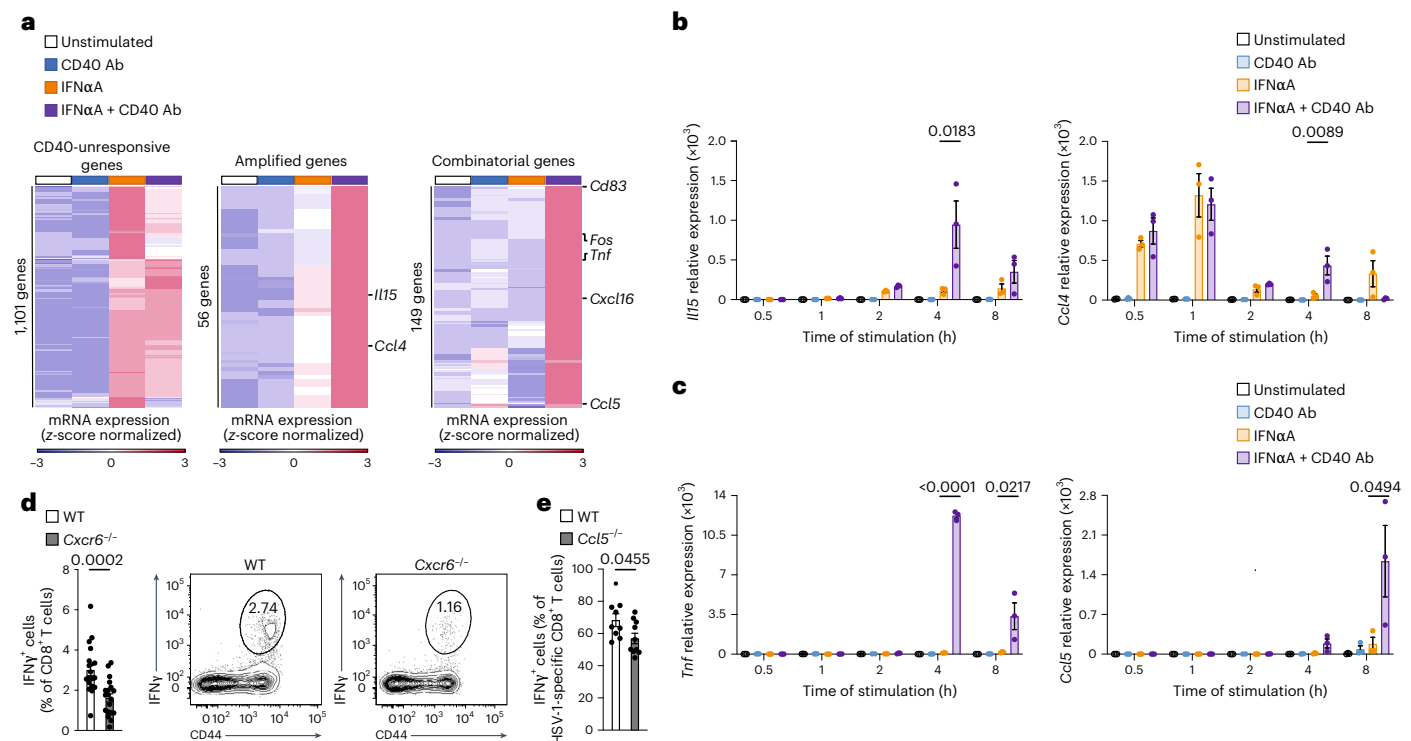


Fig. 1 | IFN α/β and CD40 induce distinct and combinatorial responses in cDC1s. **a**, Changes in gene expression of BMDC1s stimulated for 4 h with IFN α (n = 6 independent experiments), CD40 antibody (Ab) (n = 3 independent experiments) or IFN α + CD40 antibody (n = 3 independent experiments) compared to unstimulated BMDC1s (n = 6 independent experiments). Differentially expressed genes are displayed as heat maps after z-score transformation of counts per million (CPM). Statistical differences were assessed by one-way analysis of variance (ANOVA); FDR-adjusted $P \leq 0.05$ and fold change greater than 1.5. **b, c**, Relative expression of *Il15* and *Ccl4* (**b**) and *Tnf* and *Ccl5* (**c**) over time in BMDC1s stimulated with IFN α and/or CD40 antibody. Data are mean \pm s.e.m. from two to three independent experiments. Statistically significant differences between conditions were assessed by one-way ANOVA;

adjusted P values are indicated. **d**, IFN γ production after ex vivo antigen restimulation for 5 h by splenic wild-type (WT) and *Cxcr6*^{-/-} HSV-1-specific CD8⁺ T cells 10 days after HSV-1 skin infection of wild-type mice that were irradiated and reconstituted with an equal mix of *Cxcr6*^{-/-} and wild-type bone marrow cells 6–8 weeks earlier. Data are mean \pm s.e.m. from three independent experiments (n \geq 5 per experiment). **e**, IFN γ production after ex vivo antigen restimulation for 5 h by transgenic HSV-1-specific CD8⁺ T cells (gBT-1 cells) transferred as naive gBT-1 cells into wild-type or *Ccl5*^{-/-} mice 1 day before HSV-1 infection and isolated from the spleen 7 days after infection. Data are mean \pm s.e.m. from three independent experiments (n \geq 1 per experiment). Statistical significance between conditions in **d** and **e** was assessed by two-tailed Wilcoxon rank-sum test, and respective P values are indicated.

signaling cascades in the interplay between IFN α and CD40 antibody. The induction of amplified genes (*Il15* and *Ccl4*) and combinatorial genes (*Tnf* and *Cxcl16*) in BMDC1-IFN α + CD40-4h was similar between *Nfkb2*^{-/-} and wild-type BMDC1s (data not shown), indicating that the non-canonical NF- κ B pathway was not required. BMDC1-IFN α + CD40-15min resulted in I κ B α degradation and p65 phosphorylation (Fig. 3b and Extended Data Fig. 2c), and the NF- κ B inhibitor ammonium pyrrolidinedithiocarbamate (PDTC)¹² impaired the increased expression of *Tnf* and *Ccl4* in BMDC1-IFN α + CD40-4h (Fig. 3c). These findings highlight that IFN α/β conditioning enabled CD40 to trigger the canonical NF- κ B pathway in BMDC1s.

The transcriptional regulator FOS was induced in BMDC1-IFN α + CD40-15min compared to in BMDC1-IFN α , BMDC1-CD40 and BMDC1-IFN α + CD40-4h (Fig. 3d and Supplementary Table 2). We therefore deleted FOS from FLT3L-propagated BMDCs using CRISPR–Cas9 and stimulated these cells for 4 h with IFN α and CD40 antibody. Compared to non-targeting guide control (NTC) BMDCs, *Il15ra* and *Il27*, but not *Cxcl16* or *Nfkb2*, were reduced in the absence of FOS (Fig. 3e). ERK¹³ and CD40 signaling¹⁴ can activate FOS, and we found phosphorylated p38 and ERK in BMDC1-IFN α + CD40-15min (Fig. 3f). Inhibition of ERK by nimolide prevented the increase in *Ccl4* expression and partially reduced *Tnf* expression in BMDC1-IFN α + CD40-4h compared to in BMDC1-IFN α (Fig. 3c). Together, these findings indicate that

IFN α/β conditioning enables CD40 to activate FOS, likely through activation of ERK and p38.

The ‘combinatorial’ genes induced by IFN α/β and CD40 antibody were enriched in IRF1 binding sites (Fig. 3g), and expression of *Irf1* was increased in BMDC1-IFN α + CD40-30min and BMDC1-IFN α + CD40-4h compared to in BMDC1-IFN α (Fig. 3h). IRF1 binding signals were enriched in combinatorial genes in BMDC1-IFN α + CD40-4h compared to in BMDC1-NS, BMDC1-IFN α and BMDC1-CD40, as revealed by cleavage under targets and tagmentation (CUT&TAG) analysis (Fig. 3i). Endogenous IRF1 was bound to the promoter region of *Cxcl16* in BMDC1-IFN α + CD40-4h but not in BMDC1-IFN α , BMDC1-CD40 or BMDC1-NS (Fig. 3j). Moreover, *Irf1*^{-/-} BMDC1s did not induce the expression of *Cxcl16* in response to 4 h of combined IFN α/β and CD40 antibody stimulation (Fig. 3k), and transcription factor binding motifs in the vicinity of IRF1 binding sites were enriched for motifs recognized by p65 (Fig. 3l). Together, these findings show that IFN α/β conditioning enhances the capacity of cDC1s to degrade I κ B α and phosphorylate p65, p38 and ERK downstream of CD40, thus enabling CD4⁺ T cells to induce p65-, IRF1- and FOS-dependent transcriptional programs.

Mild COVID-19 is associated with IFN α/β and CD40 synergy Imbalances in IFN α/β provision¹⁵ and low-avidity CD4⁺ T cell responses¹⁶ are associated with severe COVID-19 (refs. 17,18), while milder outcomes correlate with virus-specific CD8⁺ T cells¹⁸ and the ability of individuals

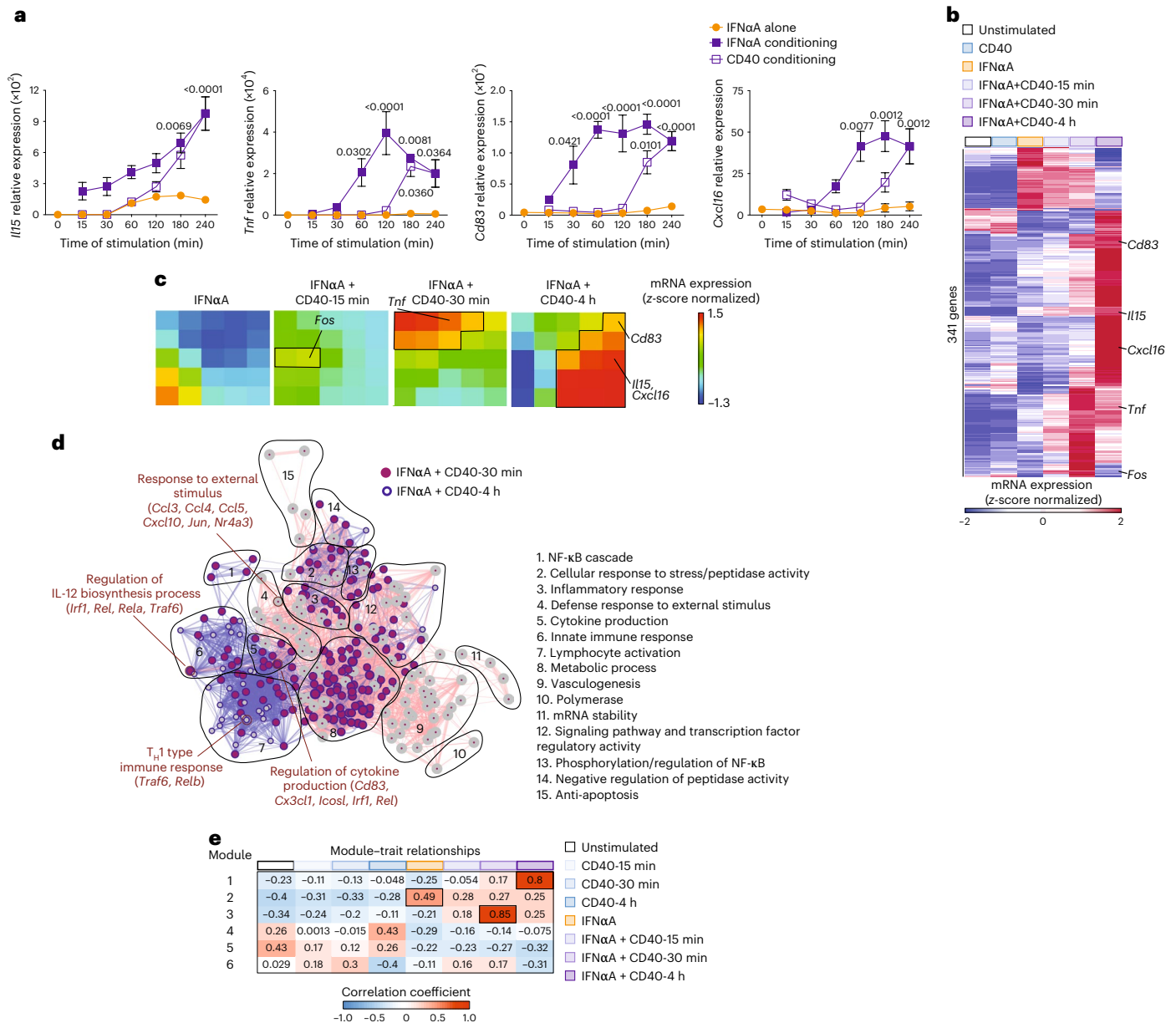


Fig. 2 | IFN α/β conditions cDC1s to enhance transcription in response to CD40 stimulation. a, Changes in the expression of *Il15*, *Tnf*, *Cd83* and *Cxcl16* in BMDCs stimulated with IFN α for 4 h and stimulated additionally with CD40 antibody for the last 15, 30, 60, 120, 180 and 240 min (‘IFN α conditioning’) or with CD40 antibody for 4 h and stimulated additionally with IFN α for the last 15, 30, 60, 120, 180 and 240 min (‘CD40 conditioning’) compared to BMDCs exposed to IFN α alone (at least three independent experiments for each time point). Error bars represent mean \pm s.e.m. Statistically significant differences between the corresponding conditions and IFN α at 4 h alone were assessed by one-way ANOVA. **b, c**, Heat map (b) and SOM (c) of differentially expressed genes between BMDCs left unstimulated or stimulated with IFN α alone (IFN α ; $n = 6$ independent experiments) or with IFN α for 4 h + CD40 for 15 min (IFN α + CD40-15min; $n = 3$ independent experiments), 30 min (IFN α + CD40-30min; $n = 3$ independent experiments) or 4 h (IFN α + CD40-4h; $n = 3$ independent experiments). The 341 genes were clustered into 25 SOM clusters that follow similar patterns of expression with the identification of

select genes in their respective clusters. **d**, Gene Ontology (GO) terms enriched in IFN α + CD40-30min SOM clusters (clusters 1–4 and 6–8, as in panel c) and IFN α + CD40-4h SOM clusters (clusters 5, 9, 10, 13–15, 18–20 and 23–25, as in panel c). Nodes represent the GO term, edges represent a score inversely proportional to the genes shared between the two GO terms, and the size of the nodes is proportional to the enrichment score. GO terms with a P value of ≤ 0.005 that relate to three or more GO terms are displayed; T_H1, type 1 helper T cell. **e**, Correlation coefficients of weighted gene correlation network analysis (WGCNA) eigengenes combining transcriptional results from RNA-seq of BMDCs that were unstimulated ($n = 6$ independent experiments) or stimulated with CD40 for 15 min (CD40-15min; $n = 3$ independent experiments), CD40 for 30 min (CD40-30min; $n = 3$ independent experiments), CD40 for 4 h (CD40-4h; $n = 3$ independent experiments), IFN α alone for 4 h (IFN α ; $n = 6$ independent experiments), IFN α for 4 h + CD40 for 15 min (IFN α + CD40-15min), IFN α for 4 h + CD40 for 30 min (IFN α + CD40-30min) or IFN α for 4 h + CD40 for 4 h (IFN α + CD40-4h; $n = 3$ independent experiments).

to respond to CCL5 (ref. 19) and CXCL16 (ref. 20). To investigate the synergy between IFN α/β and CD40 during SARS-CoV-2 infection, we isolated CD14⁺HLA-DR⁺ DCs from the blood of individuals with COVID-19 4 to 35 days after symptom onset²¹. This included mild to moderate

disease (WHO (World Health Organization) score of 2–5) and severe disease (WHO score of 6–8) (Supplementary Table 7). CD14⁺HLA-DR⁺ DCs from individuals with severe disease had significantly reduced expression of MHC class II (HLA-DR) compared to CD14⁺HLA-DR⁺ DCs from

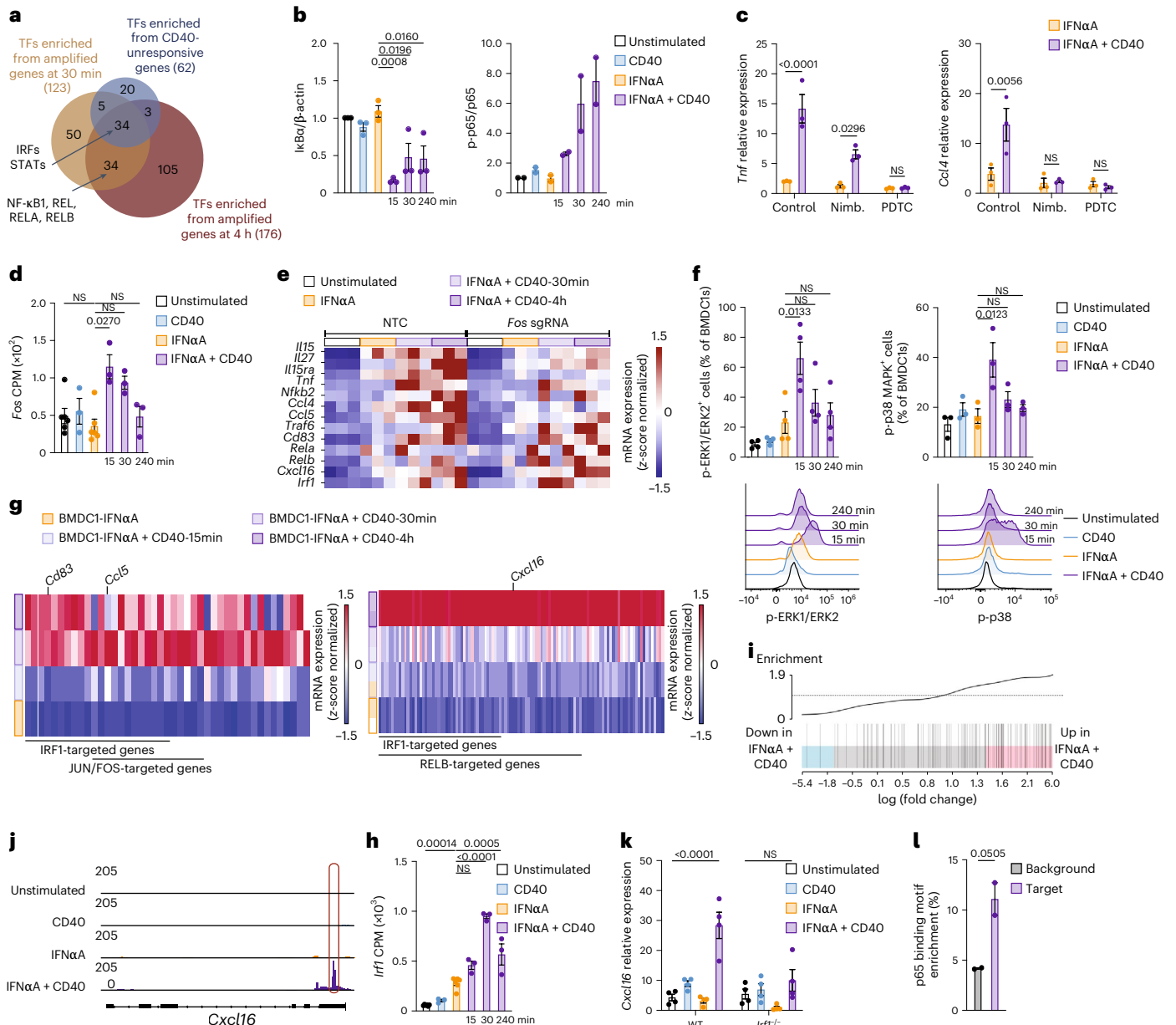


Fig. 3 | IFN α conditioning enables CD40 to activate a network of transcription factors that includes p65, IRF1 and FOS. **a**, Transcription factor (TF) motifs enriched for ‘CD40-unresponsive genes’ and ‘amplified genes’ at 30 min and 4 h (as in Fig. 2b) and displayed as Venn diagrams. **b**, IkB α degradation ($n = 3$ independent experiments) and p65 phosphorylation ($n = 2$ independent experiments) in BMDCs, as in Fig. 2b. **c**, *Tnf* and *Ccl4* expression in BMDCs stimulated as in Fig. 2b in the absence or presence of inhibitors for ERK (nimbolide) and the NF- κ B pathway (PDTC). Data are displayed relative to treatment alone and are pooled from three independent experiments. Error bars represent mean \pm s.e.m. Adjusted *P* values of the statistically significant differences as assessed by two-way ANOVA are indicated; Nimb, nimbolide; NS, not significant. **d**, *Fos* expression based on RNA-seq of BMDCs, stimulated as Fig. 2b, expressed as CPM. **e**, Relative expression of select genes (*Il15*, *Il27*, *Il15ra*, *Tnf*, *Nfkb2*, *Ccl4*, *Ccl5*, *Traf6*, *Cd83*, *Rela*, *Relb*, *Cxcl16* and *Irf1*) in BMDCs transduced with *Fos* single guide RNA (sgRNA) or NTC and stimulated as in Fig. 2b ($n = 3$ independent experiments). **f**, Phosphorylation of ERK1/ERK2

(p-ERK1/ERK2) and p38 MAPK (p-p38 MAPK) ($n = 3-4$ independent experiments) in BMDCs as in Fig. 2b. Pooled data and representative histograms are displayed. **g**, Expression of ‘combinatorial genes’ in BMDCs as in Fig. 2b. **h**, Expression of *Irf1* in RNA-seq data from BMDCs stimulated as in Fig. 2b, expressed as CPM. **i**, Enrichment of IRF1 binding signals in combinatorial genes in BMDC1-IFN α + CD40-4h ($P < 0.0001$; $n = 2$ replicates). **j**, IRF1 binding signals analyzed using CUT&Tag in BMDCs stimulated as in Fig. 2b ($n = 2$ replicates). **k**, Expression of *Cxcl16* in wild-type or *Irf1*^{-/-} BMDCs stimulated as in Fig. 2b. Data are mean \pm s.e.m. from three independent experiments. Adjusted *P* values were assessed by two-way ANOVA. **l**, p65 binding motif enrichment in DNA bound to IRF1 in BMDCs as in Fig. 2b, expressed as target relative to the entire genomic background data. Statistical testing was performed using the cumulative binomial distribution to compare target binding to background signal. Data are mean \pm s.e.m. from two replicates. Error bars in **b**, **d**, **f** and **h** represent mean \pm s.e.m. Adjusted *P* values of the statistically significant differences between the corresponding conditions as assessed by one-way ANOVA are indicated.

individuals with mild disease (Fig. 4a). A similar pattern was observed in CD14⁺CD11c⁺ monocytes, with a significant reduction in MHC class II expression compared to that observed in mild COVID-19 cases (Fig. 4a).

To test whether IFN α / β signals contribute to MHC class II expression, we collected blood samples 4 to 35 days after symptom onset from individuals with COVID-19 who had developed neutralizing antibodies

against type I IFN (IFN-AAB)²². CD14⁺HLA-DR⁺ DCs and CD14⁺CD11c⁺ monocytes from IFN-AAB⁺ individuals had an even stronger reduction of MHC class II than observed in those from individuals with mild disease (Fig. 4a). The expression of CD40 on CD14⁺HLA-DR⁺ DCs in individuals with severe disease increased irrespective of IFN-AAB but was reduced in CD14⁺CD11c⁺ monocytes in individuals with IFN-AAB (Fig. 4a), suggesting that IFN α / β regulate the ability of DCs and monocytes to receive T cell help through the expression of MHC class II^{5,23,24}.

Next, we used published single-cell RNA-seq (scRNA-seq) data from individuals with COVID-19 (ref. 25) to examine the expression of the 'CD40-unresponsive', 'amplified' and 'combinatorial' gene signatures identified above. This included peripheral blood mononuclear cells (PBMCs) from individuals with COVID-19 (mild, WHO score of 3, $n = 16$; moderate, WHO score of 4–5, $n = 11$; severe, WHO score of 7, $n = 23$) collected within the first 25 days after symptom onset before availability of vaccination. These were compared to samples from healthy or otherwise hospitalized individuals who tested negative for SARS-CoV-2, were serologically negative or had no indication of acute COVID-19 disease based on clinical or laboratory parameters (HC; $n = 13$)²⁵. We analyzed 31,736 classical monocytes and 722 myeloid DCs using reference-based cell-type annotation and clustering (Methods), referred to here as CD14⁺ monocytes and CD1c⁺ DCs, respectively. CD14⁺ monocytes from individuals with mild disease²⁵ were significantly enriched for the 'amplified' and 'combinatorial' responses (that is, *CD83*, *CXCL16*, *NFKB2* and *JUND*) compared to CD14⁺ monocytes from individuals with moderate or severe disease or from healthy control individuals (Fig. 4b,c and Supplementary Table 5). Also, CD1c⁺ DCs from individuals with mild COVID-19 had increased transcription of genes of the 'amplified' and 'combinatorial' responses, such as *CD83*, *EGR1* and *REL*, compared to CD1c⁺ DCs from individuals with severe COVID-19, which in turn had increased expression of CD40-unresponsive genes, such as *IFIT3*, *MXI* and *IRF7* (Fig. 4d and Supplementary Table 6). Similar patterns were observed in scRNA-seq data of a second cohort²⁶, which included three individuals with moderate disease (respiratory symptoms and pneumonia), four individuals with severe disease (supplemental oxygen requirement) collected 2–16 days after symptom onset and five asymptomatic healthy control individuals from whom samples were collected before the widespread circulation of SARS-CoV-2 (Extended Data Fig. 3a).

We also performed scRNA-seq on PBMC samples from the COVID-19 cohort above, which included IFN-AAB⁺ individuals²²

(Supplementary Table 7). CD14⁺ monocytes from IFN-AAB⁺ individuals had lower induction of prototypical ISGs, such as *ISG15* and *IFIT2*, than CD14⁺ monocytes from healthy individuals and individuals with disease without IFN-AAB (Extended Data Fig. 3b). Furthermore, the expression of *HLA-DRA*, *HLA-DRB1*, *TNF*, *CD83* and *CCL4* was reduced in CD14⁺ monocytes from individuals with severe COVID-19 and in IFN-AAB⁺ individuals compared to in healthy individuals and in individuals with COVID-19 without IFN-AAB (Extended Data Fig. 3b). To gain more robust insights into data distribution, we integrated our data with comparable published scRNA-seq data sets^{21,27,28}, including a study examining four IFN-AAB⁺ individuals²⁸. This yielded 179,012 single-cell CD14⁺ monocyte transcriptomes across 263 samples (HC, $n = 39$; WHO score of 1–3, mild, $n = 79$; WHO score of 4–5, moderate, $n = 82$; WHO score of 6–8, severe, $n = 52$; WHO score of 7–8, severe + IFN-AAB, $n = 11$). *HLA-DRB1*, *CD83* and *TNF* were significantly reduced in individuals with COVID-19 with increasing disease severity, reaching a minimum in individuals with IFN-AAB (Extended Data Fig. 3b). Furthermore, the 'amplified' and 'combinatorial' signatures were reduced in CD14⁺ monocytes from individuals with severe COVID-19, with and without IFN-AAB, compared to in CD14⁺ monocytes from individuals with mild disease (Extended Data Fig. 3c). Together, these findings indicate that IFN α / β signals are critical drivers of 'amplified' and 'combinatorial' responses during SARS-CoV-2 infection.

Reanalysis of published single-cell assay for transposase-accessible chromatin with sequencing (scATAC-seq) data sets²⁹ from PBMCs of individuals with COVID-19 indicated that CD14⁺ monocytes from individuals with mild disease had significantly increased accessibility of more than 300 genes, including *IL15*, *CD83*, *TNF* and *CXCL16*, compared to CD14⁺ monocytes from individuals with moderate and severe COVID-19 (Fig. 4e,f). Furthermore, Hallmark enrichment analysis of more accessible genes in CD14⁺ monocytes from individuals with mild COVID-19 compared to CD14⁺ monocytes from healthy control individuals identified 'IFN γ response' and 'TNF signaling via NF- κ B' as major pathways differentially regulated in mild COVID-19 (Fig. 4g). To investigate whether these responses can be elicited in vitro in human cDC1s, we differentiated human CD141⁺CADMI⁺CLEC9A⁺ cDC1s (hDC1s) from blood-derived CD34⁺ stem cells using FLT3L, stem cell factor and IL-4 (ref. 30) and stimulated them with human recombinant IFN α and human CD40 Ab separately or in combination for 18 h. hDC1s

Fig. 4 | Combinatorial responses to IFN α / β and CD40 antibody by DCs and monocytes correlate with milder outcomes of COVID-19. a, HLA-DR

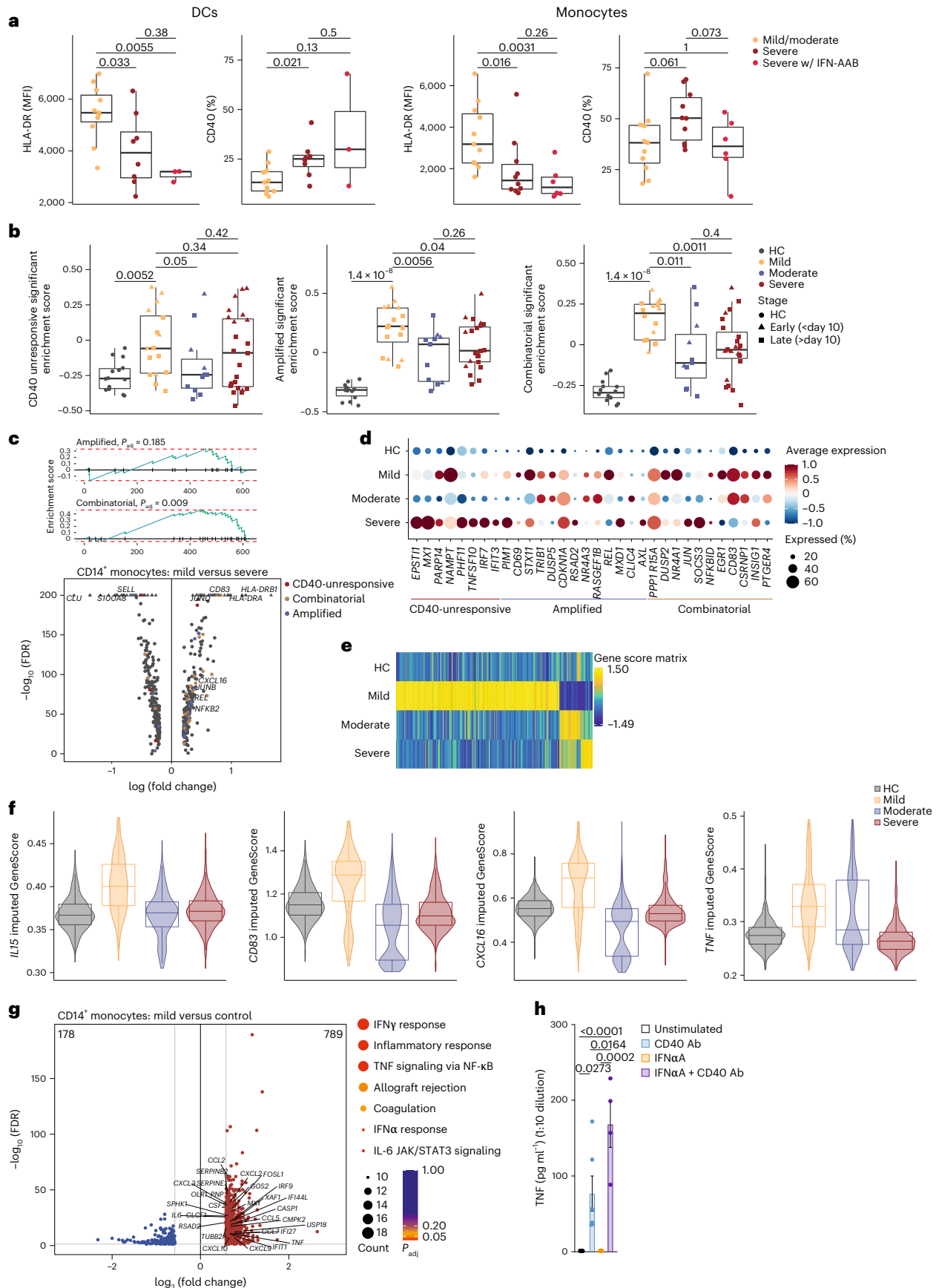
expression of CD14⁺CD11c⁺ monocytes and CD14⁺HLA-DR⁺ DCs from individuals with COVID-19 with mild or moderate symptoms (WHO score of 2–5; $n = 11$) or severe disease with (WHO score of 6–8; $n = 3–6$) and without ($n = 10$) IFN-AAB. Data are displayed as box and whisker plots showing the median and the 25th and 75th percentiles and two whiskers at 1.5 \times the interquartile range (IQR) of the mean fluorescence intensity (MFI) and percentage of CD40⁺ cells.

b, Single-sample gene set variation analysis (GSVA) of the 'CD40-unresponsive', 'amplified' and 'combinatorial' gene signatures in scRNA-seq data from CD14⁺ monocytes and CD1c⁺ DCs from PBMCs of individuals with mild (WHO score of 3; $n = 16$), moderate (WHO score of 4–5; $n = 11$) or severe (WHO score of 7; $n = 23$) COVID-19 and healthy control (HC) individuals ($n = 13$; reanalyzed from ref. 25). Box plots as in panel **a**. Data points are colored and shaped according to disease severity and stage based on days after onset of symptoms, respectively. Wilcoxon rank-sum test P values are shown. **c**, Gene set enrichment analysis plots (top) showing enrichment curves of the 'amplified' and 'combinatorial' signatures in the differentially expressed genes (two-sided Wilcoxon rank-sum test, minimum percentage = 0.1, \log_2 (fold change) > 0.2) in CD14⁺ monocytes from mild compared to severe COVID-19 cases as in **b**. The \log_{10} (FDR P values) and the \log_2 (fold change) values of the differentially expressed genes are shown as a volcano plot (bottom). Genes are colored according to the 'CD40-unresponsive', 'amplified' or 'combinatorial' signature; P_{adj} , adjusted P value.

d, Differential expression of 'CD40-unresponsive', 'amplified' and 'combinatorial' signature genes in CD1c⁺ DCs from healthy control individuals and individuals with mild, moderate and severe cases of COVID-19, as in **a**, determined using a two-sided Wilcoxon rank-sum test. **e**, Heat map showing GeneScores for disease-specific, significantly differentially accessible genes in scATAC-seq data of CD14⁺ monocytes from PBMC samples derived from individuals with mild (WHO score of 1–3; $n = 7$ samples), moderate (WHO score of 4–5; $n = 4$) or severe (WHO score of 6–7; $n = 6$) COVID-19 and healthy control individuals ($n = 6$; reanalyzed from ref. 29) determined using a two-sided Wilcoxon rank-sum test (FDR \leq 0.01 and \log_2 (fold change) \geq 0.58). **f**, Imputed GeneScores of *IL15*, *CD83*, *CXCL16* and *TNF* in CD14⁺ monocytes grouped according to COVID-19 severity as in **e**. Data are displayed as violin plots with overlaying box and whisker plots showing the median and 25th and 75th percentiles and two whiskers at 1.5 \times IQR. **g**, Differentially accessible genes (FDR \leq 0.01 and \log_2 (fold change) \geq 0.58) in CD14⁺ monocytes from individuals with mild COVID-19 compared to healthy control individuals, as in **e**, visualized as a volcano plot showing $-\log_{10}$ (FDR) and \log_2 (fold change) values (left) and the corresponding enriched Hallmark terms for the 789 genes with increased accessibility in mild COVID-19 CD14⁺ monocytes compared to healthy control monocytes displayed as dot plots showing gene counts and adjusted P values per term (right). **h**, Secretion of TNF in hDC1s stimulated with IFN α and/or CD40 antibody for 18 h. Data are mean \pm s.e.m. from six donors. Statistical significance for differences between conditions was assessed by one-way ANOVA, and adjusted P values are indicated.

secreted TNF in response to IFN α when aided by CD40 triggering, but not after treatment with IFN α alone (Fig. 4h). These observations indicated that APCs from individuals with mild, but not severe,

COVID-19 had increased chromatin accessibility and transcription of genes requiring the synergy between IFN α/β and CD40 described in the mouse experiments.



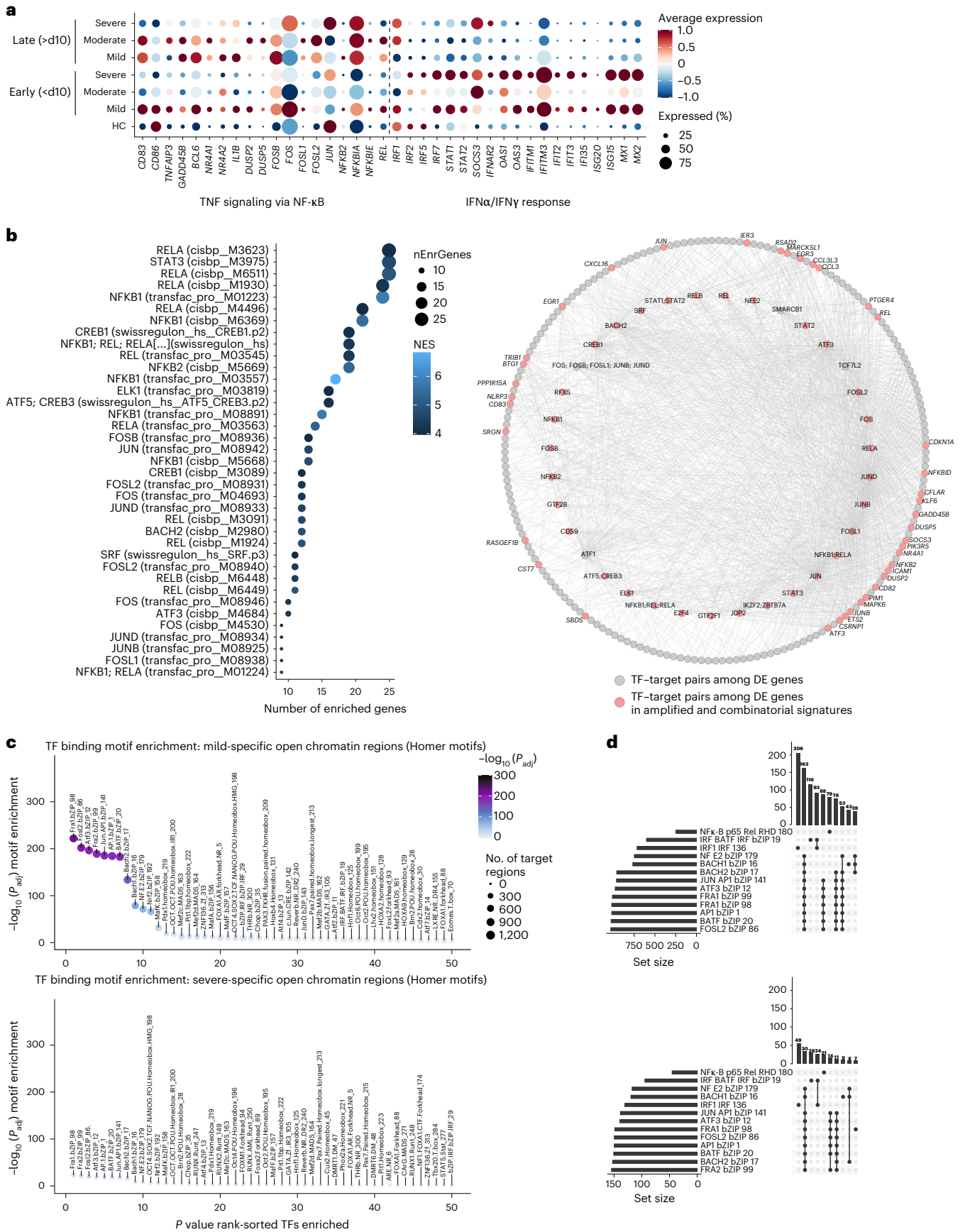


Fig. 5 | Enrichment of NF- κ B- and FOS-dependent transcriptional responses in APCs from individuals with mild, but not severe, COVID-19. **a**, Differentially expressed genes between disease severities and stages in CD14⁺ monocytes representing the significantly enriched Hallmark terms ‘IFN γ response’, ‘IFN α response’ and ‘TNF signaling via NF- κ B’, displayed as dot plots. **b**, RcisTarget transcription factor binding motif enrichment based on differentially expressed genes (two-tailed Wilcoxon rank-sum test, minimum percentage = 0.1, \log_2 (fold change) > 0.2) in CD14⁺ monocytes from individuals with mild compared to severe COVID-19, as in Fig. 4a. Data are visualized as a dot plot (left) showing the number of enriched genes and the normalized enrichment score per motif. The inner circle (right) shows the enriched transcription factors for all differentially expressed (DE) genes, and the outer circle shows the respective target genes responsible

for their enrichments. Transcription factors enriched for the genes overlapping with the ‘amplified’ and ‘combinatorial’ gene signatures and the target genes are colored in red. NES, normalized enrichment score. **c**, Transcription factor binding motif enrichment based on significantly differentially accessible peaks in CD14⁺ monocytes from individuals with mild or severe COVID-19 compared to CD14⁺ monocytes from healthy control individuals. Data are based on scATAC-seq data²⁹ and are displayed as dot plots showing FDR-adjusted *P* values of the enrichments and the number of target regions per transcription factor binding motif. **d**, Target regions of the top 10 highest enriched transcription factor binding motifs and motifs corresponding to IRF1 and p65 (RELA), shown as UpSet plots comparing the number of target regions.

CD40 triggers NF- κ B and FOS-dependent transcription in mild COVID-19

To explore whether IFN α / β also affected the signaling cascade downstream of CD40 in human APCs, we subjected the differentially expressed genes that were significantly higher in CD14⁺ monocytes from individuals with mild COVID-19 than in CD14⁺ monocytes from individuals with severe COVID-19 to enrichment analyses using the Hallmark database³¹ and transcription factor binding motifs³². There was a significant enrichment of genes associated with the NF- κ B pathway, including *CD83*, *CD86*, *TNFAIP3*, *IL1B*, *DUSP2*, *NFKB2* and *REL* (Fig. 5a and Supplementary Table 5). We also observed preferential involvement of the NF- κ B family (NFKB1, RELA and RELB) and the FOS and JUN families (AP-1; Fig. 5b). Visualization of the links between predicted transcription factors and their target genes within the differentially expressed genes between mild and severe COVID-19 indicated a dense regulatory network controlled by NF- κ B, FOS and JUN transcription factors (Fig. 5b).

Similarly, transcription factor binding motif enrichment analyses in differentially accessible chromatin regions of CD14⁺ monocytes from individuals with mild or severe COVID-19 compared to those from healthy control individuals²⁹ predicted members of the FOS family as key regulators (Fig. 5c). The enrichment score and number of accessible target regions of the predicted transcription factors, including FRA1/FRA2, FOSL2 and JUN, were higher in CD14⁺ monocytes from individuals with mild COVID-19 than in CD14⁺ monocytes from individuals with severe COVID-19 (Fig. 5c,d). Furthermore, the top 10 predicted transcription factor binding motifs and motifs corresponding to IRF1 and p65 (RELA) revealed large and distinct sets of target regions for the identified key regulator families among more accessible chromatin regions in CD14⁺ monocytes from mild COVID-19 cases than those from healthy control individuals. There were also substantially lower numbers of target regions with increased accessibility in CD14⁺ monocytes from individuals with severe COVID-19 than in CD14⁺ monocytes from healthy control individuals (Fig. 5d). These findings suggest that the

amplified and combinatorial responses enriched in CD14⁺ monocytes in individuals with mild COVID-19 are regulated by signal integration through transcription factors of the NF- κ B, FOS and JUN families.

Mild COVID-19 is associated with ‘helped’ CD8⁺ T cells

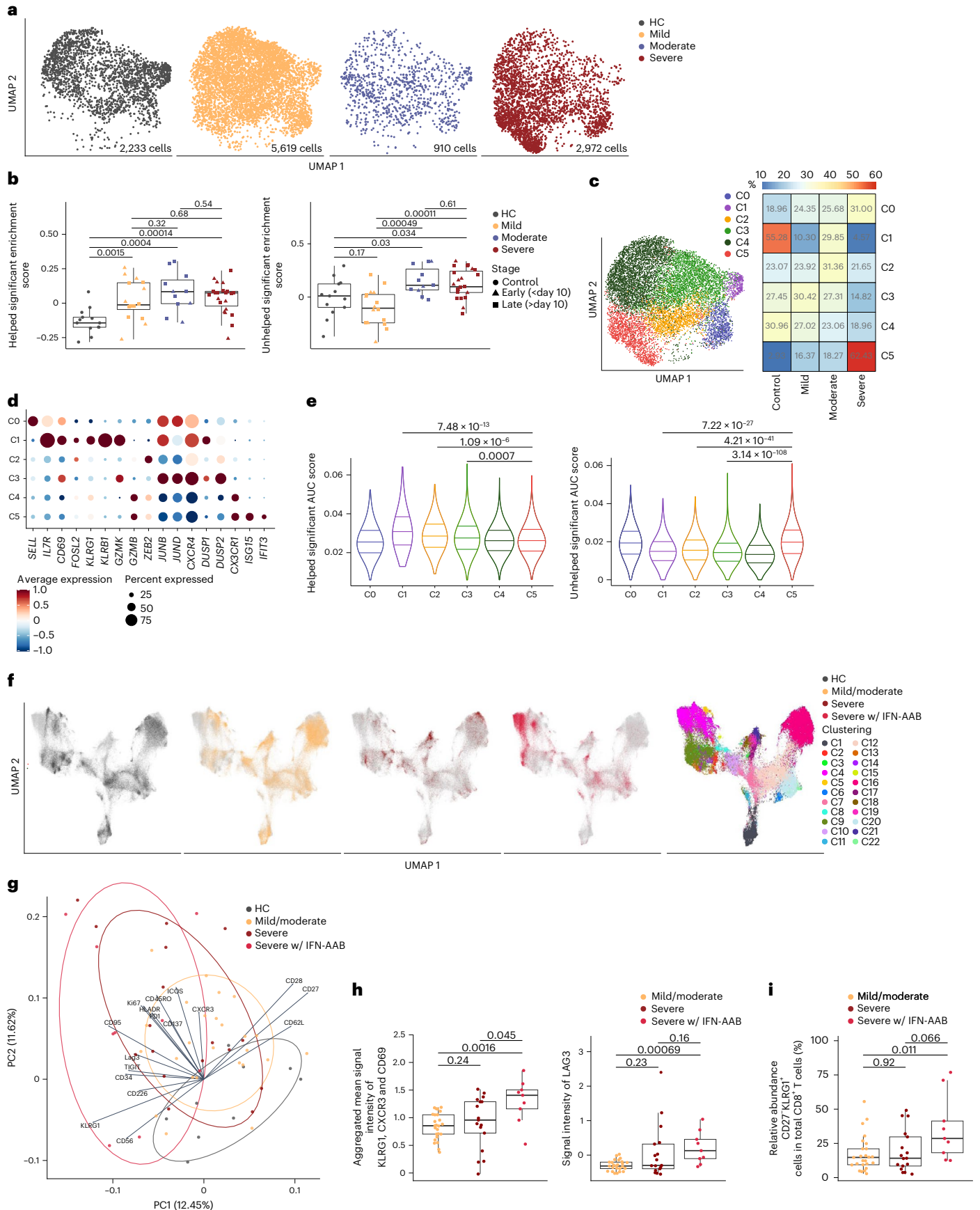
To test whether IFN α / β -dependent provision of T cell help to DCs and monocytes affects the CD8⁺ T cell response, we used the PBMC scRNA-seq data set from the cohort of individuals with COVID-19 and healthy control individuals defined above (Fig. 4b). We analyzed 11,734 CD8⁺ T cells using reference-based cell-type annotation and clustering (Methods) and compared their transcriptional profiles to published gene signatures that reflected CD8⁺ T cell priming in the presence (‘helped’) or absence (‘unhelped’) of CD4⁺ T cell help for DCs³³. CD8⁺ T cells from individuals with moderate and severe COVID-19 were enriched for ‘unhelped’ profiles (including *CD200*, *CD200R1*, *BTLA*, *ID3* and *PDCDI*) compared to CD8⁺ T cells from individuals with mild COVID-19 (Fig. 6a,b). Clustering analysis further indicated that individuals with mild and moderate COVID-19 were enriched in CD8⁺ T cell subsets with transcriptional profiles (*IL7R*, *TCF7*, *JUNB* and *JUND*) indicative of early effector or activated memory T cells^{34,35} (Fig. 6c,d and Supplementary Table 8, cluster 3). CD8⁺ T cells with characteristics of terminal differentiation (*CX3CR1* and *ISG15*, cluster 5) also dominated in individuals with severe COVID-19 (Fig. 6c,d) and had a reduction in ‘helped’ signatures (that is, *CD69*, *IL2RA* and *TNF*) and a corresponding gain in the ‘unhelped’ signature (that is, *IL6R*, *CD9*, *ISG15* and *PDCDI*) (Fig. 6e). We found comparable patterns in published scRNA-seq data from two other cohorts of individuals with COVID-19 (Extended Data Fig. 4a–c)^{36,37}. We used cytometry by time of flight (CyTOF) to examine protein expression in CD8⁺ T cells from blood samples of 9 healthy control individuals and individuals with COVID-19 with mild (WHO score of 2–3; *n* = 25) or severe (WHO score of 7–8; *n* = 18) disease and IFN-AAB⁺ individuals with severe disease (WHO score of 7–8; *n* = 9)²¹ collected 4 to 30 days after symptom onset (Supplementary Table 7). Dimensionality reduction using uniform manifold approximation and

Fig. 6 | Severe outcomes of COVID-19 are associated with ‘unhelped’ CD8⁺ T cells. **a**, UMAP visualization of scRNA-seq profiles of 11,734 CD8⁺ T cells from individuals with mild (WHO score of 3; *n* = 16), moderate (WHO score of 4–5; *n* = 11) or severe (WHO score of 7; *n* = 23) COVID-19 and healthy control individuals (*n* = 13; reanalyzed from ref. 25). Cells are split and colored according to disease severity. **b**, GSVA of ‘helped’ and ‘unhelped’ T cell signatures derived from published gene expression³³ profiles of mouse CD8⁺ T cells primed in the presence or absence of CD4⁺ T cells. Data are displayed as box and whisker plots showing the median and 25th and 75th percentiles and two whiskers at 1.5 \times IQR. Two-sided Wilcoxon rank-sum test *P* values are shown. **c**, UMAP of CD8⁺ T cells segregated into clusters 0–5 (left) and heat map of the respective proportionate cluster occupancy per disease severity (right) as in **a**. **d**, Expression of key genes associated with clusters 0–5 as in **c**. **e**, AUCell enrichment of genes derived from published gene expression³³ profiles of mouse CD8⁺ T cells primed in the presence or absence of CD4⁺ T cells as in **b**, grouped according to the clustering as in **c** and displayed as violin plots of area under the curve (AUC) scores. FDR-

corrected Dunn’s multiple comparison test *P* values are indicated. **f**, UMAP visualization of CD8⁺ T cells from whole-blood samples from healthy control individuals (*n* = 10) and individuals with COVID-19 (mild, *n* = 22; severe, *n* = 21; severe with IFN-AAB, *n* = 9) analyzed by CyTOF. The rightmost plot shows the UMAP colored according to FlowSOM clustering, while the four plots on the left show the distribution of events across the groups. **g**, PCA analysis plot showing average PC1 and PC2 values for all the events per individual as in **f**, colored according to the sample group. Ellipses show an estimated region of group accumulation, arrows represent correlation of the respective marker with either of the PC axes, and arrow length represents correlation strength. **h**, Mean scaled signal intensities for KLRG1, CXCR3 and CD69 (left) and LAG3 (right) displayed as box and whisker plots showing the median and 25th and 75th percentiles and two whiskers at 1.5 \times IQR. **i**, Relative abundance of CD27⁺ KLRG1⁺ cells in the total CD8⁺ T cell fraction displayed as box and whisker plots showing the median and the 25th and 75th percentiles and two whiskers at 1.5 \times IQR. Statistics in **h** and **i** show two-sided Benjamini–Hochberg-corrected pairwise Wilcoxon *P* values.

projection (UMAP) and clustering with the FlowSOM algorithm indicated differences in the composition of CD8⁺ T cells between individuals with COVID-19 with different disease severity (Fig. 6f). Individuals with

mild COVID-19 had increased proportions of CD27⁺CD8⁺ T cells with memory potential⁶ (Fig. 6f and Extended Data Fig. 4d,e, clusters 17, 19 and 21), while individuals with severe COVID-19 had greater proportions



of CD27⁺ KLRG1⁺ CD8⁺ T cells (clusters 3 and 8) than healthy individuals or individuals with mild disease (Fig. 6f and Extended Data Fig. 4d,e). Principal component analysis (PCA) of CD8⁺ T cells from individuals with mild and severe COVID-19 identified the expression of CD27 and KLRG1 as distinct features of CD8⁺ T cells from individuals with mild and severe disease, respectively (Fig. 6g,i), and CD8⁺ T cells from individuals with severe disease were enriched for LAG3 (Fig. 6h), a molecule induced by priming with unhelped DCs³³. These findings indicate that severe outcomes of COVID-19 are associated with unhelped phenotypes of CD8⁺ T cells.

Discussion

Our findings uncovered an iterative consolidation process, in which innate stimuli, such as IFN α/β or TLR agonists, determined broad response options in APCs, and CD4⁺ T cells subsequently partitioned these into distinct sets of co-stimulatory molecules, cytokines and chemokines through CD40L. Together, these consecutive signals endowed APCs with optimal capacities to orchestrate effective antiviral CD8⁺ T cell responses in mouse HSV-1 infections and during community-acquired SARS-CoV-2 infections, where effective consolidation of IFN α/β and CD40 signals in APCs correlated with milder outcomes of COVID-19.

The conditioning of APCs by IFN α/β to become receptive to T cell help involved increased expression of MHC class II and distinct changes in how the APCs responded to CD40 stimulation. The changes in CD40 responsiveness were not just a function of increased expression of CD40 alone⁸, as spontaneously matured CD40^{hi} DCs in mice and CD40^{hi} APCs in individuals with severe COVID-19 were unable to engage ‘helper’-dependent programs. Instead, the capacity to receive help depended on additional changes in the signaling cascade downstream of CD40. These endowed APCs with the capacity to rapidly engage a network of transcription factors, including p65, IRF1 and FOS, and likely others, such as JUN, to select a distinct group of genes that provide the DCs with optimal capacities to prime CD8⁺ T cells responding to antigen. Some of the transcription factors were directly regulated by IFN α/β and CD40 stimulation, suggesting that conditioning also enhanced the availability of relevant transcription factors. These responses were not exclusive to the cooperation between IFN α/β and CD40, as similar patterns of CD40-dependent calibration also occurred in DCs stimulated through different TLRs. Together with increased chromatin accessibility at binding sites for the above-mentioned transcription factors in promoter regions of key genes regulated through IFN α/β and CD40, our study revealed a multitude of transcriptional and post-translational changes as a functional basis for how innate cues condition APCs to become receptive to T cell help, thus enabling CD4⁺ T cells to calibrate APCs for optimal stimulation of CD8⁺ T cell responses.

We have investigated the relevance of these findings for antiviral CD8⁺ T cell immunity in a mouse model of HSV-1 skin infection and showed that optimal HSV-specific CD8⁺ T cell responses depended on contextual cues that require IFN α/β and NF- κ B signal integration by DCs. Notably, we translated these experimental insights to individuals with SARS-CoV-2 infection and demonstrated that the consecutive activation of APCs by IFN α/β and CD4⁺ T cells played an important role in regulating how APCs orchestrate CD8⁺ T cell responses during COVID-19. This interpretation not only helps align a number of currently unlinked findings in COVID-19, such as an association of milder disease with effective provision of CXCL16 (ref. 20) and CCL5 (ref. 19), high-avidity CD4⁺ T cells¹⁶ and effective CD8⁺ T cell responses¹⁸, but also raises the prospect of ‘unhelped’ APCs launching too many terminally differentiated CD8⁺ T cells that contribute to immunopathology in individuals with severe COVID-19. It is important to acknowledge limitations around our findings in individuals with COVID-19. Our study cannot discern if the observed failures in signal integration by APCs and preponderance of terminally differentiated CD8⁺ T cells are

a ‘cause’ or ‘effect’ of severe COVID-19 or are more likely a complex combination of both. Moreover, it is possible that interindividual differences in T cell antigen receptor epitopes, precursor frequencies of antigen-specific CD8⁺ T cells and a great number of many other covariates (that is, age, gender and comorbidities) influence the interaction between APCs and CD8⁺ T cells in individuals with COVID-19. However, having validated our findings across multiple unrelated clinical data sets, it is unlikely that our findings simply represent the confounding effects of any one of these covariates. We likely also missed some of the more nuanced aspects of the interaction between APCs and naive CD8⁺ T cells that take place in lymph nodes before symptom onset, which are difficult to capture as the precise time point of infection is unknown in community-acquired infections, and lymph nodes are not as amenable as blood for routine sampling, especially in individuals with mild disease.

Collectively, our findings demonstrate the reliance of antiviral immunity on a step-wise, carefully orchestrated consolidation process, whereby APCs combine and integrate innate signals and, after selection by CD4⁺ T cells, produce a discrete set of co-stimulatory molecules and soluble mediators that adapt responding CD8⁺ T cells to the specific challenge. In showing how innate and adaptive signals cooperate to partition tailored responses from multiple broad and overlapping innate pathways and demonstrating functional relevance of these processes in mouse and human virus infections, our study provides critical new insights into how the host mounts effective antiviral immunity.

Online content

Any methods, additional references, Nature Portfolio reporting summaries, source data, extended data, supplementary information, acknowledgements, peer review information; details of author contributions and competing interests; and statements of data and code availability are available at <https://doi.org/10.1038/s41590-023-01517-x>.

References

1. Chow, A., Brown, B. D. & Merad, M. Studying the mononuclear phagocyte system in the molecular age. *Nat. Rev. Immunol.* **11**, 788–798 (2011).
2. Joffre, O. P., Segura, E., Savina, A. & Amigorena, S. Cross-presentation by dendritic cells. *Nat. Rev. Immunol.* **12**, 557–569 (2012).
3. Cabeza-Cabrerizo, M., Cardoso, A., Minutti, C. M., Pereira da Costa, M. & Reis e Sousa, C. Dendritic cells revisited. *Annu. Rev. Immunol.* **39**, 131–166 (2021).
4. Ardouin, L. et al. Broad and largely concordant molecular changes characterize tolerogenic and immunogenic dendritic cell maturation in thymus and periphery. *Immunity* **45**, 305–318 (2016).
5. Borst, J., Ahrends, T., Babala, N., Melief, C. J. M. & Kastenmuller, W. CD4⁺ T cell help in cancer immunology and immunotherapy. *Nat. Rev. Immunol.* **18**, 635–647 (2018).
6. Greyer, M. et al. T cell help amplifies innate signals in CD8⁺ DCs for optimal CD8⁺ T cell priming. *Cell Rep.* **14**, 586–597 (2016).
7. Schulz, O. et al. CD40 triggering of heterodimeric IL-12 p70 production by dendritic cells in vivo requires a microbial priming signal. *Immunity* **13**, 453–462 (2000).
8. Eickhoff, S. et al. Robust anti-viral immunity requires multiple distinct T cell-dendritic cell interactions. *Cell* **162**, 1322–1337 (2015).
9. Hor, J. L. et al. Spatiotemporally distinct interactions with dendritic cell subsets facilitates CD4⁺ and CD8⁺ T cell activation to localized viral infection. *Immunity* **43**, 554–565 (2015).
10. Rusinova, I. et al. Interferome v2.0: an updated database of annotated interferon-regulated genes. *Nucleic Acids Res.* **41**, D1040–D1046 (2013).

11. Yu, X. et al. Isotype switching converts anti-CD40 antagonism to agonism to elicit potent antitumor activity. *Cancer Cell* **37**, 850–866 (2020).
12. Schreck, R., Meier, B., Mannel, D. N., Droge, W. & Baeuerle, P. A. Dithiocarbamates as potent inhibitors of nuclear factor κ B activation in intact cells. *J. Exp. Med.* **175**, 1181–1194 (1992).
13. Lavoie, H., Gagnon, J. & Therrien, M. ERK signalling: a master regulator of cell behaviour, life and fate. *Nat. Rev. Mol. Cell Biol.* **21**, 607–632 (2020).
14. Kashiwada, M. et al. Tumor necrosis factor receptor-associated factor 6 (TRAF6) stimulates extracellular signal-regulated kinase (ERK) activity in CD40 signaling along a Ras-independent pathway. *J. Exp. Med.* **187**, 237–244 (1998).
15. Hadjadj, J. et al. Impaired type I interferon activity and inflammatory responses in severe COVID-19 patients. *Science* **369**, 718–724 (2020).
16. Bacher, P. et al. Low-avidity CD4⁺ T cell responses to SARS-CoV-2 in unexposed individuals and humans with severe COVID-19. *Immunity* **53**, 1258–1271 (2020).
17. Schultze, J. L. & Aschenbrenner, A. C. COVID-19 and the human innate immune system. *Cell* **184**, 1671–1692 (2021).
18. Sette, A. & Crotty, S. Adaptive immunity to SARS-CoV-2 and COVID-19. *Cell* **184**, 861–880 (2021).
19. Galani, I. E. et al. Untuned antiviral immunity in COVID-19 revealed by temporal type I/III interferon patterns and flu comparison. *Nat. Immunol.* **22**, 32–40 (2021).
20. Pairo-Castineira, E. et al. Genetic mechanisms of critical illness in COVID-19. *Nature* **591**, 92–98 (2021).
21. Georg, P. et al. Complement activation induces excessive T cell cytotoxicity in severe COVID-19. *Cell* **185**, 493–512 (2022).
22. Akbil, B. et al. Early and rapid identification of COVID-19 patients with neutralizing type I interferon auto-antibodies. *J. Clin. Immunol.* **42**, 1111–1129 (2022).
23. Bedoui, S., Heath, W. R. & Mueller, S. N. CD4⁺ T-cell help amplifies innate signals for primary CD8⁺ T-cell immunity. *Immunol. Rev.* **272**, 52–64 (2016).
24. Wu, R. & Murphy, K. M. DCs at the center of help: origins and evolution of the three-cell-type hypothesis. *J. Exp. Med.* **219**, e20211519 (2022).
25. Schulte-Schrepping, J. et al. Severe COVID-19 is marked by a dysregulated myeloid cell compartment. *Cell* **182**, 1419–1440 (2020).
26. Arunachalam, P. S. et al. Systems biological assessment of immunity to mild versus severe COVID-19 infection in humans. *Science* **369**, 1210–1220 (2020).
27. Su, Y. et al. Multi-omics resolves a sharp disease-state shift between mild and moderate COVID-19. *Cell* **183**, 1479–1495 (2020).
28. van der Wijst, M. G. P. et al. Type I interferon autoantibodies are associated with systemic immune alterations in patients with COVID-19. *Sci. Transl. Med.* **13**, eabh2624 (2021).
29. Wilk, A. J. et al. Multi-omic profiling reveals widespread dysregulation of innate immunity and hematopoiesis in COVID-19. *J. Exp. Med.* **218**, e20210582 (2021).
30. Pearson, F. E. et al. Human CLEC9A antibodies deliver Wilms' tumor 1 (WT1) antigen to CD141⁺ dendritic cells to activate naive and memory WT1-specific CD8⁺ T cells. *Clin. Transl. Immunol.* **9**, e1141 (2020).
31. Liberzon, A. et al. The Molecular Signatures Database (MSigDB) Hallmark gene set collection. *Cell Syst.* **1**, 417–425 (2015).
32. Aibar, S. et al. SCENIC: single-cell regulatory network inference and clustering. *Nat. Methods* **14**, 1083–1086 (2017).
33. Ahrends, T. et al. CD4⁺ T cell help confers a cytotoxic T cell effector program including coinhibitory receptor downregulation and increased tissue invasiveness. *Immunity* **47**, 848–861 (2017).
34. Kaech, S. M. & Wherry, E. J. Heterogeneity and cell-fate decisions in effector and memory CD8⁺ T cell differentiation during viral infection. *Immunity* **27**, 393–405 (2007).
35. Pipkin, M. E. Runx proteins and transcriptional mechanisms that govern memory CD8 T cell development. *Immunol. Rev.* **300**, 100–124 (2021).
36. Bernardes, J. P. et al. Longitudinal multi-omics analyses identify responses of megakaryocytes, erythroid cells, and plasmablasts as hallmarks of severe COVID-19. *Immunity* **53**, 1296–1314 (2020).
37. Chua, R. L. et al. COVID-19 severity correlates with airway epithelium-immune cell interactions identified by single-cell analysis. *Nat. Biotechnol.* **38**, 970–979 (2020).

Publisher's note Springer Nature remains neutral with regard to jurisdictional claims in published maps and institutional affiliations.

Springer Nature or its licensor (e.g. a society or other partner) holds exclusive rights to this article under a publishing agreement with the author(s) or other rightsholder(s); author self-archiving of the accepted manuscript version of this article is solely governed by the terms of such publishing agreement and applicable law.

© The Author(s), under exclusive licence to Springer Nature America, Inc. 2023

¹Department of Microbiology and Immunology at the Doherty Institute for Infection and Immunity, The University of Melbourne, Melbourne, Victoria, Australia. ²Life and Medical Sciences (LIMES) Institute, University of Bonn, Bonn, Germany. ³Systems Medicine, Deutsches Zentrum für Neurodegenerative Erkrankungen (DZNE), Bonn, Germany. ⁴Translational Immunology, Berlin Institute of Health (BIH) & Charité University Medicine, Berlin, Germany. ⁵Infectious Diseases and Respiratory Medicine, Charité, Universitätsmedizin Berlin, Berlin, Germany. ⁶Berlin Institute of Health at Charité, Universitätsmedizin Berlin, Core Unit Bioinformatics, Berlin, Germany. ⁷Institute of Innate Immunity, University of Bonn, Bonn, Germany. ⁸Sydney Cytometry Core Research Facility, Charles Perkins Centre, Centenary Institute and University of Sydney, Sydney, New South Wales, Australia. ⁹Centre for Innate Immunity and Infectious Diseases, Hudson Institute of Medical Research, Clayton, Victoria, Australia. ¹⁰Department of Molecular and Translational Science, Monash University, Clayton, Victoria, Australia. ¹¹Würzburg Institute of Systems Immunology, Max Planck Research Group, Julius-Maximilians-Universität Würzburg, Würzburg, Germany. ¹²Institute of Experimental Immunology, University of Bonn, Bonn, Germany. ¹³Mater Research Institute, The University of Queensland, Brisbane, Queensland, Australia. ¹⁴Department of Biochemistry, Biomedicine Discovery Institute, Monash University, Clayton, Victoria, Australia. ¹⁵PRECISE Platform for Single Cell Genomics and Epigenomics, DZNE and University of Bonn, Bonn, Germany. ¹⁶These authors contributed equally: Elise Gressier, Jonas Schulte-Schrepping. ¹⁷These authors jointly supervised this work: Susanne V. Schmidt, Sammy Bedoui.

✉ e-mail: elise.gressier07@gmail.com; sbedoui@unimelb.edu.au

Methods

Mice

C57BL/6, *Ccl5*^{-/-}, *Cxcr6*^{-/-}, *Ifnar2*^{-/-}, *Irf1*^{-/-} and CD45.1⁺ gBT-I mice were bred and maintained at the animal facility of the Department of Microbiology and Immunology, The University of Melbourne. All animal experiments were approved by The University of Melbourne Animal Ethics Committee.

Human samples

This study includes a subset of individuals enrolled between March 2020 and April 2021 in the Pa-COVID-19 study, a prospective observational cohort study assessing pathophysiology and clinical characteristics of individuals with COVID-19 at Charité Universitätsmedizin, Berlin³⁸. The study was approved by the Institutional Review board of Charité (EA2/066/20). Written informed consent was provided by all individuals or legal representatives for participation in the study. Specifics about the participants per application (flow cytometry, CyTOF and scRNA-seq), including COVID-19 status, time point of sampling after onset of symptoms, sex, age and outcome, are listed in Supplementary Table 7 and are described elsewhere^{21,22}. Human umbilical cord blood was obtained with written informed consent from the Queensland Cord Blood Bank and approval from the Mater Human Research Ethics Committee (HREC13/MHS/86).

In vitro generation of BMDCs

Single-cell suspensions from mouse bone marrow were cultured with FLT3L to generate BMDCs⁶. Red blood cells were removed using 1 ml of red blood cell lysis buffer (Sigma-Aldrich) per mouse for 90 s. Cells were cultured at 1.5×10^6 cells per ml in complete medium supplemented with 1.32 mM L-glutamine, 10% fetal calf serum, 90 μ M β -mercaptoethanol, 100 U ml⁻¹ penicillin, 0.2 g liter⁻¹ streptomycin and 150 ng ml⁻¹ FLT3L (BioXCell). Following 8 days of culture at 37 °C, cells were stained for 30 min on ice with CD45R/B220 (RA3-6B2), SIRP α (P84), CD11c (N418), CD11b (M1/70), I-A/E (M5114) and CD24 (M1/69) antibodies. cDC1 or CD8⁺ DC equivalents were identified by CD24^{high}SIRP α ^{low}CD11b^{low}CD45R/B220⁻ and were sorted using a FACS Aria III (BD Biosciences). Following sorting, BMDCs were washed and resuspended before stimulation. Stimulation was performed on bulk BMDCs or sorted BMDCs with IFN α A (PBL; 1,000 U ml⁻¹), IFN β (R&D Systems; 1 μ g ml⁻¹), LPS (Sigma-Aldrich; 10 μ g ml⁻¹), CpG (1668, GeneWorks; 1.6 nmol ml⁻¹) or poly(I:C) (InvivoGen; 10 μ g ml⁻¹) in the presence or absence of monoclonal antibody to CD40 (CD40 Ab; FGK45.5, Miltenyi Biotec; 10 μ g ml⁻¹). Cells and supernatants were collected at different time points thereafter. Pharmacological inhibition of NF- κ B and ERK pathways was achieved with 1 h pretreatment using PDTC (ab141406, 10 μ M) and nimbolide (ab142138, 10 μ M), respectively.

Cytokine and chemokine determination

Supernatants were subjected to BD Cytometric Bead Array measurement of CCL4 (limit of detection of 4.88 pg ml⁻¹), CCL5 (limit of detection of 1.22 or 4.88 pg ml⁻¹) and TNF- α (limit of detection of 39.07 or 9.7 pg ml⁻¹), according to the manufacturer's instructions. Samples were assessed using an LSRFortessa and FACS Diva software 6.1.3, and all concentrations were determined relative to a standard curve.

Real-time PCR

Cells were resuspended in TRIzol (Life Technologies), and mRNA was extracted using a Direct-zol RNA MicroPrep kit (Zymo Research) following the manufacturer's instructions. cDNA was synthesized with an Omniscript RT kit for reverse transcription (Qiagen) using oligo(dT) primers (Promega) and RNaseOUT recombinant ribonuclease inhibitor (Thermo Fisher Scientific). Real-time PCR was performed with Taqman Universal PCR master mix (Life Technologies) with primers/probes for 18S (Mm03928990_g1), *B2m* (Mm00437762_m1), *Ccl4* (Mm00443111_m1), *Ccl5* (Mm01302427_m1), *Cd83* (Mm00486868_m1), *Cxcl16*

(Mm00469712_m1), *Gapdh* (Mm99999915_g1), *Hprt* (Mm00446968_m1), *Il15* (Mm00434210_m1), *Il15ra* (Mm04336046_m1), *Il27* (Mm00461162_m1), *Irf1* (Mm01288580_m1), *Nfkb2* (Mm00479807_m1), *Rela* (Mm00501346_m1), *Relb* (Mm00485664_m1), *Tnf* (Mm00443258_m1) and *Traf6* (Mm00493836_m1).

RNA-seq and data analysis

Gene expression changes were investigated using RNA-seq. Up to 100 ng of total RNA was used for library preparation, according to the manufacturer's protocol, and was either sequenced in a 125-base pair (bp) paired-end run on a HiSeq HT sequencer (Illumina) or in a 50-bp single-read QuantSeq 3'-mRNA (Lexogen) run. Reads were aligned against the mouse genome mm10 by STAR v2.5.3a. Gene quantification was performed via the E/M algorithm in PartekFlow (v8.0.19.0707) and normalized as CPM. Genes with a mean expression of ≤ 1 CPM under all conditions were excluded from further analysis, resulting in 10,222 present genes for ANOVA in the Partek Genomics Suite (PGS, v7.18.0402). Genes with a fold change of 1.5 and an FDR-adjusted *P* value of ≤ 0.05 were defined as differentially expressed between two tested conditions. GO enrichment for the modules was performed using DAVID³⁹ with the GOTERM_BP_DIRECT annotation. GO terms were filtered by unadjusted *P* ≤ 0.05 and visualized using ggplot2. Biological interpretation of differentially expressed genes was performed with the following tools. Gene set enrichment analysis was performed using the GSEA application (v4.0.3) and the Hallmark gene set published by the Broad Institute. Enrichments were plotted using ggplot2 (v3.3.3)⁴⁰. Cytoscape was used to visualize enriched GO terms as a network with the two plugins BiNGO (v3.0.3) and EnrichmentMap (v3.2.1). WordCloud plugin (v3.1.3) was used to visualize the most frequent annotation associated within a cluster of GO terms. All present genes were used as input for a WGCNA, performed using the WGCNA R package (v1.70-3), to identify correlations of gene expression within the data set in an unbiased approach. The β -value was set at 23. For the module dissimilarity, a threshold of 0.42 was chosen, and the minimal cluster size was set to 30 genes. The prediction of transcription factor binding motifs was performed using the Cytoscape plugin iRegulon (v1.3) with a minimum normalized enrichment score of 3 and a maximum FDR on motif similarity of 0.001. All potential transcription factors annotated to the enriched binding motifs were used in the Venn diagram to illustrate their overlaps.

CUT&Tag and analysis

The CUT&Tag experiments were performed as previously described⁴¹ with a hyperactive in situ ChIP library prep kit purchased from Epiccypher (CUTANA CUT&Tag Assays) following the manufacturer's recommendations. A minimum of 1×10^5 stimulated BMDCs were bound to activated concanavalin A-coated magnetic beads and were subjected to immunoprecipitation with 0.5 μ g of primary antibody (anti-IRF1, D5E4, Cell Signaling Technology; rabbit anti-mouse IgG control). Immunoprecipitated DNA was amplified with high-fidelity 2 \times PCR mix (Epiccypher) using universal barcodes i5 and uniquely barcoded i7 primers and 21 cycles. PCR products were purified with AMPure XP beads and eluted in water. Libraries were sequenced on an Illumina NextSeq platform, and 150-bp paired-end reads were generated. Fastq reads for each sample were aligned to the mm39 reference genome using bwa (v0.7.17). PCR duplicates were removed using picard tools' MarkDuplicates (v2.25.0), and peaks were called using macs2 (v2.2.7.1) with the '-nomodel' parameter. To establish consensus peaks between all conditions, peak sets were merged using homer's mergePeaks (v4.11.1), and reads in consensus peaks were counted for each replicate using subread's featureCounts (v2.0.0). PCA plots were generated using R (v4.1) and the prcomp function. Differentially occupied peaks were established using the limma package (v3.46.0) and its voom, lmFit and eBayes functions. Motif occupancy at peaks was established with homer and the findMotifsGenome function (v4.11.1).

Immunoblotting

BMDCs were lysed in resuspension with RIPA buffer containing 50 mM Tris-HCl (pH 8), 150 mM sodium chloride, 1% NP-40, 0.5% sodium deoxycholate and 0.1% SDS (Sigma-Aldrich) supplemented with PhosSTOP phosphatase inhibitor cocktail tablets (Roche) and cComplete protease inhibitor cocktail tablets (Roche). Cell lysates were rotated at 4 °C for 30 min and clarified at 4 °C at 13,000g for 10 min. Proteins were denatured for 5 min at 90 °C with sample buffer containing 350 mM Tris-HCl (pH 6.8–5), 5% β -mercaptoethanol, 10% SDS, 36% glycerol and 0.0012% bromophenol blue. Proteins were then separated using NuPAGE 4–12% Bis-Tris gels (Thermo Fisher Scientific). Proteins were transferred onto nitrocellulose membranes (Bio-Rad) and blocked for 30 min with either 5% milk or 5% bovine serum albumin (BSA; for phosphorylated proteins) in PBS or TBS (for phosphorylated proteins) with 0.1% Tween 20. The following primary antibodies were used: rabbit anti-NF- κ B p65 (D14E12), mouse anti-phospho S536 NF- κ B p65 (7F1), rabbit anti-I κ B α (44D4) and rabbit anti- β -actin (I3E5), all purchased from Cell Signaling Technology. Membranes were incubated with horseradish peroxidase-conjugated secondary antibodies goat anti-rabbit IgG and horse anti-mouse IgG (Cell Signaling Technology) and subsequently with a Novex ECL chemiluminescent substrate reagent kit before imaging. Quantitative analysis of the signal intensity was performed using ImageJ software.

PhosFlow cytometry

Following in vitro stimulation of BMDCs, 100 μ l of warm PhosFlow Lyse/Fix Buffer (BD Biosciences) was directly added to the samples and incubated for 10 min at 37 °C. Samples were then resuspended in PhosFlow Perm Buffer III (BD Biosciences) and incubated for 30 min on ice. After being washed twice, samples were stained for 1 h at room temperature with the antibodies described above supplemented with antibody to phospho-P44/42 MAPK (ERK1/ERK2; Thr 202/Tyr 204; 197G2; Cell Signaling Technology) and phospho-p38 MAPK (Thr 180/Tyr 182; 4NIT4KK; Thermo Fisher Scientific). A Biosciences Cytek Aurora was used for the measurement of samples, and FlowJo software (TreeStar) was used for analysis.

CRISPR–Cas9 gene editing

Freshly isolated bone marrow precursors were edited via electroporation before culture with FLT3L, as described previously⁴². In brief, per 10×10^6 mouse bone marrow precursors to be electroporated, 61 pmol of Cas9 nuclease (IDT) and 300 pmol of sgRNA (Synthego) were combined and incubated for 10 min at room temperature, generating Cas9–sgRNA ribonucleoprotein complex. Bone marrow precursors (10×10^6) were then washed with $1 \times$ PBS twice and resuspended in 20 μ l of P3 buffer (Lonza) combined with the Cas9–sgRNA complex and electroporated using 4D-Nucleofector (Lonza) using the pulse code CM-137. Prewarmed medium was immediately added in electroporation wells to allow cells to recover for 10 min at 37 °C. Cells were subsequently cultured for 8 days in complete medium supplemented with FLT3L, as described above. sgRNA sequences used were *Fos* (UAGUGCCAAC-UUUAUCCCCA) and *NTC* (GCACUACCAGAGCUAACUCA).

Virus infection and viral titers

HSV-1 KOS was grown using Vero cells (CSL). Mice were epicutaneously infected with 10^6 plaque-forming units of HSV-1, as previously described⁶.

Flow cytometry analysis of in vivo HSV-1 responses

Endogenous HSV-specific CD8⁺ T cells were analyzed using H-2K^b-restricted gB_{498–505}-specific tetramers, as previously described⁶. In some experiments, *Ccl5*^{−/−} and wild-type mice were transferred with 50,000 naive HSV-specific CD8⁺ T cells (gBT-I cells) before infection, and their expansion was measured 10 days later in the spleen, as described previously⁶. IFN γ production in gB_{498–505}-specific CD8⁺

T cells was measured after restimulation for 5 h ex vivo in the presence of brefeldin A. Single-cell suspensions were stained with antibodies to CD16/CD32 (2.4G2, Fc block), CD8 (53-6.7), CD44 (IM7), CD45.2 (104) and CD3 (145-2C11) and, when necessary, with either CD45.1 monoclonal antibody (A20) or tetramer staining. After fixation and permeabilization with BD Cytofix/Cytoperm (BD Biosciences), cells were stained for 20 min at room temperature with antibodies to IFN γ (XMG1.2) in BD Perm/Wash buffer (BD Biosciences) before analysis on a flow cytometer. Dead cells were excluded by using a LIVE/DEAD fixable dead cell stain kit (Thermo Fisher Scientific). A BD LSRFortessa and a FACS Diva or Biosciences Cytek Aurora and SpectroFlo were used for measurement of samples, and FlowJo software (TreeStar) was used for analysis. In some experiments, CD8⁺ DCs from wild-type versus *Irfnar2*^{−/−} mice were analyzed in the brachial lymph node 2 days after HSV-1 skin infection, as previously described⁶. Cells were stained with antibodies to CD11c (N418), CD8 (53-6.7), CD3 (145-2C11, BD Biosciences), CD19 (1D3), NK1.1 (PK136) and IA/E (2G9), and CD8⁺ DCs were then processed on an analytic flow cytometer (LSRFortessa BD Biosciences).

BM chimeras

Mixed chimeras were generated as previously described⁶. C57BL/6 mice were lethally irradiated with 2×550 cGy and were reconstituted with a total of 5×10^6 bone marrow cells, previously depleted for T cells, from *Cxcr6*^{−/−} and wild-type mice in a 1:1 ratio.

scRNA-seq data generation and analysis

scRNA-seq data of PBMCs from individuals with COVID-19 and healthy control individuals collected from April to July 2020 in Bonn, Germany, were used, as previously reported²⁶. Samples were classified by disease severity according to the WHO ordinal scale (WHO score of 3, mild; WHO score of 4–5, moderate; WHO score of 7, severe) and by the time after onset of first symptoms (early: days 0–10, late: >day 11) at the date of sampling. Details about sample procurement and processing, sequencing and data analysis have been previously described²⁵, and an extensive description of the protocol has also been published⁴³. Processed and annotated scRNA-seq data²⁵ were used as published previously and are available at https://beta.fastgenomics.org/p/schulte-schrepping_covid19. The data were imported into R version 4.0.3 and were mainly analyzed using Seurat v3.9.9.

Subset analysis of DCs and monocytes

PBMCs were subjected to Seurat v4 reference mapping following the developer vignette (satijalab.org/seurat/articles/multimodal_reference_mapping.html) using the multimodal PBMC reference data set⁴⁴. Only those cells classified as DC or monocyte subsets were selected to remove any possible cellular contaminations in the data set. Subsequently, the remaining 37,100 cells were reclustered after scaling and regressing for unique molecular identifier (UMI) count per cell, identification of variable genes and PCA in this cellular subspace using the Louvain algorithm with a resolution of 0.2 based on the first 10 PCs. Clusters representing DCs or classical CD14⁺ monocytes were then subsetted, respectively, and the resulting 31,736 monocytes and 722 DCs were analyzed in detail, including rescaling, identification of variable genes, PCA and subsequent UMAP based on the first 10 PCs. Disease severity-specific marker gene analysis was performed using the Wilcoxon rank-sum test with the following cutoffs: genes had to be expressed in more than 10% of the cells of the respective condition and exceed a logarithmic fold change cutoff of at least 0.2. Before dot plot visualization and functional enrichment analyses, sets of differentially expressed genes were filtered for ribosomal protein-coding genes (*RPL/RPS*), mitochondrial genes (MT-) and hemoglobin genes (*HBA1*, *HBA2* and *HBB*). Hallmark enrichment analysis of differentially expressed gene sets was performed using the Hallmark v7.3 database and the enricher function implemented in the R package clusterProfiler v3.18.0 (ref. 45). Gene set enrichment analyses of

'CD40-unresponsive', 'amplified' and 'combinatorial' gene signatures in the differentially expressed genes in monocytes from individuals with mild COVID-19 compared to those from individuals with severe disease were performed using the *fgsea* package v1.16.0. Single-sample GSEA using the 'CD40-unresponsive', 'amplified' and 'combinatorial' signatures derived from the mouse bulk RNA-seq analysis of this study was performed using GSEA v1.38.2 (ref. 46). For this, aggregated expression values of all cells of each sample were calculated using the *AggregateExpression* function in Seurat and were used as input for the sample-specific analysis. Of note, the IFN α A response signature was intersected with the top 100 IFN-response genes derived from an integrated analysis of eight microarray data sets on IFN response of myeloid cells listed in the Interferome database (<http://www.interferome.org/>)⁴⁰ ranked by their combined \log_2 (fold change) values to reduce the signature to a length comparable to the amplified and combinatorial signatures. Transcription factor binding motif enrichment analysis based on the significantly differentially expressed genes in monocytes derived from individuals with mild COVID-19 compared to cells from individuals with severe disease and those differentially expressed genes that intersected with the 'amplified' and 'combinatorial' gene signatures was performed using *RcisTarget*³², the *hg38_refseq-r80_10kb_up_and_down_tss.mc9nr.feather* database and a normalized enrichment score threshold of 4. Enriched transcription factor binding motifs were filtered for the *transfac_pro*, *cisbp* and *swissregulon* databases and those motifs with high-confidence transcription factor annotation (TF_highConf). A network linking enriched target genes and predicted transcriptional regulators based on the *Rcistarget* transcription factor binding motif enrichment results was constructed and visualized in a circular layout using *Cytoscape* v3.7.1.

scRNA-seq analysis of CD14⁺ monocytes from individuals with IFN-AAB and corresponding healthy individuals

PBMC scRNA-seq data were produced from five control samples, five samples from individuals with moderate COVID-19, five samples from individuals with severe COVID-19 and seven samples from individuals with severe COVID-19 with IFN-AAB, which were tested for each individual in virus neutralization assays described in Akbil et al.²². On the day of the experiment, frozen live PBMCs were thawed in prewarmed medium (RPMI 1640 (Gibco), 2% fetal calf serum (Sigma) and 0.01% Pierce Universal Nuclease (Thermo Fisher)). The PBMCs were then labeled with 0.5 μ g of TotalSeq-C hashtag antibodies (Biolegend) in DPBS supplemented with 0.5% BSA and 2 mM EDTA for 30 min at 4 °C and washed at least three times with DPBS + 1% BSA. Subsequently, the PBMCs were counted, and up to seven different samples were pooled in equal proportions. The resulting cell pool was filtered through a 40- μ m mesh (Flowmi Cell Strainer, Merck) and super loaded with 50,000 cells per lane in the Chromium Controller for partitioning single cells into nanoliter-scale Gel Bead-In-Emulsions (GEMs). For reverse transcription, cDNA amplification and library construction of the gene expression libraries, the Chromium Next GEM Single Cell kit 5' v2 (10x Genomics) was used. The Chromium Single Cell 5' Feature Barcode Library kit (10x Genomics) was used for preparing additional hashtag libraries. All libraries were prepared according to the protocols provided by 10x Genomics, quantified by Qubit Flex fluorometer (Thermo Fisher) and quality checked using the 4150 TapeStation system. Sequencing was performed in paired-end mode (R1 26 cycles, R2 90 cycles) on a NovaSeq 6000 (Illumina) with a NovaSeq 6000 S2 reagent kit (100 cycles). After demultiplexing, raw sequencing data were processed with Cell Ranger v5 and aligned against the GRCh38 reference, including TotalSeq-C hashtag barcodes. scRNA-seq UMI count matrices were imported into R 4.0.3, and gene expression data analysis was performed using the R/Seurat package 3.9.9. Cells from pooled samples were demultiplexed using a combination of HTODemux implemented in Seurat and *vireo* (v0.5.6)⁴⁷ after scoring common variants from the 1000Genomes project with *cellsnr-lite* (v1.2.0)⁴⁸.

Events classified as 'negative' and 'doublet' by the HTODemux algorithm were assigned an ID via *vireo* classification. Subsequently, cells were filtered by number of features (over 200 and less than 5,000), percentage of mitochondrial genes (<10% mitochondrial UMIs) and number of counts per cell (<20,000) to exclude debris and doublets. Gene expression values were normalized by total UMI counts per cell, multiplied by 10,000 (TP10K) and log transformed by \log_{10} (TP10k + 1). For cell-type annotation, cells were subjected to Seurat v4 reference mapping following the developer vignette using the multimodal PBMC reference data set⁴⁴. Cells classified as CD14⁺ classical monocytes were selected and reclustered after scaling and identification of variable genes using *vst* and PCA using the Louvain algorithm with a resolution of 0.2 based on the first 10 PCs. A cluster characterized by the expression of T cell marker genes was removed to exclude potential T cell contamination in the CD14⁺ monocyte subset. Averaged gene expression values per sample of selected key genes were visualized as box plots across disease severity groups.

To increase the number of samples per severity group, scRNA-seq data of PBMCs from other COVID-19 cohorts produced using the same scRNA-seq protocol (10x Genomics, 5') by us²¹ and others^{27,28} were included in the analysis and processed as described above. The total number of samples combined in this analysis was 263. All samples were grouped according to their WHO ordinal scale classification into mild (WHO score of 1–3), moderate (WHO score of 4–5) and severe (WHO score of 6–8) COVID-19 disease. In addition, samples known to be derived from individuals with IFN-AAB were subgrouped accordingly. PBMC scRNA-seq data from Van der Wijst et al.²⁸ were downloaded and filtered for the earliest sample available per donor, resulting in 11 control samples and 35 samples from individuals with moderate COVID-19, 26 samples from individuals with severe COVID-19 and 4 samples from individuals with severe COVID-19 with IFN-AAB. PBMC scRNA-seq data from Su et al.²⁷ were downloaded and filtered for the earliest sample available per donor, resulting in 17 control samples and 69 samples from individuals with mild COVID-19, 45 samples from individuals with moderate COVID-19 and 15 samples from individuals with severe COVID-19. PBMC scRNA-seq data from Georg et al.²¹ included six control samples, five samples from individuals with mild COVID-19, two samples from individuals with moderate COVID-19 and six samples from individuals with severe COVID-19. Single-sample GSEA using the 'CD40-unresponsive', 'amplified' and 'combinatorial' signatures derived from the mouse bulk RNA-seq analysis of this study was performed using GSEA v1.38.2.

For validation, we additionally analyzed scRNA-seq data from DCs from PBMC data enriched for DCs as previously published²⁶. After downloading the respective data from the public domain, we selected those cells originally classified as monocytes and DCs and followed the same procedure of filtering the cells using the Seurat v4 reference mapping approach, as outlined above. Differential gene expression analyses and signature enrichment analyses of the 'CD40-unresponsive', 'amplified' and 'combinatorial' signatures were performed as described above.

Subset analysis of CD8⁺ T cells

For detailed analysis of the CD8⁺ T cell compartment, cells classified as T cells according to the original annotation provided were selected from the PBMC data set. These cells were subjected to Seurat v4 reference mapping following the developer vignette (satijalab.org/seurat/articles/multimodal_reference_mapping.html) using the multimodal PBMC reference data set⁴⁴. Only those cells classified as T cells were selected to remove any possible cellular contaminations in the T cell data set. Subsequently, the remaining 45,516 cells were reclustered after scaling, regressing for UMI count per cell, identification of variable genes and PCA in this cellular subspace using the Louvain algorithm with a resolution of 0.2 based on the first 10 PCs. Cluster 1, representing CD8⁺ T cells, was then subsetted, and the resulting 12,386 cells were analyzed in detail, including rescaling, identification of variable

genes, PCA and subsequent UMAP⁴⁹ based on the first 10 PCs. Ribosomal protein-coding genes (*RPL/RPS*), mitochondrial genes (MT-) and hemoglobin genes (*HBA1*, *HBA2* and *HBB*) were excluded from the set of variable features to remove potential sources of technical differences. Single-sample GSVA using the ‘helped’ and ‘unhelped’ T cell signatures derived from RNA-seq analysis of CD8⁺ T cells primed in the presence or absence of CD4⁺ T cell responses was performed using GSVA v1.38.2. For this, aggregated expression values of all CD8⁺ T cells of each sample were calculated using the `AggregateExpression` function in Seurat and were used as input for the sample-specific analysis. Clustering of the CD8⁺ T cells was performed using the Louvain algorithm with a resolution of 0.4 based on the first 10 PCs, and cells identified as $\gamma\delta$ T cells were removed. To investigate proportional cluster occupancy per disease severity, cell counts per condition were normalized before calculation of per-cluster percentages. Single-cell gene set enrichment analysis across cells of each CD8⁺ T cell subcluster using the ‘helped’ and ‘unhelped’ T cell signatures derived from RNA-seq analysis of CD8⁺ T cells primed in the presence or absence of CD4⁺ T cell responses was performed using AUCell v1.12.0 (ref. 32). For validation, we analyzed CD8⁺ T cells from two other data sets^{36,37}. After downloading the respective data from the public domain, we followed the same procedure of filtering the cells using the Seurat v4 reference mapping approach and performed signature enrichment analysis using the above-mentioned T cell signatures.

Analysis of scATAC-seq data

scATAC-seq data of PBMCs from individuals with COVID-19 and healthy individuals produced using a Chromium Next GEM Single Cell ATAC reagent kit version 1.1 (10x Genomics, PN-1000175) was used, as previously published²⁹. Processed and annotated scATAC-seq data from Wilk et al.²⁹ were downloaded from Gene Expression Omnibus (GEO) under accession number [GSE174072](https://www.ncbi.nlm.nih.gov/geo/query/acc.cgi?acc=GSE174072) and https://github.com/ajwilk/COVID_scMultiome and were imported to R version 4.1.0. After creation of Arrow files and a respective ArchRproject using the R package ArchR version 1.0.1 (ref. 50), the resulting single-cell data were filtered based on the published cell annotation and subsetted to CD14⁺ monocytes. Imputation weights on GeneScores were calculated using MAGIC⁵¹ implemented in ArchR’s `addImputeWeights` function. Severity-specific accessible genes were identified using the Wilcoxon rank-sum test comparing gene scores of monocytes from individuals with mild COVID-19 to cells from control donors with the following cutoffs: $FDR \leq 0.05$ and $\log_2(\text{fold change}) \geq 0.58$. Hallmark enrichment analyses were performed using clusterProfiler version 4.0.5 and the Hallmark gene set v6.2. After generation of pseudo-bulk replicates across cells of each COVID-19 severity group, peaks were called using MACS3 (ref. 52) and annotated using ChIPseeker version 1.28.3 (ref. 53). Subsequently, transcription factor binding motifs were identified in the peak regions using the homer motif set. After calculation of severity-specific differentially accessible peak regions ($FDR \leq 0.01$ and $\log_2(\text{fold change}) \geq 2$) comparing chromatin profiles of monocytes from individuals with mild and severe COVID-19 to cells from control donors, motif enrichment analysis was performed using ArchR’s `peakAnnoEnrichment` function.

CytoF data and analysis

For mass cytometry data from a publicly available publication²¹, please refer to the Methods part of the work for detailed descriptions of the cohort, data collection and analysis workflows. Here, CD8⁺ T cells were separately reanalyzed and pre-gated using OMIQ cloud-based cytometry analysis software, also in relation to the presence of IFN- γ AAB²². In addition to the steps described²¹, we performed a PCA using R (4.0.2), where principal components were first calculated for all the events, and averages of principal component values per individual were used in plotting. Figures were rendered with the help of the R package `ggfortify` and function `autoplot`, which allows plotting of eigenvectors of input variables when used on precalculated principal components.

An ellipse was calculated with `ggplot2` to visually estimate the localization of different groups. Marker intensity box plots show average z-score-normalized intensity signals for all the CD8⁺ T cells per individual. Z-score normalization was performed beforehand over all the immune cells acquired in CyTOF.

Flow cytometry analysis of monocytes and DCs in individuals with COVID-19

Fixed whole-blood samples from individuals with COVID-19 were collected, processed and stored, as previously described²⁵. The samples were subsequently thawed to room temperature, and erythrocytes were lysed with Thaw-Lysis buffer (Smart Buffer). After 5 min of treatment with 50 U ml⁻¹ Pierce Universal Nuclease for Cell Lysis (Thermo Scientific) and 20 min of blocking with 1 mg ml⁻¹ beriglobin (CSL Behring), the samples were stained for 30 min at 4 °C with antibodies to CD45 (HI30), CD11c (Bu15), CD14 (M ϕ P9), CD3 (UCHT1), CD19 (SJ25C1), CD40 (5C3), CD83 (HB15e), CD86 (IT2.2), HLA-DR (G46-6), CD16 (3G8), CD141 (1A4) and CD163 (GHI/61). A BD LSRFortessa was used for the measurement of samples, and FlowJo software (TreeStar) was used for analysis. Expression of CD45, CD3, CD19 and HLA-DR was used for granulocyte, T cell, B cell and natural killer cell exclusion, respectively. Monocytes were gated as CD14⁺CD11c⁺ and DCs as CD14⁺HLA-DR⁺ events.

In vitro generation of human CD34⁺ stem cell-derived cDC1s

Human umbilical cord blood was obtained with written informed consent from the Queensland Cord Blood Bank and approval from the Mater Human Research Ethics Committee (HREC13/MHS/86). cDC1s were differentiated in a 9- to 10-d culture of in vitro expanded cord blood CD34⁺ progenitors in 100 ng ml⁻¹ FLT3L (Peprotech), 100 ng ml⁻¹ stem cell factor (Peprotech), 2.5 ng ml⁻¹ IL-4 (Invitrogen) and 2.5 ng ml⁻¹ granulocyte-macrophage colony-stimulating factor (Invitrogen), as previously described³⁰, but with the addition of an irradiated OP9-DL1 stromal cell feeder layer to maximize cDC1 yields⁵⁴. CD141⁺CADM1⁺CLEC9A⁺ cDC1s were enriched to >80% purity by labeling with biotinylated antibodies to human CADM1 (CM004-6) or CD141 (M80) and anti-biotin microbeads, followed by positive selection on an LS column according to manufacturer’s instructions (Miltenyi). Purified cDC1s were cultured at a density of 1×10^6 per ml in the presence of 1,000 U ml⁻¹ human IFN α 2a (PBL), 5 μ g ml⁻¹ CD40 agonistic antibody¹¹ (34G12-h2, a gift from M. Cragg at University of Southampton) or a combination. TNF- α was detected in the supernatant after 18 h using a LegendPlex kit (Biolegend) on a CytoFLEX-S (Beckman Coulter) flow cytometer.

Quantification and statistical analysis

Prism v8.4.3 (GraphPad Software) was used to assess statistical significance of non-RNA-seq data; z score = $(x - \text{mean})/s.d.$ The sample size (n), statistical significance and statistical tests are indicated in the legends. Data distribution was assumed to be normal, but this was not formally tested. Data collection and analysis were not performed blind to the conditions of the experiments and no formal randomization was used. No data points were excluded.

Reporting summary

Further information on research design is available in the Nature Portfolio Reporting Summary linked to this article.

Data availability

The RNA-seq data set generated in this study can be accessed via the GEO accession number [GSE171690](https://www.ncbi.nlm.nih.gov/geo/query/acc.cgi?acc=GSE171690).

Code availability

Code used for the analysis of scRNA-seq and scATAC-seq data is available at https://github.com/schultzelab/Gressier_2022. We also provide

the scRNA-seq data sets used in this study and the code to analyze the respective data sets via FASTGenomics (https://beta.fastgenomics.org/p/gressier_2022).

References

38. Kurth, F. et al. Studying the pathophysiology of coronavirus disease 2019: a protocol for the Berlin prospective COVID-19 patient cohort (Pa-COVID-19). *Infection* **48**, 619–626 (2020).
39. Huang da, W., Sherman, B. T. & Lempicki, R. A. Systematic and integrative analysis of large gene lists using DAVID bioinformatics resources. *Nat. Protoc.* **4**, 44–57 (2009).
40. Subramanian, A. et al. Gene set enrichment analysis: a knowledge-based approach for interpreting genome-wide expression profiles. *Proc. Natl Acad. Sci. USA* **102**, 15545–15550 (2005).
41. Kaya-Okur, H. S. et al. CUT&Tag for efficient epigenomic profiling of small samples and single cells. *Nat. Commun.* **10**, 1930 (2019).
42. Freund, E. C. et al. Efficient gene knockout in primary human and murine myeloid cells by non-viral delivery of CRISPR–Cas9. *J. Exp. Med.* **217**, e20191692 (2020).
43. De Domenico, E. et al. Optimized workflow for single-cell transcriptomics on infectious diseases including COVID-19. *STAR Protoc.* **1**, 100233 (2020).
44. Hao, Y. et al. Integrated analysis of multimodal single-cell data. *Cell* <https://doi.org/10.1016/j.cell.2021.04.048> (2021).
45. Wu, T. et al. clusterProfiler 4.0: a universal enrichment tool for interpreting omics data. *Innovation* **2**, 100141 (2021).
46. Hanzelmann, S., Castelo, R. & Guinney, J. GSEA: gene set variation analysis for microarray and RNA-seq data. *BMC Bioinformatics* **14**, 7 (2013).
47. Huang, Y., McCarthy, D. J. & Stegle, O. Vireo: Bayesian demultiplexing of pooled single-cell RNA-seq data without genotype reference. *Genome Biol.* **20**, 273 (2019).
48. Huang, X. & Huang, Y. Cellsnp-lite: an efficient tool for genotyping single cells. *Bioinformatics* **37**, 4569–4571 (2021).
49. McInnes, L., Healy, J. & Melville, J. UMAP: Uniform Manifold Approximation and Projection for dimension reduction. Preprint at <https://doi.org/10.48550/arXiv.1802.03426> (2018).
50. Granja, J. M. et al. ArchR is a scalable software package for integrative single-cell chromatin accessibility analysis. *Nat. Genet.* **53**, 403–411 (2021).
51. van Dijk, D. et al. Recovering gene interactions from single-cell data using data diffusion. *Cell* **174**, 716–729 (2018).
52. Zhang, Y. et al. Model-based analysis of ChIP-seq (MACS). *Genome Biol.* **9**, R137 (2008).
53. Yu, G., Wang, L. G. & He, Q. Y. ChIPseeker: an R/Bioconductor package for ChIP peak annotation, comparison and visualization. *Bioinformatics* **31**, 2382–2383 (2015).
54. Balan, S. et al. Large-scale human dendritic cell differentiation revealing notch-dependent lineage bifurcation and heterogeneity. *Cell Rep.* **24**, 1902–1915 (2018).

Acknowledgements

We thank L. Loyal, A. Thiel, C. Iwert, C. Meisel, R. Rudraraju and K. Subbarao for discussions, F. Koay and D. Godfrey for *Cxcr6*^{-/-} mice and M. Cragg for the human CD40 antibody. The technical expertise in breeding, maintaining and manipulating specific pathogen-free mice by the Doherty Bioresources facility is gratefully acknowledged. We also thank D. Kunkel and J. Keye from the BIH Flow and Mass Cytometry Core Facility for sample acquisition. We are grateful to

the Genomics platform at the Walter & Eliza Hall Institute for Medical Research in Melbourne. Our research is supported by the National Health and Medical Research Council of Australia (APP1124815, APP1071916, APP1103895 and APP1154540), the Sylvia & Charles Viertel Charitable Foundation, a 350th Anniversary Research Grant from Merck KgGA, The Advanced Genomic Collaboration and the International Research Training Group (IRTG2168) funded by the German Research Council and The University of Melbourne. B.S. received support from the European Union's Horizon 2020 research and innovation program (INSTRuCT, 860003) and the German Federal Ministry of Education and Research (BMBF) project RECAST (01K120337). A.H. is supported by the Jürgen Manchot Foundation. E.L. and S.V.S. were supported by the German Federal Ministry of Education and Research through the COVIMMUN project (grant 01K120343). Furthermore, E.L. received support by the Deutsche Forschungsgemeinschaft (DFG, German Research Foundation), grant 397484323, TRR259. We thank the NGS Core Facility of the University Hospital Bonn for library preparation and the generation of the sequencing data. We also would like to thank the German COVID-19 OMICS Initiative (DeCOI) for providing access to scRNA-seq data. J.L.S. was supported by the DFG (IRTG2168, INST 217/1011-1 and INST 217/1017-1, Excellence Cluster ImmunoSensation² (EXC2151/1) under project number 390873048) and SYSCID, receiving funding from the European Union's Horizon 2020 research and innovation program under grant agreement number 733100. We are indebted to the participants, their families and the hospital staff for support, without whom this study would not have been possible.

Author contributions

Conceptualization: S. Bedoui, E.G., J.S.-S. and S.V.S. Methodology: P.G.W., A.B., K.H., M.K., M. Clarke, T.H.O.N., P.S., K.W., C.V.L.O., B.O., C.v.d.S., Y.-C.E.C., K.J.R., T.M., M. Chopin, S. Brumhard, S.S.G., K.K. and S.L.L. Formal analysis: E.G., J.S.-S., A.O., J. Spitzer, L.J.G., P.J.H., L.P., T.K., T.A., F.K., J. Schroeder and B.S. Investigation: E.G., J.S.-S., P.G.W., A.B., M.G. and F.K. Writing, original draft: S. Bedoui and E.G. Writing, review and editing: S. Bedoui, E.G., J.S.-S., S.V.S., J.L.S., W.K., A.K., T.G., E.L., C.K. and L.E.S. Funding acquisition: S. Bedoui, T.G., E.L., J.L.S. and S.V.S.

Competing interests

The authors declare no competing interests.

Additional information

Extended data is available for this paper at <https://doi.org/10.1038/s41590-023-01517-x>.

Supplementary information The online version contains supplementary material available at <https://doi.org/10.1038/s41590-023-01517-x>.

Correspondence and requests for materials should be addressed to Elise Gressier or Sammy Bedoui.

Peer review information *Nature Immunology* thanks Teunis Geijtenbeek, and the other, anonymous, reviewer(s) for their contribution to the peer review of this work. Primary Handling Editor: Ioana Visan, in collaboration with the *Nature Immunology* team. Peer reviewer reports are available.

Reprints and permissions information is available at www.nature.com/reprints.

4 Discussion with references

4.1 Antibody-response to SARS-CoV-2 vaccines

In the first part of this thesis, I could demonstrate sustained antibody reactions to SARS-CoV-2; these reactions did not differ in their magnitude, regardless of choice of vaccine and vaccination scheme. While at the time, these results were a novel insight into the response to varying vaccination schemes, the size of the study, especially with regard to the mixed-booster regimens, did leave room for improvement. Later, a study by Atmar *et al.* could confirm a similar lack of strong differences in a study with 458 participants (Atmar *et al.*, 2022). Another limitation of the study herein presented is the underrepresentation of later, namely Omnicron variants. The Omnicron variants show a strong immune escape (Cao *et al.*, 2022) and interestingly do not confer cross-protection with other variants after infection (Dejnirattisai *et al.*, 2022). As such, it would have been a good inclusion into this study, but sample collection for the largest part was conducted before Omnicron variants became widespread within central Europe (Anand *et al.*, 2023; Maier *et al.*, 2023).

With regard to the antibody response post infection, a longer-term follow-up could have yielded interesting results; previously, Wang *et al.* had shown that antibody-responses post infection remain stable between 6 months and 1 year after infection (Wang *et al.*, 2021). In this regard, the study was hampered by vaccination recommendation by the German regulatory authorities, as they recommend a booster post-infection after 3-6 months (RKI, 2023).

In the first study, we could not demonstrate any strong effects with regards to comorbidities such as obesity, hypertension, or diabetes. With the second study, focussing on the influence of liver cirrhosis and the immune dysfunction induced by it, a cohort of participants with cirrhosis was analysed with regards to their SARS-CoV-2 vaccination response: indeed, a weaker vaccine response could be demonstrated in this cohort. Other studies have also found a similar detrimental effects of IL-10 levels on vaccine response, although in this case not cirrhosis-induced (Azaiz *et al.*, 2022; Ponciano-Gómez *et al.*, 2022).

4.2 IFN-induced IL10 weakens the T cell response

The second publication in this thesis demonstrates that IL-10 drives an exhaustion-like phenotype in T cells. The IL-10 is derived from myeloid cells in the liver as they respond to microbial-induced IFN. Due to the chronic nature of the cirrhosis model, one could

assume the T cell exhaustion to be established by long-term exposure to IFN or IL-10, but we could demonstrate that IL-10Ra antibodies in cirrhosis models have a quick positive effect on the exhausted T cells. Direct targeting of IFN signalling in chronic diseases has been successfully used in chronic disease settings (Wilson *et al.*, 2013), the effects can be detrimental (Murira and Lamarre, 2016), so a focus on downstream effects of IFN may be appropriate target for future intervention. While the study did focus on the T cell compartment, the underlying mechanism is one of myeloid-T cell interaction and can be targeted at either side. In COVID-19 infections, IL10 has been linked to severe infections (Islam *et al.*, 2021) and is being discussed as a predictor and driver of more severe forms (Dhar *et al.*, 2021; Lu *et al.*, 2021). Moreover, together with my colleagues, we demonstrate for the first time a link between IL-10 levels and survival: while patients with severe disease show higher levels of IL-10, the survival of patients with severe disease appears to be correlated with IL-10 levels in our limited cohort.

4.3 Interactions of T cells and antigen presenting cells

The third study presented here elucidated the interaction of antigen presenting cells (APCs) and T cells at the centre of COVID-19 infection: while initial IFN signalling can precondition APCs, only through interaction with CD4⁺ T cells, APCs participate in the antiviral defence. Here, the direct contact between cells is needed as the cluster of differentiation (CD) 40 – CD40 ligand interaction is what licenses myeloid cells to their fullest potential. As such, these results explain a number of findings in the literature, such as the lower IFN response in more severe cases (Hadjadj *et al.*, 2020), i.e. lack of preconditioning, and missing myeloid-T cell interactions (Zhang *et al.*, 2021).

In summary, the studies presented as part of this thesis characterise and explain aspects of the immune response to SARS-CoV-2, both to the disease itself and to human-made analogues in the form of vaccines. The first study characterises various vaccines as well as the accompanying cytokines. The second study describes the specific cytokine environment made up of IFN and IL-10 created by liver cirrhosis in the context of viral infections and vaccinations, and explores the potential therapeutic strategy of altering the IL-10 response to allow for more successful vaccinations as well as anti-viral treatments. In the third study, the direct contact between myeloid and T cell compartments is described; after preconditioning with IFN, CD40-CD40L interaction can fully license APC action against COVID-19.

4.4 References

Anand, U. *et al.* (2023) 'The spread of the omicron variant: Identification of knowledge gaps, virus diffusion modelling, and future research needs', *Environmental Research*, 225, p. 115612. Available at: <https://doi.org/10.1016/j.envres.2023.115612>.

Atmar, R.L. *et al.* (2022) 'Homologous and Heterologous Covid-19 Booster Vaccinations', *New England Journal of Medicine*, 386(11), pp. 1046–1057. Available at: <https://doi.org/10.1056/NEJMoa2116414>.

Azaiz, M.B. *et al.* (2022) 'Deciphering the balance of IL-6/IL-10 cytokines in severe to critical COVID-19 patients', *Immunobiology*, 227(4), p. 152236. Available at: <https://doi.org/10.1016/j.imbio.2022.152236>.

Cao, Y. *et al.* (2022) 'Omicron escapes the majority of existing SARS-CoV-2 neutralizing antibodies', *Nature*, 602(7898), pp. 657–663. Available at: <https://doi.org/10.1038/s41586-021-04385-3>.

Dejnirattisai, W. *et al.* (2022) 'SARS-CoV-2 Omicron-B.1.1.529 leads to widespread escape from neutralizing antibody responses', *Cell*, 185(3), pp. 467-484.e15. Available at: <https://doi.org/10.1016/j.cell.2021.12.046>.

Dhar, S.K. *et al.* (2021) 'IL-6 and IL-10 as predictors of disease severity in COVID-19 patients: results from meta-analysis and regression', *Heliyon*, 7(2), p. e06155. Available at: <https://doi.org/10.1016/j.heliyon.2021.e06155>.

Hadjadj, J. *et al.* (2020) 'Impaired type I interferon activity and inflammatory responses in severe COVID-19 patients', *Science*, 369(6504), pp. 718–724. Available at: <https://doi.org/10.1126/science.abc6027>.

Islam, H. *et al.* (2021) 'Elevated Interleukin-10 Levels in COVID-19: Potentiation of Pro-Inflammatory Responses or Impaired Anti-Inflammatory Action?', *Frontiers in Immunology*, 12. Available at: <https://www.frontiersin.org/articles/10.3389/fimmu.2021.677008> (Accessed: 17 August 2023).

Lu, L. *et al.* (2021) 'A Potential Role of Interleukin 10 in COVID-19 Pathogenesis', *Trends in Immunology*, 42(1), pp. 3–5. Available at: <https://doi.org/10.1016/j.it.2020.10.012>.

Maier, B.F. *et al.* (2023) 'Modeling the impact of the Omicron infection wave in Germany', *Biology Methods & Protocols*, 8(1), p. bpad005. Available at: <https://doi.org/10.1093/biomethods/bpad005>.

Murira, A. and Lamarre, A. (2016) 'Type-I Interferon Responses: From Friend to Foe in the Battle against Chronic Viral Infection', *Frontiers in Immunology*, 7. Available at: <https://www.frontiersin.org/articles/10.3389/fimmu.2016.00609> (Accessed: 17 August 2023).

Ponciano-Gómez, A. *et al.* (2022) 'High baseline expression of IL-6 and IL-10 decreased CCR7 B cells in individuals with previous SARS-CoV-2 infection during BNT162b2 vaccination', *Frontiers in Immunology*, 13, p. 946770. Available at: <https://doi.org/10.3389/fimmu.2022.946770>.

RKI (2023). Available at: https://www.rki.de/SharedDocs/FAQ/COVID-Impfen/FAQ_Genesene_Impfdosis.html (Accessed: 17 August 2023).

Wang, Z. *et al.* (2021) 'Naturally enhanced neutralizing breadth against SARS-CoV-2 one year after infection', *Nature*, 595(7867), pp. 426–431. Available at: <https://doi.org/10.1038/s41586-021-03696-9>.

Wilson, E.B. *et al.* (2013) 'Blockade of Chronic Type I Interferon Signaling to Control Persistent LCMV Infection', *Science*, 340(6129), pp. 202–207. Available at: <https://doi.org/10.1126/science.1235208>.

Zhang, D. *et al.* (2021) 'Frontline Science: COVID-19 infection induces readily detectable morphologic and inflammation-related phenotypic changes in peripheral blood monocytes', *Journal of Leukocyte Biology*, 109(1), pp. 13–22. Available at: <https://doi.org/10.1002/JLB.4HI0720-470R>.

5 Acknowledgement

I want to thank Eicke Latz and in the last year Gunther Hartmann for providing me with the possibility to perform research in their laboratories, as well as any advice and input they provided. I want to thank my supervisor Susanne Schmidt for providing me with interesting challenges and problems during my PhD, the freedom to overcome them and advise and help when I could not. I want to thank my colleagues and fellow PhD students, for the support during work times and distraction and fun afterwards. A special thanks belongs to my family and friends, chief among them my girlfriend, for their support.